8071-15-P

# COLLECTION AND ANALYSIS OF SEISMIC-WAVE PROPAGATION DATA
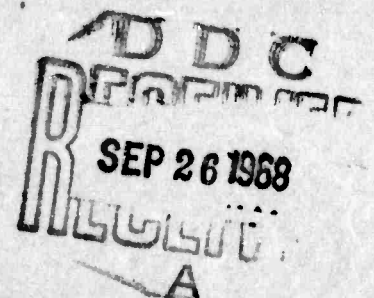
## (Annual Report)

September 1968

Prepared For
Geophysics Division
Air Force Office of Scientific Research
Arlington, Virginia 22209

By
DAVID E. WILLIS
PHILIP L. JACKSON
Principal Investigators

Geophysics Laboratory
Willow Run Laboratories
Institute of Science and Technology
The University of Michigan
Ann Arbor, Michigan

Sponsored By

Advanced Research Projects Agency
Nuclear Test Detection Office
Project VELA UNIFORM
ARPA Order No. 292, Amendments 32 and 37

Distribution of this document is unlimited.

8071-15-P

# COLLECTION AND ANALYSIS OF SEISMIC-WAVE PROPAGATION DATA

## (Annual Report)

September 1968

By
DAVID E. WILLIS
PHILIP L. JACKSON
Principal Investigators

Geophysics Laboratory
Willow Run Laboratories
Institute of Science and Technology
The University of Michigan
Ann Arbor, Michigan

## ABSTRACT

This report discusses the results of an extensive long-range reversed refraction profile which traverses the Michigan Basin and the Appalachian Mountains. Particular emphasis is placed on the attenuation of first compressional wave arrivals and on crustal-upper mantle structure. Also included are results of a survey on lake bottom seismic background noise in Lake Superior. Although large signal levels were obtained in the lake bottom, long periods of high background noise indicated that land based seismographs are superior. Theoretical studies in elastic wave scattering were made to evaluate the effect of nonhomogeneities on the propagation of elastic waves. Theoretical development of mode filtering, (previously demonstrated empirically), is nearly completed. A LASA digital data convertor was designed, constructed, and put into operation. Two- and three-dimensional seismic ray-tracing techniques using digital modeling were developed. These techniques enable the seismologist to determine the effects of lateral inhomogeneities and irregularities in velocity interface on travel time and attenuation of seismic waves.

# CONTENTS

## FIGURES

## ACRONYMS

ECOOE  East Coast On-Shore Off-Shore Experiment

LASA   Large Aperture Seismic Array

LRSM   Long Range Seismic Measurement

SAAC   Large Aperture Seismic Array Analysis Center, Washington, D. C.

USCG   United States Coast and Geodetic Survey

USGS   United States Geological Survey

## SYMBOLS

$f_0$       fundamental frequency

h           layer thickness

$\eta$       geometrical spreading

P           compressional wave

$P_g$       crustal compressional wave

$P_n$       upper-mantle compressional wave

$P_o$       observed travel time

Q           attenuation factor

$Q_\alpha$   compressional wave attenuation factor

S           shear wave

T           time

$T_o$       observed travel time

$T_r$       residual travel time

v           layer

$v_N$       upper-mantle layer

$v_o$       upper layer

V           voltage

X           distance

$\alpha$     seismic-wave absorption

$\Delta$     distance

Other symbols are defined where they are used in text.

# COLLECTION AND ANALYSIS OF SEISMIC-WAVE PROPAGATION DATA
## Annual Report
### 1 June 1967 Through 31 May 1968

## SUMMARY

An extensive long-range reversed refraction profile was obtained in the eastern United States. This profile traversed the Michigan Basin and the Appalachian Mountains. Close station control (25 km or less) over most of the profile permitted detailed studies of travel time and attenuation anomalies. Crustal and upper-mantle structure was determined along the profile. A mountain-root system similar to the Rocky Mountains was indicated under the Appalachian Mountains. A two-layered crust with a high-velocity (7.7 km/sec) lower layer was found in the Lake Superior area, and a single-layered crust was determined in the Atlantic Coast area. High upper-mantle Q values ($Q_\alpha \cong 1900$) for first compressional wave arrivals were disclosed in the Lake Superior area and across the Michigan Basin; considerably lower values ($Q_\alpha \cong 960$) were indicated farther east. Lower crustal Q's ($Q_\alpha \cong 160$ and 200) were found for the two-layered crust in the Lake Superior area; a considerably higher value ($Q_\alpha \cong 870$) was determined for the single-layered crust along the East Coast.

A new method of displaying seismic attenuation and spectral data was developed; it permits the presentation of the data in three dimensions (distance, frequency, and ground-particle velocity amplitude). Meaningful and consistent anomalies in the spectrum of seismic waves were found that could be correlated with variations in the source and in propagation effects.

Theoretical studies in elastic-wave scattering were made to evaluate the effect of non-homogeneities on the propagation of elastic waves. A general solution was obtained to determine the scattering of plane waves in an elastic medium by elliptical obstacles. The degenerate case of a slit (fault) was also computed. Current studies are directed toward evaluating the scattering effects caused by imperfections or irregularities at a velocity discontinuity on the reflected and transmitted seismic waves.

A series of seismic recordings was obtained on the bottom of Lake Superior to determine the nature of the background noise and to check the reciprocity in signal amplitudes of tele-seismic sources. Previous research had disclosed that shots fired in Lake Superior were very efficient in the coupling of seismic energy. If teleseismic sources recorded on the bottom of Lake Superior had large amplitudes and the background noise were low, consideration might be given to establishing a permanent station or array for monitoring small distant events. The results of this investigation disclosed that larger amplitude signals were obtained on the lake bottom but that the signal-to-noise ratios were no better and in many cases worse than those obtained on land stations. Long periods of high background noise were encountered on the lake-bottom seismograph and could be correlated with local meteorological conditions and with water-wave action.

1

Analysis of travel-time and amplitude data from the SHOAL event at distances of 200 to 1200 km has revealed significant azimuthal variation in velocity and attenuation. $P_n$ travel-time residuals east of the Sierras are negatively correlated with teleseismic P residuals and can be explained in terms of rather localized velocity variations in the uppermost mantle. Average apparent Q values were 276 for $P_n$ and 225 for $P_g$. Higher Q's were observed to the north for $P_n$ and to the southeast for $P_g$. These results indicate that explosions detonated in areas of complex crust and upper-mantle structure may be expected to radiate seismic energy in a highly asymmetrical manner.

The mode-filtering techniques developed at the Geophysics Laboratory by optical processing methods have moved from an empirical basis to a nearly complete theoretical basis.

Given the sampling geometry described in the previous annual report under this contract [1], it can be shown that filters which are merely opaque and transparent quadrants symmetrically placed with respect to the origin yield an output which is the sum of the original seismic traces and those whose phase spectrum has been shifted by $\pi/2$. The use of banded filters of the same symmetry as above provides (no proof has been given yet) amplitude equalization before (or along with) the phase shift to further attenuate Rayleigh waves. Of course, the phase shifting must not be applied to signal components; they must be identified in the Fourier plane and the fiters applied only to noise patterns in that plane. To date this technique has been directed toward extracting P-wave signals out of Rayleigh wave noise where signal-to-noise ratios are frequently less than unity. Plans are being made to extend the technique to include S-wave signal enhancement.

A digital data convertor for LASA data was designed, constructed, and is operational. It permits viewing up to 50 data channels directly from a LASA digital tape without the use of a digital computer. The convertor is a flexible device with either an analog or a digital output. Wiggly line seismograms or variable-density film records can be readily obtained. An investigation of on-line optical techniques (velocity filtering, beam forming, cross correlation, etc.) for the detection of significant events is now under consideration. While the system would not be as versatile and as accurate as the elaborate digital facilities at SAAC, the technique may provide a low-cost means of viewing LASA data in a routine manner and aid in the selection of events for more elaborate processing by a digital computer.

A three-dimensional seismic-ray-tracing technique and travel-time computation using digital modeling is under development; this will enable the seismologist to determine the effects of lateral inhomogeneities and irregularities in velocity interfaces on the travel times and amplitudes of seismic waves emerging at the surface. The geological model in any or all portions of the wave path from the source to receiver can be varied, including the underlying structure of an array. It is anticipated that simulation of the type of anomalies observed at LASA will be possible. The preliminary results of this investigation have been quite encouraging. Calcomp plots of the digital computer output are shown for two-and three-dimensional models. The output will

2

also be displayed on a CRT to allow the interpreter to rapidly vary the geological structure. Also, iterative perturbation of the velocity structure, planned for the computer, will alter the velocity structure until travel-time data is duplicated.

# SEISMIC-WAVE PROPAGATION— TRAVEL TIME AND ATTENUATION
## D. E. Willis

## 1.1. INTRODUCTION

During the past five years, The University of Michigan has participated in a number of cooperative investigations of the earth's crust. A large portion of this work involved a long-range reversed seismic refraction profile extending along a line from International Falls, Minnesota, to Jacksonville, North Carolina, a distance of approximately 2000 km. The shot location and recording stations are shown in figure 1. The major shot programs include:

    1962  North Carolina Experiment
    1963  Lake Superior Experiment
    1964  July Lake Superior Experiment
    1964  October USGS Shots
    1965  ECOOE
    1966  EARLY RISE
    1965  CHASE III, 700 tons
    1965  CHASE IV, 310 tons
    1966  CHASE VII, 400 tons

The section of the map shown here is from a Calcomp plot made through use of an IBM 7090 computer. All of the geographical features, the shot points, and recording stations were machine plotted.

In this report we present some of our data on reduced travel times, record sections, and attenuation, correlating as much of them as possible with the geological environment.

## 1.2. REDUCED TRAVEL TIMES

In figure 2 the reduced travel times are shown for the 1- and 5-ton shots recorded on the ECOOE northern profile. An upper-mantle velocity of 8.2 km/sec was used for these computations. There appears to be considerable scatter on this graph. However, if each station were separated, it could be seen that the stations located east of the Appalachians group together, giving an intercept time of approximately +7 1/2 sec, and those over the crest and just west of the Appalachians group together with an intercept time of approximately 9 to 9.5 sec. This could be caused by a mountain-root system similar to that of the Rocky Mountains.

Figure 3 shows the reduced travel-time data for the 1- and 10-ton shots of the ECOOE southern profile and the CHASE III and VII shots. Also included are data from the 1962 North Carolina shots. The consistency of the smaller residuals at a distance of 400 to 450 km, obtained at a station located in the Piedmont, is indicative of a thinner upper crust in that region. The

larger residuals at 550 to 650 km again reflect a thicker crustal section under the Appalachians.

Figure 4 is a composite of the travel-time residuals of the ECOOE 5- and 10-ton shots of the northern and southern profiles and the CHASE III, IV, and VII shots. A smaller scale is used to show the data obtained at distances between 1000 and 2000 km. Of particular interest in this figure is the apparent increase in P velocity to 8.5 km/sec at distances beyond 1100 km. A similar velocity increase at comparable distances was noted by other participants of the EARLY RISE program. This increase in velocity also coincides with a substantial increase in particle-velocity amplitude beyond 1100 km. Across the Michigan Basin the first arrival amplitudes were approximately 10 to 15 dB larger than the signals recorded at The University of Michigan's Botanical Garden Station, located near the southeast rim of the Basin ($\Delta \cong 975$ km).

Figure 5 shows the reduced travel times for the shots fired by the USGS in Lake Superior during the month of October 1964. A series of 1-, 2-, 3-, 6-, and 10-ton shots were fired at several locations. A crustal velocity of 6.17 km/sec and an upper-mantle velocity of 8.29 km/sec were obtained.

Figure 6 shows the reduced travel-time data for the EARLY RISE shots which were fired in Lake Superior and were recorded along the same line as shown in the previous figures. Many of the same recording sites were reoccupied. An upper-mantle velocity of 8.0 was used for these computations. A crustal velocity of 6.3 km/sec verifies the results shown in the figure 5. However, a clear 7.7-km lower crustal layer is indicated. (This is illustrated in figure 9.) Considerable scatter can be seen in the $P_n$ arrivals beyond 700 km. This is due primarily to the high background noise caused by increased cultural activity across southeastern Michigan, Ohio, and West Virginia. The evidence for an Appalachian mountain-root system is not as convincing on this profile. The mountains are 1175 to 1360 km from the shot point. The residuals on the western half of the mountains are smaller than those on the eastern half and those located just to the east of the mountains. However, the scatter of data closer to the shot point would cause one to think this anomaly could also be due to scattering. For the shots recorded at distances of 1500 to 1650 km, the first arrival could not be read accurately. At our most distant station the signal amplitude was larger even though the background noise was high.

The vertical-component recordings for four shots recorded at the same station are shown in figure 7. These four individual shots were dubbed onto one magnetic tape, taking into account zero times of the shots and slight differences in shot-point locations. The times were aligned so that each shot is within ±2 msec at the time of the first arrival. The maximum deviation over the entire record is ±5 msec. The vertical components shown here were filtered on playback with a 1- to 4-cps passband, which greatly improved the signal-to-noise ratio. The summed vertical, longitudinal, and transverse components for the four shots are also shown on figure 7. At this distance it can be seen that most of the arrival energy of the first compressional wave is recorded on the vertical component. The summing technique (type of array processing) gives

5

a 12-dB improvement in signal-to-noise ratio of the first arrival. Such techniques allow a more accurate determination of the first arrival times.

Figure 8 shows a composite of a section of the EARLY RISE recordings. The details at this scale are difficult to see; however the increased noise beyond 750 km is quite evident. One feature particularly interesting is the small-amplitude first arrivals at stations located at 160 to 275 km. This is illustrated more clearly in figure 9. At these distances the high-gain channels were deliberately used to permit overrecording; this provided better record gains for the low-amplitude first arrivals. (Figure 9 shows the first arrivals on the vertical component with the overrecorded later phases omitted. The records are adjusted so that arrivals with a velocity of 7.7 km/sec are aligned vertically on this section. The first three traces are on the 6.2-km/sec branch of the travel-time curve. If the record gains used in the field had been set so the later phases would not be overrecorded, this early arrival would have been very difficult if not impossible to detect.)

The travel-time data for this reversed profile are shown in table I.

## 1.3. ATTENUATION DATA

Figure 10 shows the first-arrival vertical component of ground displacement versus distance for the EARLY RISE data. Although there is considerable scatter, an average slope proportional to the inverse 3/2 power of the distance fits these data reasonably well. On the reversed profile, the ECOOE shots, the 1962 North Carolina data, and the CHASE shots fit more closely to a curve whose slope is proportional to the inverse third power of the distance. Furthermore, size for size, the shots fired in Lake Superior were more efficient in coupling energy into seismic waves than the shots fired in the Atlantic Ocean. The signal amplitudes for the Lake Superior shots ranged from 6 to 18 dB, or a factor of 2 to 8 larger for shots recorded at comparable distances. A partial explanation for this phenomenon may be that the shots in Lake Superior (especially in EARLY RISE) were fired at an optimum depth for signal enhancement due to reinforcement by the bubble pulse (optimum depth between 593 and 607 ft). However, it is believed that Lake Superior is an anomalous region for the coupling of seismic energy.

For a clearer interpretation of the attenuation data, isoparticle-velocity maps were prepared from the spectral data of the first compressional-wave arrival at each station. This technique showed that many of the fluctuations in spectral data persisted from shot to shot where the station remained fixed and from station to station when the shot point was fixed. These trends are difficult to follow when the individual spectral curves are examined. Figure 11 shows the vertical component of the ground-particle velocity for the first three cycles of the first compressional-wave arrival recorded on the EARLY RISE shots. The gap in data from 270 to 380 km occurs where the profile crosses Lake Michigan. The dots correspond to data points (the values have been omitted for sake of clarity). The particle-velocity amplitudes are contoured at 6-dB (factor of 2) intervals. These amplitudes correspond to true ground motion. All instrument responses have been corrected out. The spectra of the EARLY RISE shots are strongly

6

TABLE I. TRAVEL-TIME DATA

| | ECOOE (Southern Profile) | ECOOE (Northern Profile) | EARLY RISE |
|---|---|---|---|
| $v_0/h_1$ | 2.0/0.48 | 2.0/1.7 | 4.75/2.9 |
| $v_1/h_2$ | 6.0/28.7 | 6.0/25.8 | 6.2/22.5 |
| $v_2/h_3$ | ----- | ----- | 7.7/25.0 |
| $v_n/h_4$ | 8.2/70.0 | 8.2 | 8.3/21.6 |
| $v$ | 8.5 | ----- | 8.4 |
| Total crustal thickness | 29.2 km | 27.5 km | 50.4 km |
| Depth to high-velocity upper-mantle layer | 99.2 | ----- | 72 km |

7

influenced by the bubble-pulse frequency and the reverberation of the sound waves between the lake bottom and the surface. The bubble-pulse frequency is approximately 2 cps and would be in phase at that water depth. The organ-pipe frequencies for constructive and destructive interference are:

| Constructive | Destructive |
|---|---|
| $f_0$ = 2 cps | $2f_0$ = 4 cps |
| $3f_0$ = 6 cps | $4f_0$ = 8 cps |
| $5f_0$ = 10 cps | $6f_0$ = 12 cps |
| $7f_0$ = 14 cps | |

A rather remarkable correlation with these frequencies can be seen on the particle-velocity highs and lows shown on figure 11. The major peaks along the entire profile occur at approximately 2 and 5-6 cps. The former coincides with the bubble-pulse frequency and the fundamental organ-pipe mode, and the latter coincides with the third harmonic. A high can also be correlated with the fifth harmonic. The particle-velocity lows correlate quite well with the second and fourth harmonic, where destructive interference should occur. A particle-velocity low at all frequencies can be seen near the crossover point (160 km) of the 6.2- and the 7.7-km/sec branches of the travel-time curves. Unfortunately, the $P_n$ cross overpoint falls near that section of Lake Michigan where we have no data. One other predominant feature should be pointed out. A pronounced particle-velocity high occurs at approximately 885 km. This same high was observed at a group of four stations located near Anna, Ohio, at the same distance. The latter area is 150 km southwest of the main profile and is an area where small earthquakes have been recorded in the past. The cause of this large amplitude is not known. It may possibly correlate with a cusp in the travel-time curves. Its buildup is observable at seven stations.

Figure 12 shows the isoparticle-velocity map for the 1963 Lake Superior south line. This profile was obtained by two crews which changed sites each night. They recorded nine different shots along a line perpendicular to the center of the line of shot points. The particle-velocity highs correlated well with the bubble-pulse and organ-pipe modes that would cause reinforcement. The predominant signal along the entire profile is 4 cps, which correlates with the first odd harmonic of the organ-pipe mode. The sharp decrease in particle-velocity amplitude at 160 to 170 km correlates with the data on the EARLY RISE shot made at the crossover point on the travel-time curve from the 6.2 to 7.7 branch.

In order to investigate the attenuation of a seismic wave, using the type of data shown in this figure, an equation of the type

$$A_{ij} = A_{oj} X_i^{-n} e^{-\alpha f_j X_i} \tag{1}$$

was employed. It accounts for geometrical spreading (n) and for the absorption ($\alpha$) of the seismic waves. $A_{ij}$ represents the particle-velocity amplitude for the i-th shot and the j-th frequency;

8

$A_{oj}$ represents a constant assumed to be independent of distance but dependent on the j-th frequency; $X_i$ represents the distance from the seismometer to the i-th shot; and $f_j$ is the j-th frequency.

To derive equation 1, we begin with

$$A_{ij} = A_{ij}^O X_i^{-n} e^{-\alpha f_j X_i} \quad \begin{cases} i = 1, 2, \ldots, M \\ j = 1, 2, \ldots, N \end{cases}$$

and solve for $A_{ij}^O$:

$$A_{ij}^O = A_{ij} X_i^n e^{\alpha f_j X_j}$$

If we now let

$$A_{ij}^O = \frac{1}{M} \sum_{i=1}^{M} A_{ij}^O$$

where M is the number of shots, we have arrived at equation 1. Hence, for each $A_{ij}$, an $A_{ij}^O$ was calculated so that a matrix was obtained whose rows $(1, 2, \ldots, j, \ldots, N)$ represent the N different frequencies, and whose columns $(1, 2, \ldots, i, \ldots, M)$ represent the M different shot distances (in increasing order). An average $A_{oj}$ was found for each frequency across the distances, by summing the $A_{ij}^O$ for a constant j and dividing the sums by M. There are then N $A_{oj}$'s, which are in a respect independent of distance. This matrix represents an average spectrum $(A_{oj})$.

Using equation 1 and the computed $A_{oj}$, new $A_{ij}$'s (designated $A_{ij}'$) are computed, which in general will be different from the original $A_{ij}$'s.

The $A_{ij}$'s and $A_{ij}'$'s are converted from particle-velocity amplitudes to the equivalent amplitudes in decibels by using the following relationship:

$$A_{ij} \text{ (in./sec)} = 20 \log_{10} \frac{A_{ij}(dB)}{0.01}$$

A matrix of residuals $(S_{ij})$ are formed where

$$S_{ij} = A_{ij} - A_{ij}'$$

The $S_{ij}$'s are plotted on a graph whose abscissa is the distance and whose ordinate is the frequency.

Figure 13 shows the summation of the residuals versus the absorption coefficient for values of n, the geometrical spreading factor, ranging from 0 to 3. The best fit for n and $\alpha$ would correspond to the residual minimum. For this profile a value of $n = 2.5$ and $\alpha = 7 \times 10^{-4}$ yields the smallest residual. However, a value of $n = 1.5$ would correspond to geometrical spreading due to head-wave propagation (perhaps a value of $n = 2$ for these distances). For $n = 1.5$, $\alpha = 1 \times 10^{-3}$ gives the best fit.

9

In the foregoing discussion we have assumed that the absorption would be proportional to the first power of the frequency. In order to examine this assumption, residuals were computed for $f^P$, where P ranged from 0 to 2. The results are shown in figure 14. It can be seen that $f^{1/2}$ gives the smallest residual at $\alpha = 5 \times 10^{-3}$ for n = 1.0.

Figure 15 shows the reduced isoparticle-velocity residuals after the geometrical spreading factor and absorption factor have been removed. In this case values of n = 1.0 and $\alpha = 1.5 \times 10^{-3}$ were used. This does not give the best fit from the data shown in figure 14, but it does show the technique that can be used to help study the anomalous amplitudes encountered along the profile. The bubble-pulse frequency is indicated by the X's on this graph.

Figure 16 shows the particle-velocity amplitudes for the 150-km site on the ECOOE southern profile. Most of those data fall on the 6.0 branch of the travel-time curve. The relief or change in signal here is less than that of the EARLY RISE or 1963 Lake Superior data. One reason is that the bubble-pulse frequency is below 1.5 cps for all but the two furthest shots and the fundamental organ-pipe frequency is above 10 cps for all but the last three shots. The particle-velocity highs for the last three shots correlate with the bubble-pulse frequency and the fundamental-mode organ-pipe frequency.

Figure 17 shows the sum of the residuals versus $\alpha$ for n ranging from 0.5 to 3 for the ECOOE southern-profile 150-km site. The best fit is for n = 0.5 and $\alpha = 6 \times 10^{-4}$. For n = 1.5, $\alpha = 1 \times 10^{-4}$ would give the best fit.

From data of this type it is anticipated that we will be able to determine the mathematical expression that will be best suited to predict signal amplitudes versus distance and to make accurate determinations of crustal and mantle Q's.

10
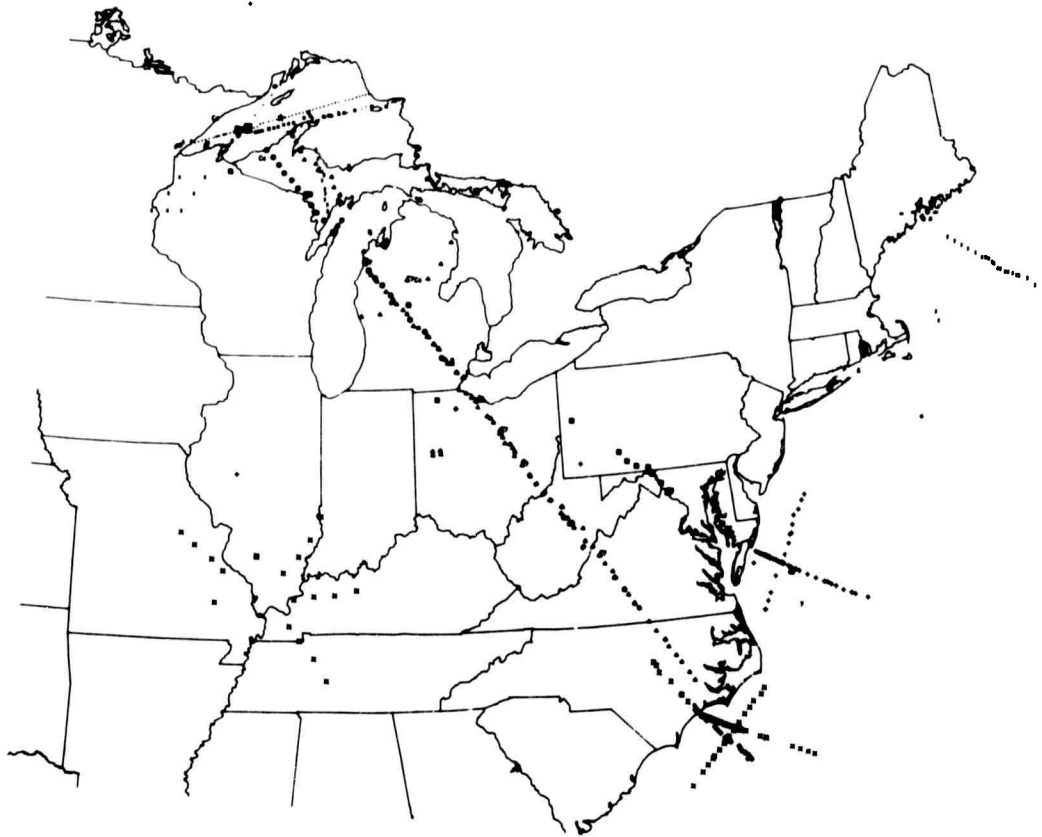
FIGURE 1. MAP OF SHOT POINTS AND RECORDING STATIONS
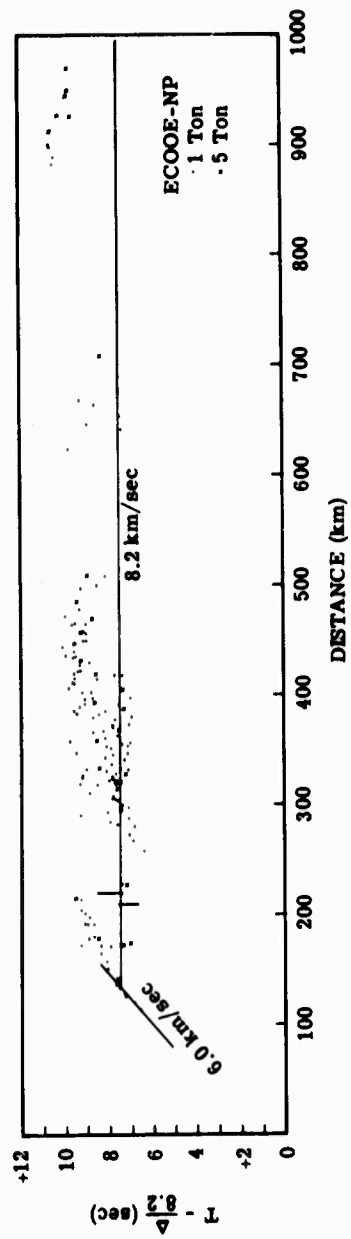
FIGURE 2. COMPOSITE TRAVEL-TIME RESIDUALS FOR ECOOE NORTHERN PROFILE

12
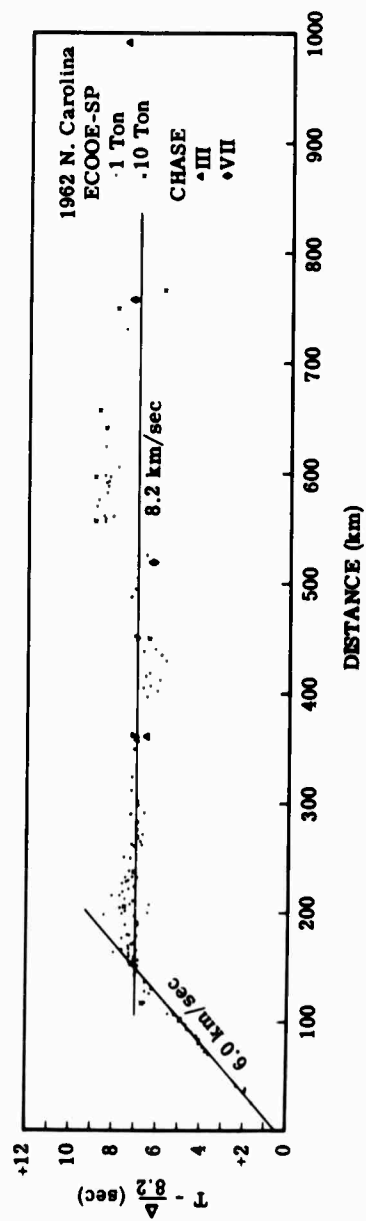
FIGURE 3. COMPOSITE TRAVEL-TIME RESIDUALS FOR 1962 NORTH CAROLINA EXPERI-
MENT, ECOOE SOUTHERN PROFILE, AND CHASE III AND VII
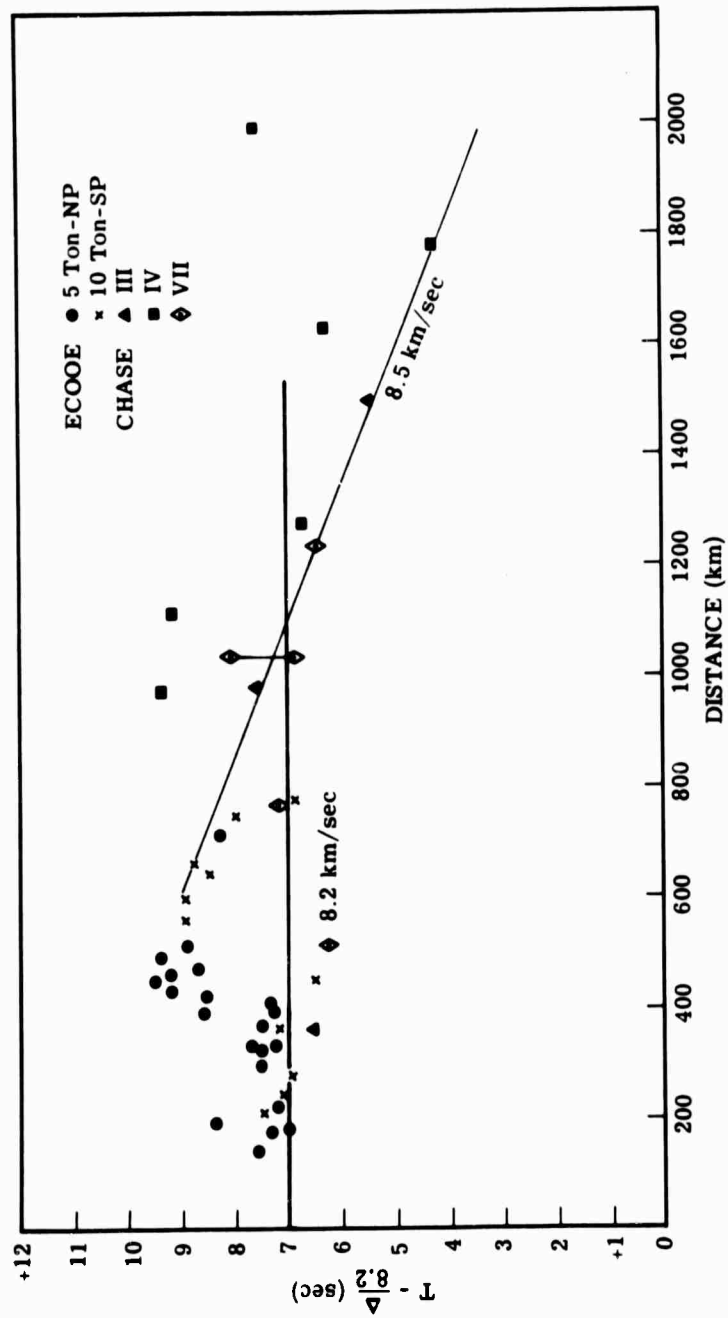
FIGURE 4. COMPOSITE TRAVEL-TIME RESIDUALS FOR 5- AND 10-TON SHOTS OF THE
ECOOE SERIES AND CHASE III, IV, AND VII

14
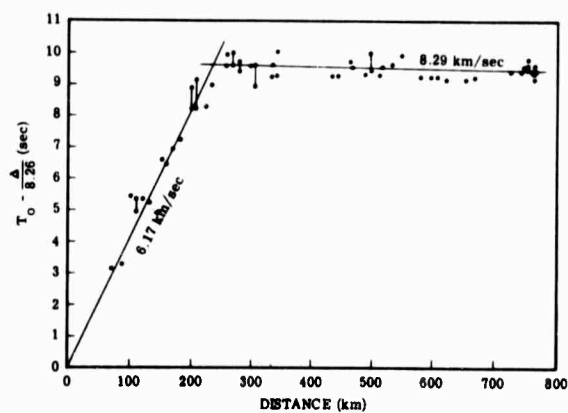
FIGURE 5.  TRAVEL-TIME RESIDUALS FOR OCTOBER 1964 LAKE SUPERIOR EXPERIMENT
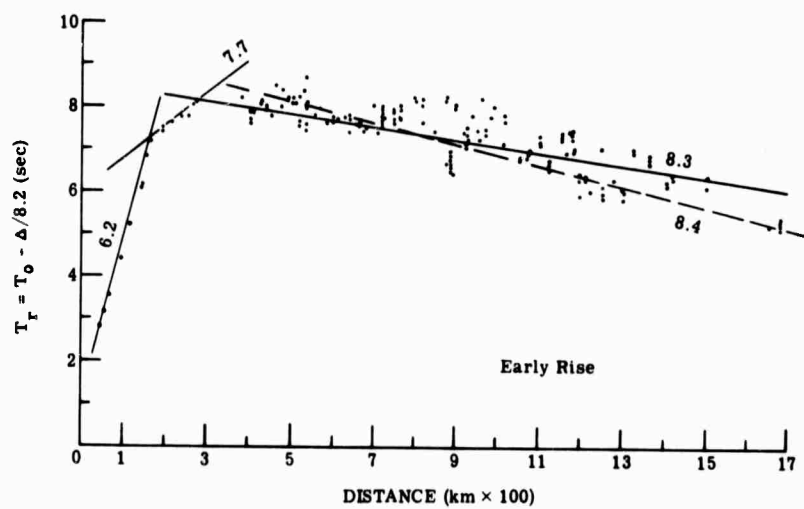


FIGURE 6.  TRAVEL-TIME RESIDUALS FOR THE 1966 EARLY RISE EXPERIMENT

15

Early Rise
Δ = 1681.9 km
1.0-4.0 cps

ΣL

ΣT

ΣV

ΣV + ΣL

Vert. - Shot 18

Vert. - Shot 19

Vert. - Shot 20

Vert. - Shot 21

3 min.　10　20　30　40　50　4 min.　10　20　30　40　50　5 min.
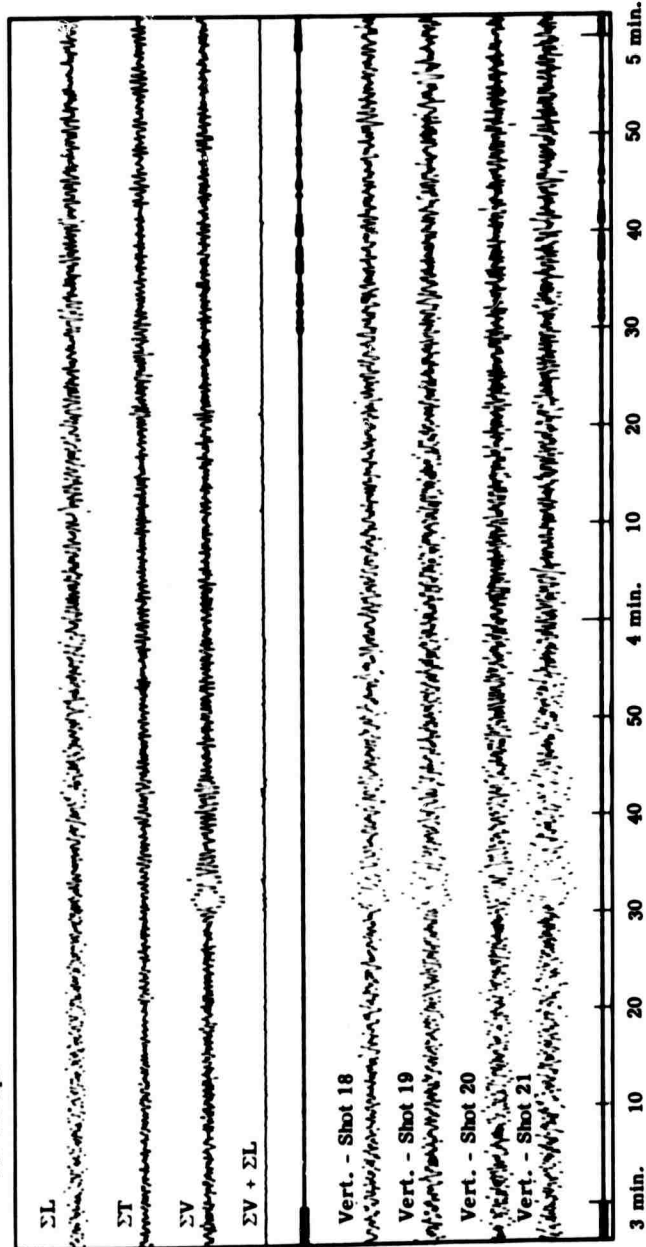
FIGURE 7. EARLY RISE SHOTS 18-21 RECORDED AT POTTER'S HILL, NORTH CAROLINA

16
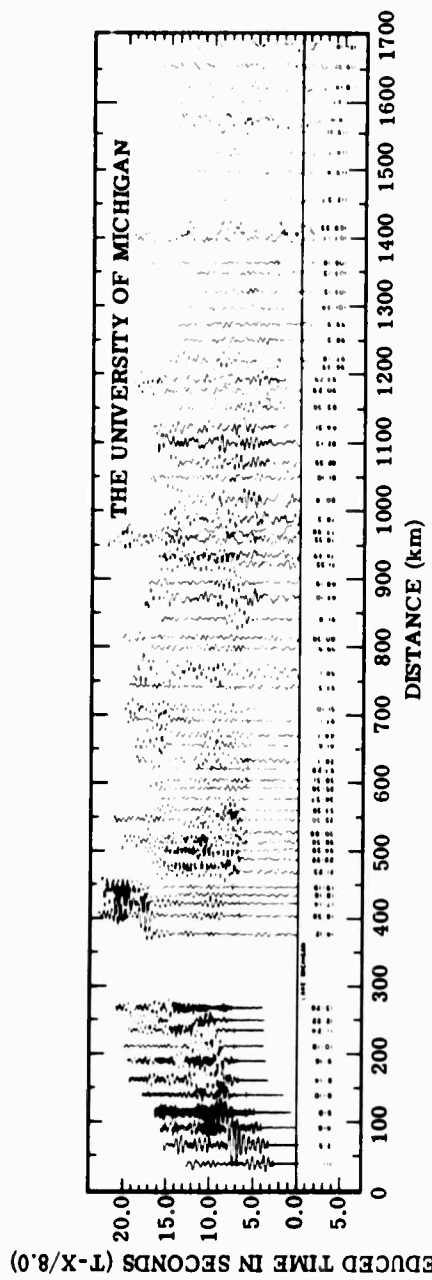
FIGURE 8. COMPOSITE OF A SECTION OF THE EARLY RISE RECORDINGS

17
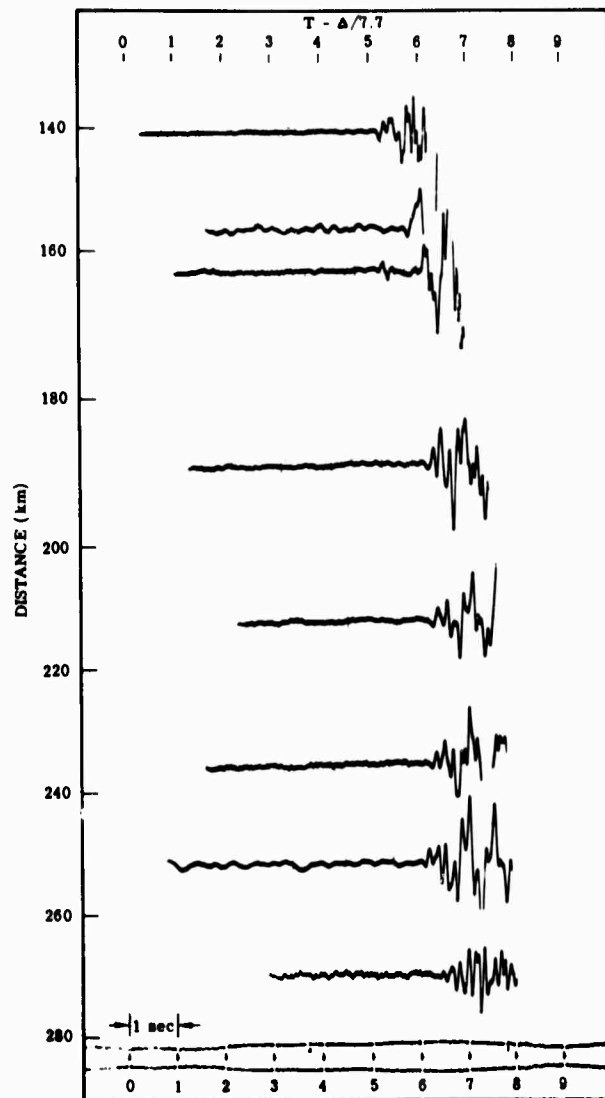
FIGURE 9. COMPOSITE SEISMOGRAM SHOWING ARRIVAL
AT 7.7 km/sec, EARLY RISE

18
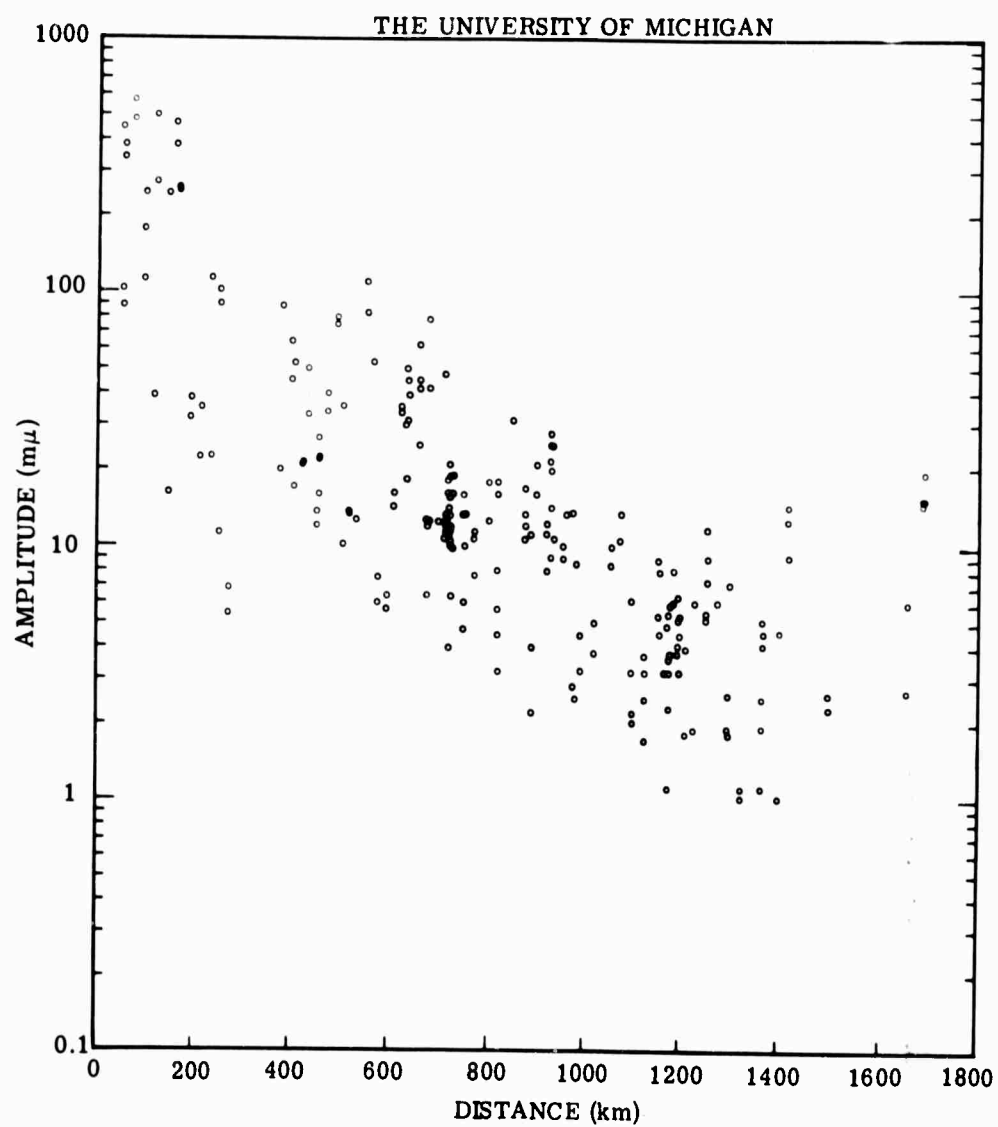
FIGURE 10. GROUND DISPLACEMENT VS. DISTANCE FOR PROJECT EARLY RISE

19
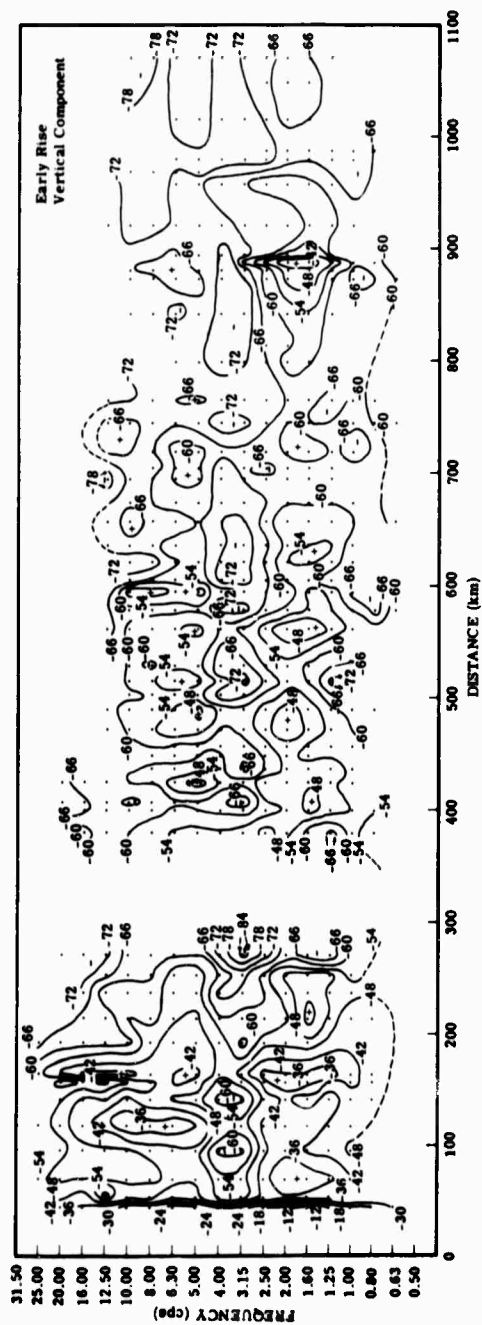
FIGURE 11.  ISOPARTICLE-VELOCITY MAP OF FIRST P-WAVE ARRIVAL FOR EARLY RISE

20
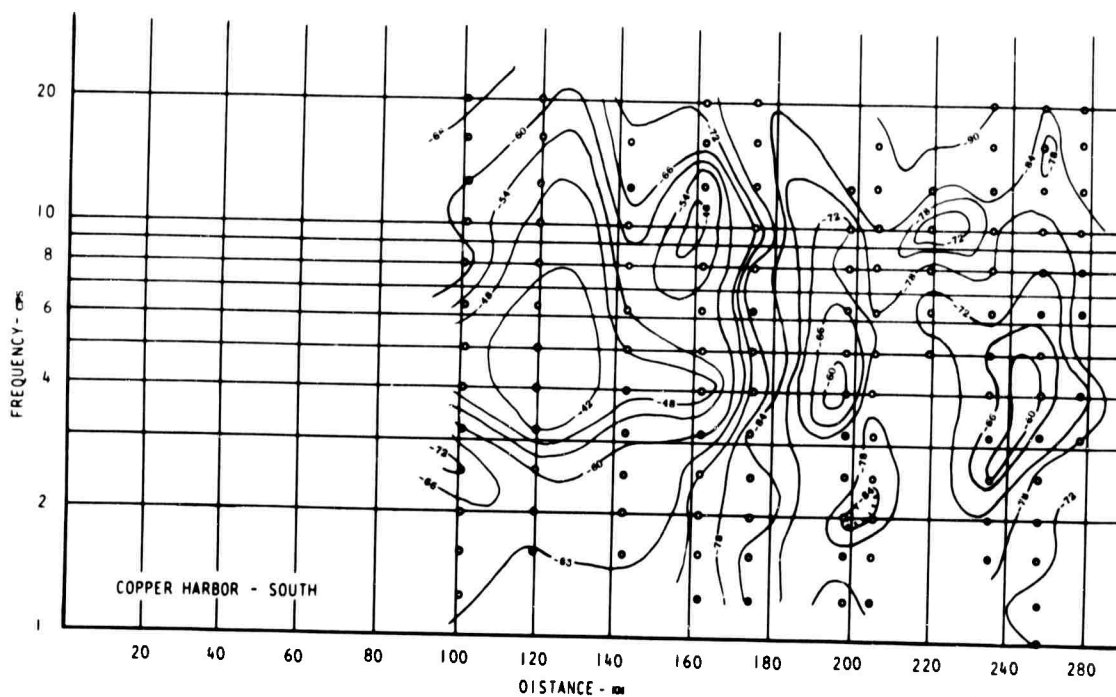
FIGURE 12.   ISOPARTICLE-VELOCITY MAP OF THE FIRST P-WAVE ARRIVAL FOR 1963
LAKE SUPERIOR SOUTH LINE
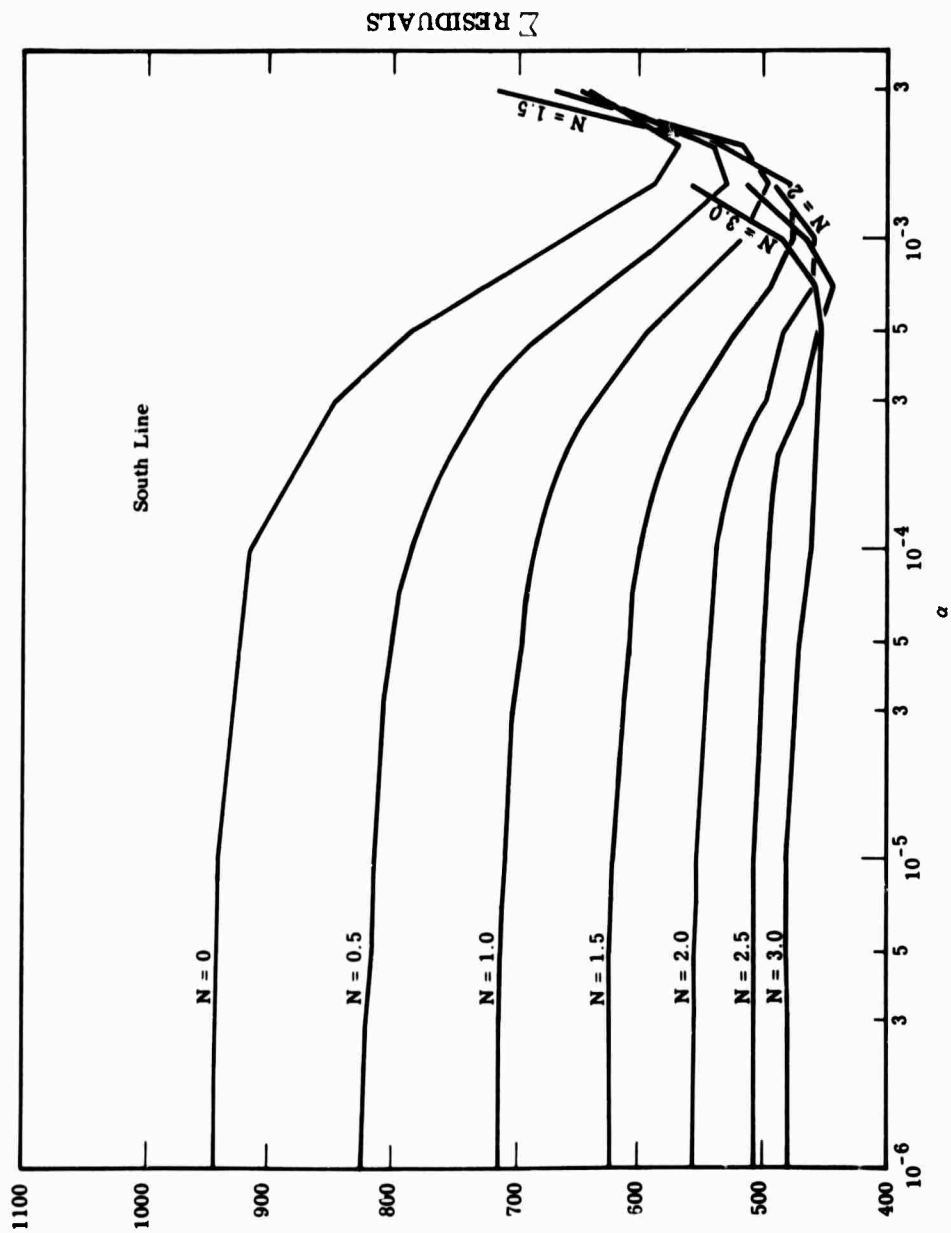
FIGURE 13.  SUMMATION OF RESIDUALS VS. α FOR 1963  LAKE SUPERIOR SOUTH LINE

22

FIGURE 14. SUMMATION OF RESIDUALS VS. $\alpha$ FOR 1963 LAKE SUPERIOR SOUTH LINE;
N = 1.0

23
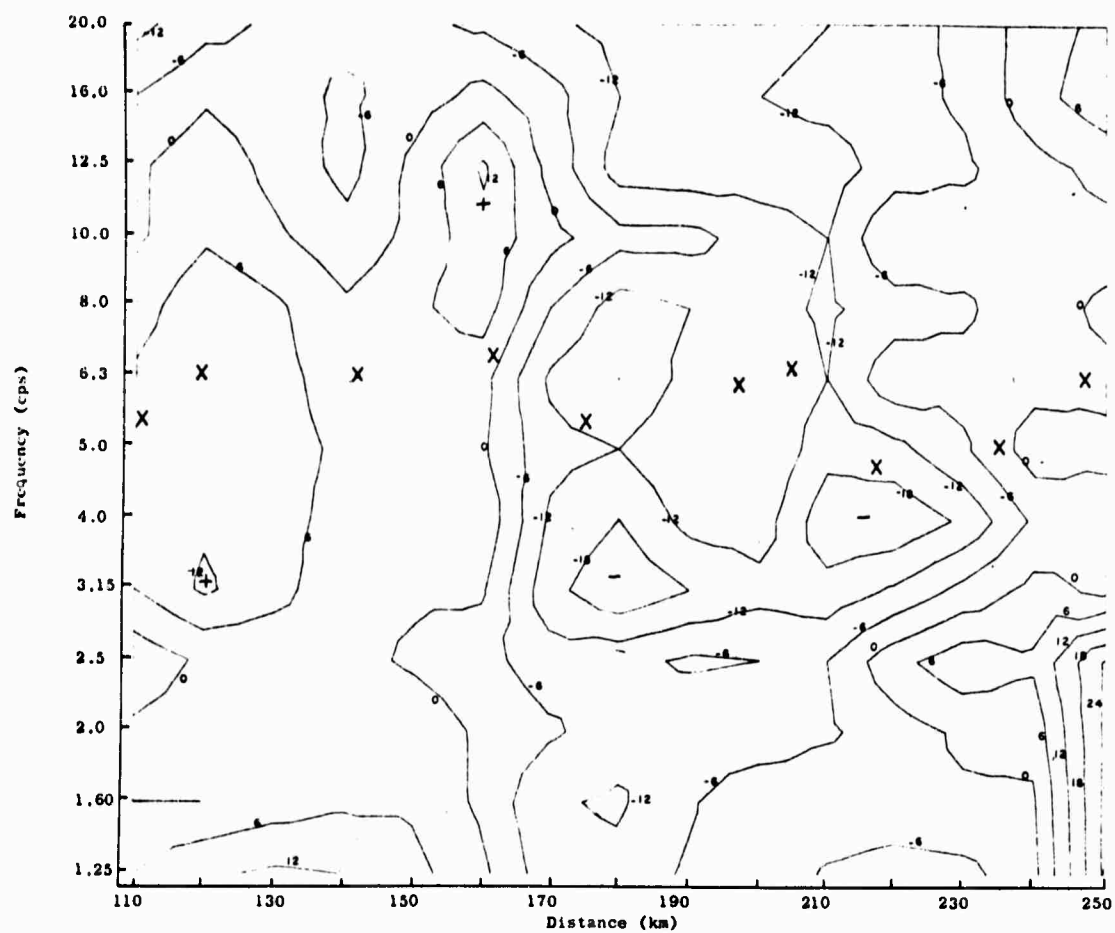
FIGURE 15. PARTICLE VELOCITY RESIDUAL MAP, SOUTH LINE, LAKE SUPERIOR, JULY 1963,
$\alpha = 1.5 \times 10^{-3}$; n = 1.0
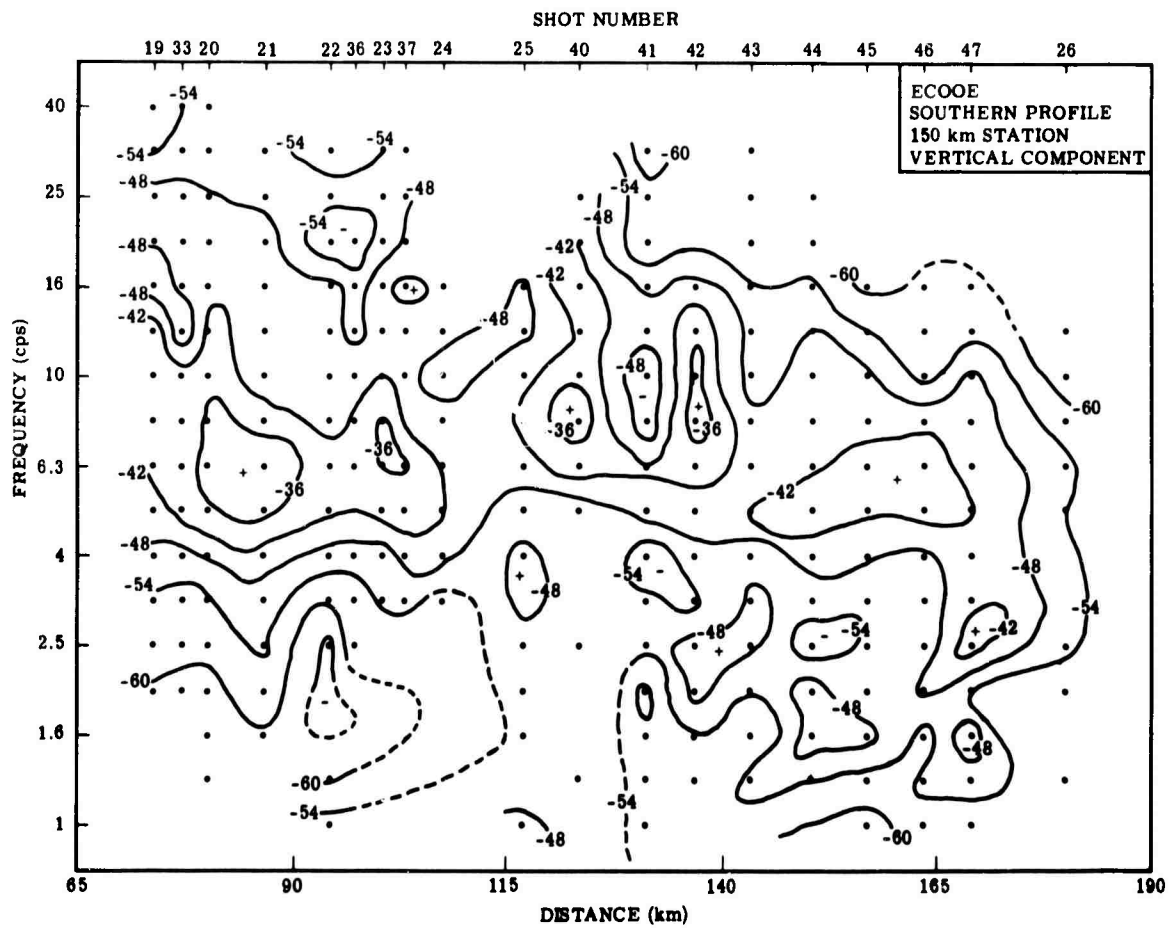
FIGURE 16. ISOPARTICLE-VELOCITY MAP FOR FIRST P-WAVE ARRIVALS ON ECOOE
150-KM STATION ON SOUTHERN PROFILE
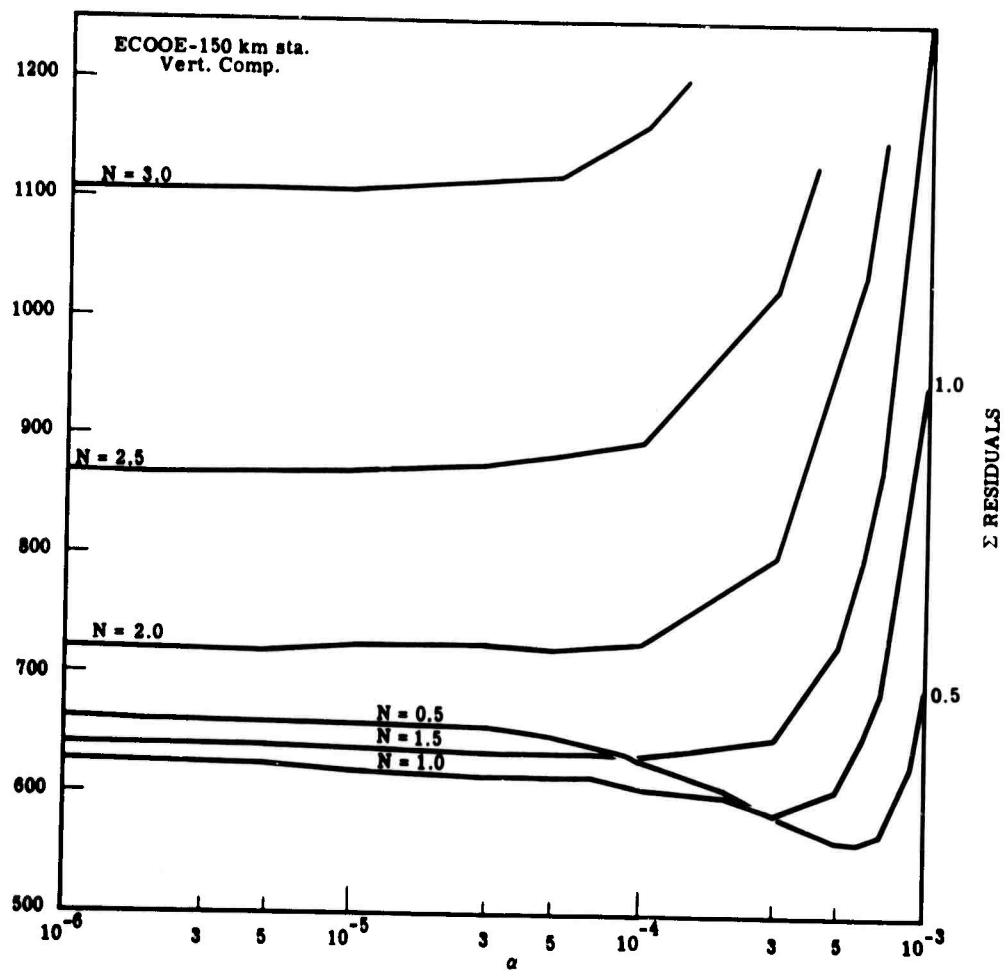
FIGURE 17.  SUMMATION OF RESIDUALS VS. $\alpha$ FOR ECOOE SOUTHERN PROFILE
150-KM SITE

## THEORETICAL STUDIES IN ELASTIC-WAVE SCATTERING
### I. K. McIvor

To evaluate the effect of nonhomogeneities on the propagation of elastic waves, a continuing analytical investigation of elastic-wave scattering is being carried out. The initial investigation considered the scattering of plane waves in an elastic media by elliptical obstacles or cavities. A general solution was obtained, and illustrative numerical calculations were made for the degenerate case of a slit. It was found that the scattered field exhibited strong directional selectivity.

The major area of investigation at present is the scattering effect of small imperfections at the interface of elastic media. A perturbation method has been developed which is applicable to a wide range of problems. A specific solution has been obtained for the scattering of body waves by surface irregularities on a half space. The solution is expressed as a surface convolution of a known kernel with the imperfection. Thus numerical results for arbitrary imperfection shapes are readily obtained. In the present problem the surface displacements and total scattered energy have been computed for a number of different scatterers.

It is anticipated that the method will be applied to other problems of seismic interest, including the scattering of surface waves and the effect of imperfections on the reflection and transmission of body waves at a material discontinuity. Finally, an effort needs to be made to compare the theoretical results with actual seismic data to see if major structural imperfections can account for observed anomalies.

# LAKE-BOTTOM SEISMIC-NOISE STUDIES
## D. E. Willis

The series of underwater shot programs conducted in Lake Superior during 1963, 1964, and 1966 ranged in size from 1 to 10 tons of high explosives and have been detected at distances in excess of 2000 km. Underwater shots provide a very efficient coupling mechanism for seismic waves. The increased signal level for a properly tamped water shot can generate ground displacements that are a factor of 20 or more larger than equivalent shots fired in rock. The seismic signals generated by these shots in Lake Superior were found to have larger amplitudes (up to a factor of 8) at comparable distances than equivalent shots fired in the Atlantic or the Pacific Oceans.

Since the Lake Superior area was found to have an efficient coupling of seismic energy it was deemed highly desirable to ascertain whether or not there would be any reciprocity in the recording of teleseismic events; that is, whether seismic sources generated at teleseismic distances in other areas would cause larger ground displacements in the vicinity of the shot points in Lake Superior where particularly good coupling was observed. The EARLY RISE shot point, located near shot point 51 (see fig. 18) of the 1963 Lake Superior Experiment, was chosen as the site to conduct these tests.

Figure 18 is a map of the portion of Lake Superior that is of interest to this study. The shot points of the 1963 experiment are shown along with the water depths and contours of the water depth [2]. The contours are not in complete agreement with the indicated water depths. The Obenhoff land station located on the Keweenaw Peninsula is also indicated. The dashed line shown in this figure is the location of a sub-bottom seismic reflection profile made by Dr. R. J. Wold of the University of Wisconsin. This profile is shown in figure 19.

A pronounced structural high having approximately 350 ft of relief was disclosed by this profile. This feature is approximately 9 km in diameter and has a more or less flat plateau on its southeast flank. This plateau was chosen as the site to install a lake-bottom seismograph since the lake-bottom sediments appeared to be thin. The plateau has a water depth of approximately 530 to 550 ft.

The lake-bottom seismograph was obtained on loan from Professor Hugh Bradner of the Institute of Geophysics and Planetary Physics, University of California at San Diego, LaJolla. A detailed description of this unit may be found in reference 3. The package consists of matched three-component equiangular seismometers, amplifiers, power supplies, a tape recorder, and an electronic clock. The following modifications of these units were made to adapt them to the purposes of this investigation. The high-frequency response of the amplifiers and tape recorder was extended to 17 cps; the seismometers were tuned to a natural period of 1.1 sec with 0.7

critical damping; the power supply was modified to provide 13 days of recording time; the interval clock was modified to provide 1-min and 1-hr time pulses with a 10-cps carrier lasting 1 sec and 1 min, respectively.

The response of the seismometers used in the lake-bottom unit and the Obenhoff land station is shown in figure 20. The land-station seismometers (matched three-component) have approximately 14 dB more output at 1 to 2 cps and 22 dB at 10 cps than the lake-bottom unit.

The lake-bottom seismograph was tethered in the manner shown in figure 21. Nylon line was used to secure the seismograph, anchor, and buoy. Ample slack was used to reduce the buoy motion being transmitted through the nylon line to the seismograph.

The package was emplaced with the assistance of the USCG cutter WOODRUSH and was operated for three periods during June-August 1967. The times of operation are shown in table II.

Very high background noise was encountered on all three drops. Long periods of high background noise were found that can be correlated with meteorological conditions and with wave action. This is illustrated in table III and figures 22 and 23. Table III shows the average seismometer output voltage from the three-component lake-bottom seismograph and the three-component land-station seismograph at 4-hr intervals for the time period 0800, June 7, to 0800, June 10, 1967. Also shown is the wind velocity and direction as well as the lake-wave height and direction. No correction has been made for the difference in seismometer response for the land and lake-bottom seismographs, so this difference should be kept in mind when responses at the two stations are compared.

The periods of peak wind velocity and lake-wave height which occur between 0800 and 1600 on June 8 correlate quite closely with the maximum signal levels at both the land station and the lake-bottom unit. The three lake-bottom seismometers have nearly identical outputs at any given time. The land-station seismograph displays the lowest levels on the vertical component and the highest on the east-west component. The prevailing winds could account for the latter.

Figure 22 shows the variation in average background noise at 15-min intervals for the time period 1000, June 7, to 2330, June 8. The land-station vertical-component seismometer output is shown. Since the output of the land-station seismometers is 14 to 22 dB greater than that of the lake-bottom seismometers, it can be seen that the difference in noise levels between these two sites is quite large.

This slow buildup and decay of background noise was found to be rather common during the three drop periods. The maximum levels persisted for intervals ranging from several hours to several days.

Spectral analysis of the average background noise for four 1-hr intervals is shown in figure 23. These time intervals include the quiet period prior to the buildup, the maximum noise levels, and the intermediate levels on buildup and decay. Several significant features can be seen in

29

### TABLE II.  OPERATION OF
### LAKE-BOTTOM UNIT

First Drop
|          |          |
|----------|----------|
| 6/5/67   | 1943 EDT |
| 6/15/67  | 1630 EDT |

Second Drop
|          |          |
|----------|----------|
| 7/5/67   | 1900 EDT |
| 7/17/67  | 2226 EDT |

Third Drop
|          |          |
|----------|----------|
| 8/7/67   | 2045 EDT |
| 8/15/67  | 0310 EDT |

TABLE III. DATA FOR THE THREE DROPS

| Date | Time | Wind Direction | Wind Velocity (knots) | Lake Waves Direction | Lake Waves Height (ft) | Background Noise* Lake Bottom (3 components) | | | Land N-S | Land E-W | Vert. |
|------|------|-----------|---------|-----------|--------|-----|-----|-----|-----|-----|-----|
| 6/7/67 | 08 | NNE | 08 | | calm | -81 | -80 | -81 | -89 | -86 | -92 |
| | 12 | NE | 12 | NE | 1 | -76 | -77 | -77 | -86 | -77 | -88 |
| | 16 | NE | 06 | | calm | -75 | -76 | -76 | -79 | -72 | -78 |
| | 20 | E | 04 | | calm | -73 | -74 | -73 | -84 | -77 | -88 |
| 6/8/67 | 00 | SSE | 07 | | calm | -74 | -73 | -74 | -89 | -81 | -87 |
| | 04 | E | 10 | E | 1 | -70 | -70 | -70 | -83 | -75 | -87 |
| | 08 | SE | 17 | SE | 2 | -65 | -66.5 | -66 | -76 | -72 | -76 |
| | 12 | ESE | 15 | ESE | 3 | -64 | -64.5 | -64 | -78 | -74 | -78 |
| | 16 | W | 14 | W | 3 | -61 | -61 | -61 | -80 | -74 | -80 |
| | 20 | SW | 10 | SW | 2 | -64 | -65 | -65 | -85 | -77 | -85 |
| 6/9/67 | 00 | SW | 10 | SW | 1 | -68 | -68.5 | -69 | -89 | -84 | -87 |
| | 04 | WSW | 10 | WSW | 1 | -71 | -71 | -71 | -89 | -87 | -90 |
| | 08 | W | 10 | W | 2 | -70 | -70 | -70 | -88 | -79 | -89 |
| | 12 | WNW | 10 | W | 2 | -70 | -71 | -70 | -86 | -78 | -88 |
| | 16 | NW | 10 | NW | 1 | -75 | -75 | -75 | -86 | -82 | -90 |
| | 20 | NW | 04 | | calm | -77 | -77 | -77 | -89 | -88 | -92 |
| 6/10/67 | 00 | SSE | 06 | | calm | -80 | -80 | -80 | -92 | -90 | -94 |
| | 04 | SE | 05 | | calm | -83 | -82 | -83 | -91 | -90 | -90 |
| | 08 | SE | 06 | | calm | -83 | -82 | -83 | -91 | -90 | -94 |

*Seismometer output voltage with reference of 1 V.

31

this figure. The minimum and maximum velocities at 1 cps are indicated for both stations. The peak ground displacement ranges from 33 to 1500 m$\mu$ on the lake bottom and from 0.4 to 10 m$\mu$ on the land station. These stations are located approximately 60 km apart. It can be seen that the lake-bottom noise is nearly two orders of magnitude higher than that at the land station. The lake-bottom noise has three prominent peaks occurring at 0.5, 1.0, and 5.0 cps, with a pronounced minimum at 2 to 3 cps. The land station has a pronounced peak at 2.5 cps with a minor peak at 5 cps and a pronounced minimum at 1.6 to 2 cps. The peak on the land station is centered near the minimum on the lake-bottom station.

Figure 24 shows a similar buildup and decay in background noise on the third drop. The shapes of the spectral curves are similar to those of figure 23, with the higher frequency peak occurring at 4 cps. A second lake-bottom seismograph was also used on the third drop. This unit was a free-fall untethered station that was used to compare background noise with the tethered unit. No significant difference in signal level was observed.

Shown in figures 25 and 26 are seismograms obtained with both the Lake Superior units during the Buffalo, New York, earthquake (magnitude 3.9) of June 13, 1967. The bottom trace of figure 25 is the summed output of the three lake-bottom seismometers and would correspond to a true vertical component. Two significant facts can be observed on these seismograms. Taking into account the difference in response of the seismometer and the difference in record gains, the ground amplitudes on the lake-bottom unit are larger than those on the land-station seismograph. The time duration of the event on the lake-bottom unit is a factor of 2 or more longer than that of the land station. Spectral analyses of this event show a pronounced peak at 1 cps. The important factor in comparing these two recordings is the signal-to-noise ratio as a function of frequency. This is shown in figure 27. It can be seen from this figure that, although the signal level on the land station was lower than that on the lake-bottom station, the maximum signal-to-noise ratio was obtained by the land station.

For comparison purposes the signal-to-noise ratios for this same event recorded at The University of Michigan's Botanical Garden intermediate-depth well station and at the surface in Ann Arbor, Michigan, are also shown in figure 27. The superiority of the well recording is quite evident in spite of the fact that the well is not of the proper depth (the surface reflection interference for the seismometers at a depth of 1206 feet causes a minimum at 2-2.5 cps).

The Denver earthquake (magnitude 5.3) of August 9, 1967, was also recorded by the lake-bottom and the land seismograph units. The spectral curves and signal-to-noise ratios were similar to those of the Buffalo earthquake. Pronounced peaks at 1 cps were observed on the lake-bottom unit.

Numerous quarry shots were also recorded by both units. A striking feature of these local events was a very sharp spectral peak at 4 cps on the lake-bottom unit. The seismograms display a pronounced ringing effect that were very dissimilar to the land-station recordings.

32

The lake-bottom units and the land-station equipment have been used to record teleseismic and local events at the Geophysics Laboratory (near Ypsilanti, Michigan). Absolute signal levels and the spectral data from both units are in very good agreement. Hence, if the lake-bottom seismograph "plant" is not introducing a resonance effect, the pronounced ringing and sharp spectral peaks for local events probably can be correlated with some sort of water reverberation effect. Teleseismic events with peak signals below 4 cps do not produce this sharp ringing effect. However, the distant events recorded on the lake-bottom unit persist for longer time intervals than on the land station.

It can be concluded that the operation of lake bottom seismographs in Lake Superior would not be desirable on a permanent basis because of the poor signal-to-noise ratios compared with those of land stations, because of long periods of very high background noise, and because of the ringing character of the seismograms.
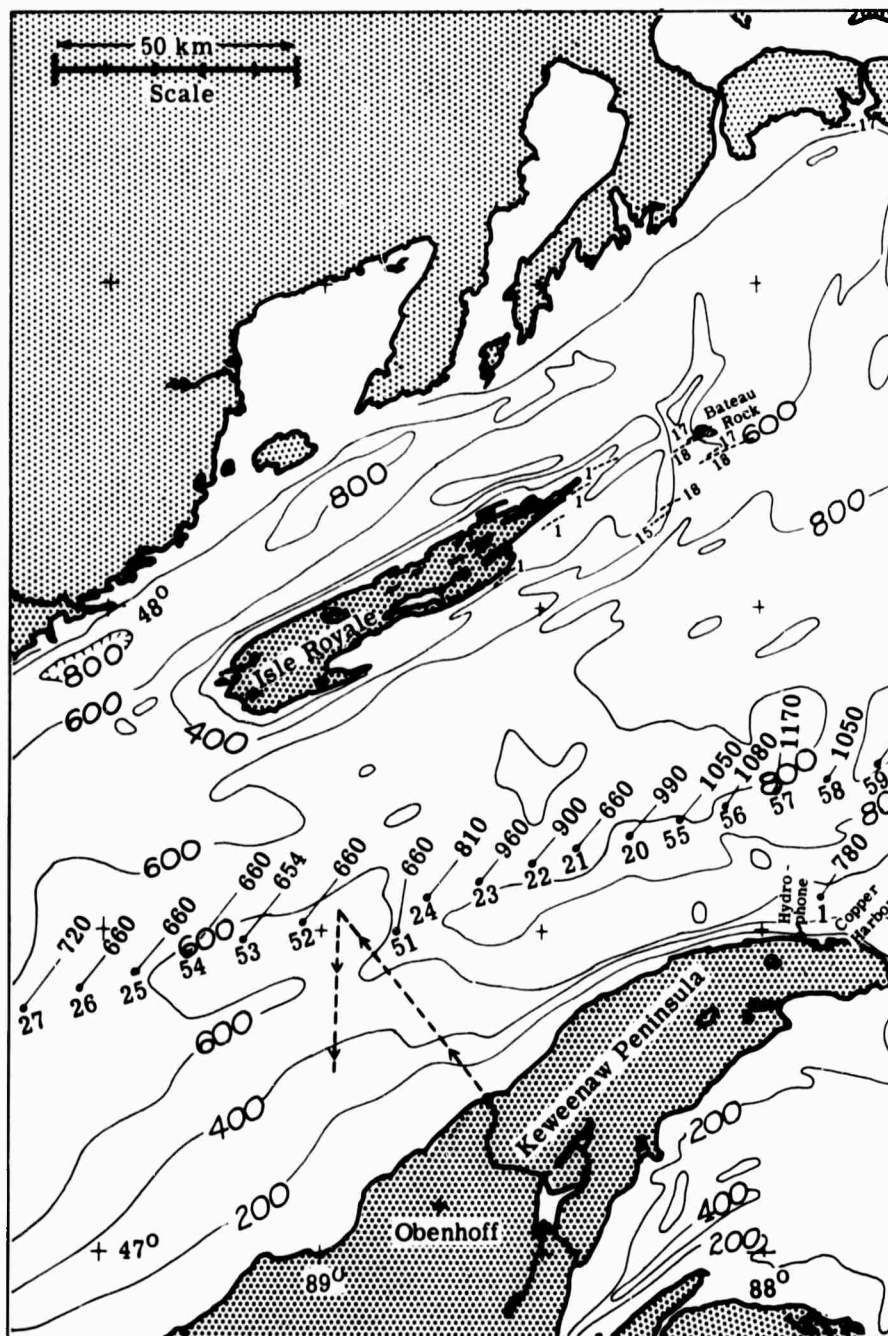
FIGURE 18. LOCATION MAP OF LAKE-BOTTOM AND LAND-STATION SEISMO-
GRAPHS, LAKE SUPERIOR

34
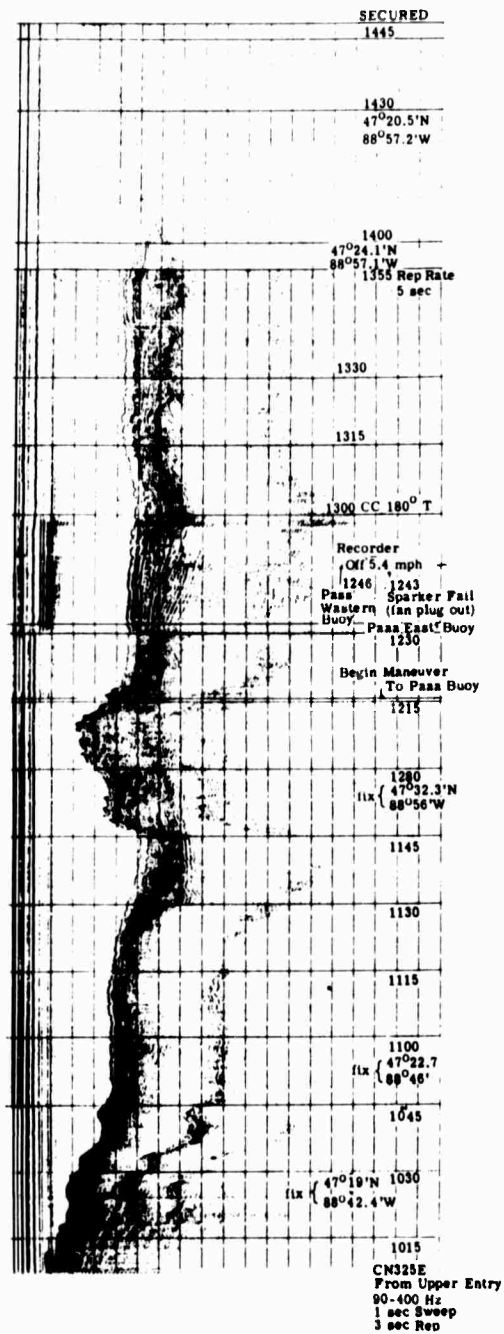
FIGURE 19. SUB-BOTTOM SEISMIC REFLEC-
TION PROFILE, LAKE SUPERIOR (COURTESY
OF DR. R. J. WOLD)
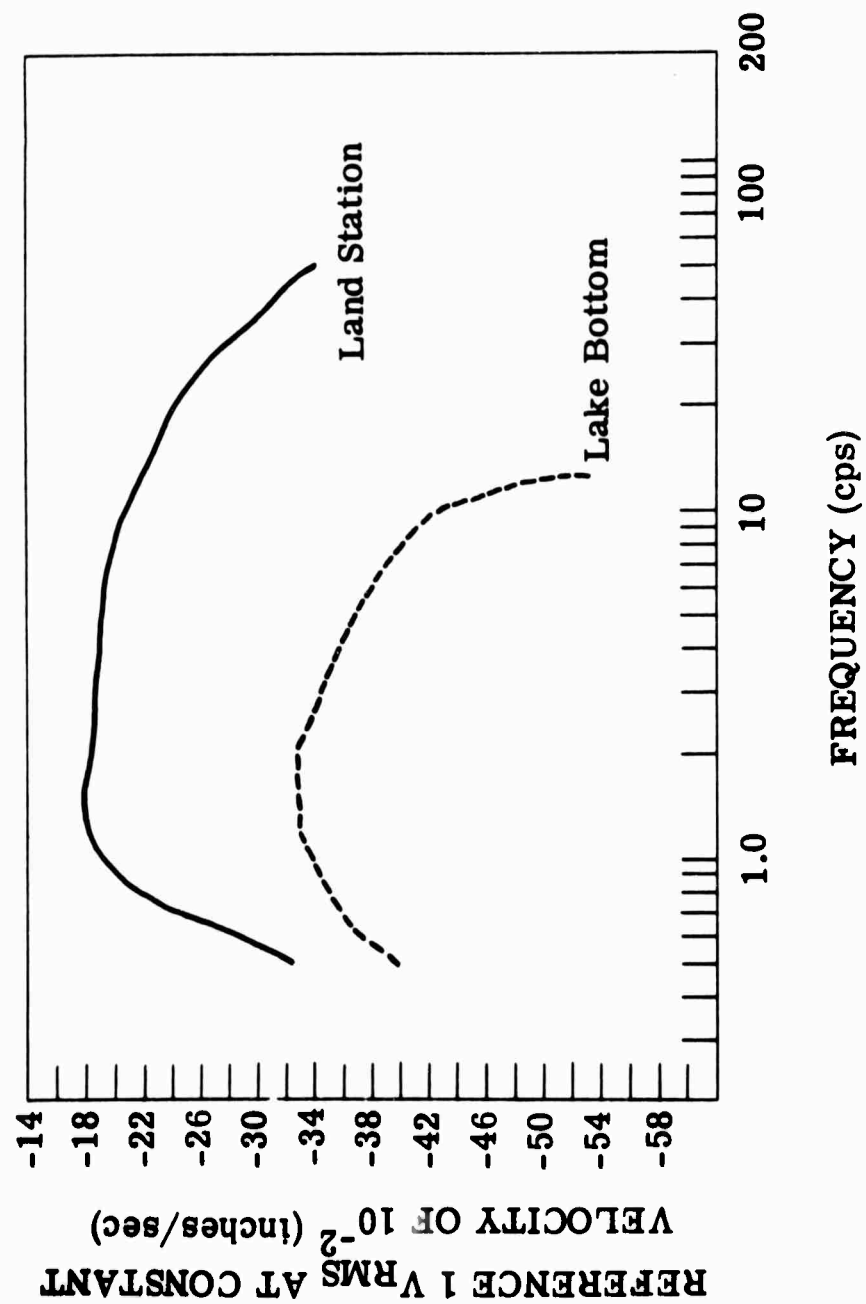
FIGURE 20. LAKE BOTTOM AND LAND SEISMOMETER RESPONSE CURVES, LAKE SUPERIOR

36
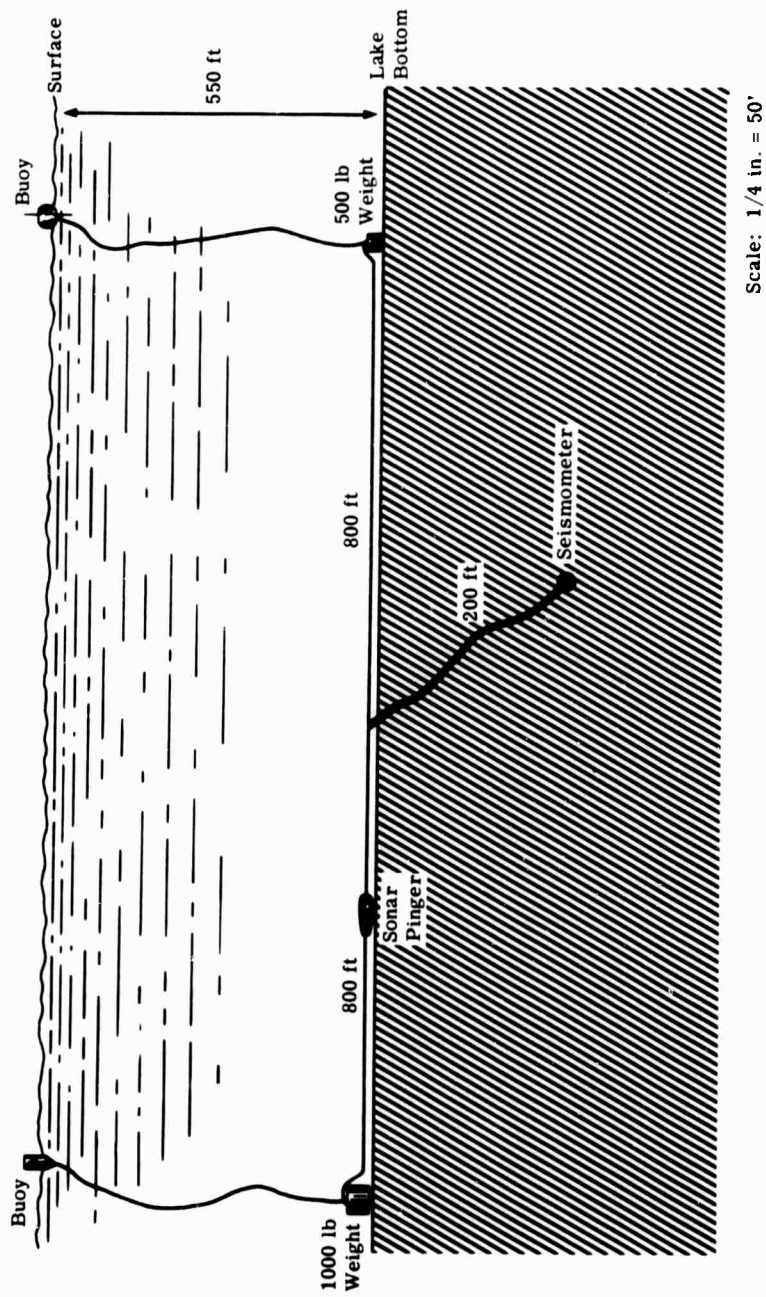
FIGURE 21. DIAGRAM OF LAKE-BOTTOM SEISMOGRAPH DEPLOYMENT, LAKE SUPERIOR

Scale: 1/4 in. = 50'

37
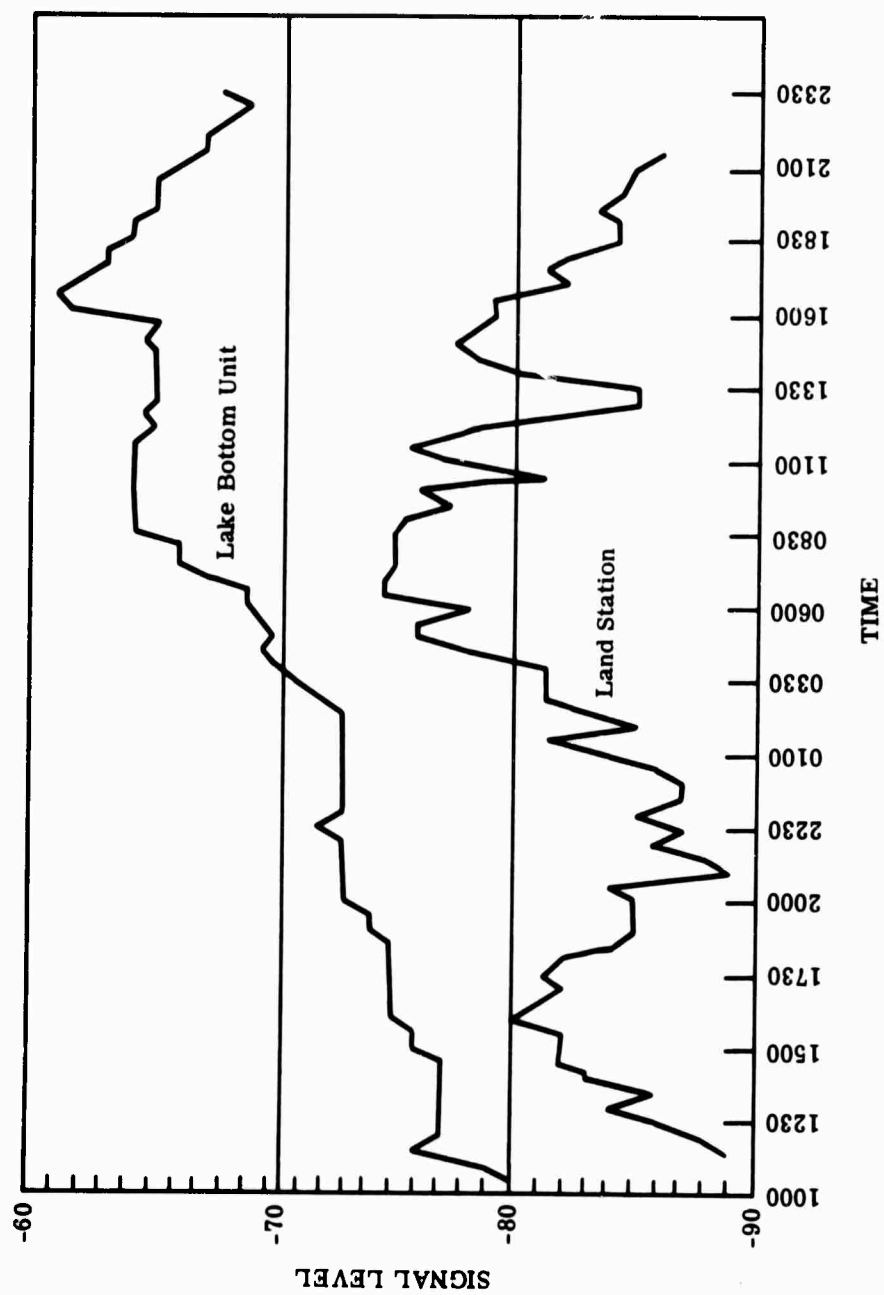
FIGURE 22. COMPARISON OF SEISMIC BACKGROUND NOISE AT 15-min INTERVALS FOR
JUNE 7 AND 8, 1967, LAKE SUPERIOR LAND STATION

38
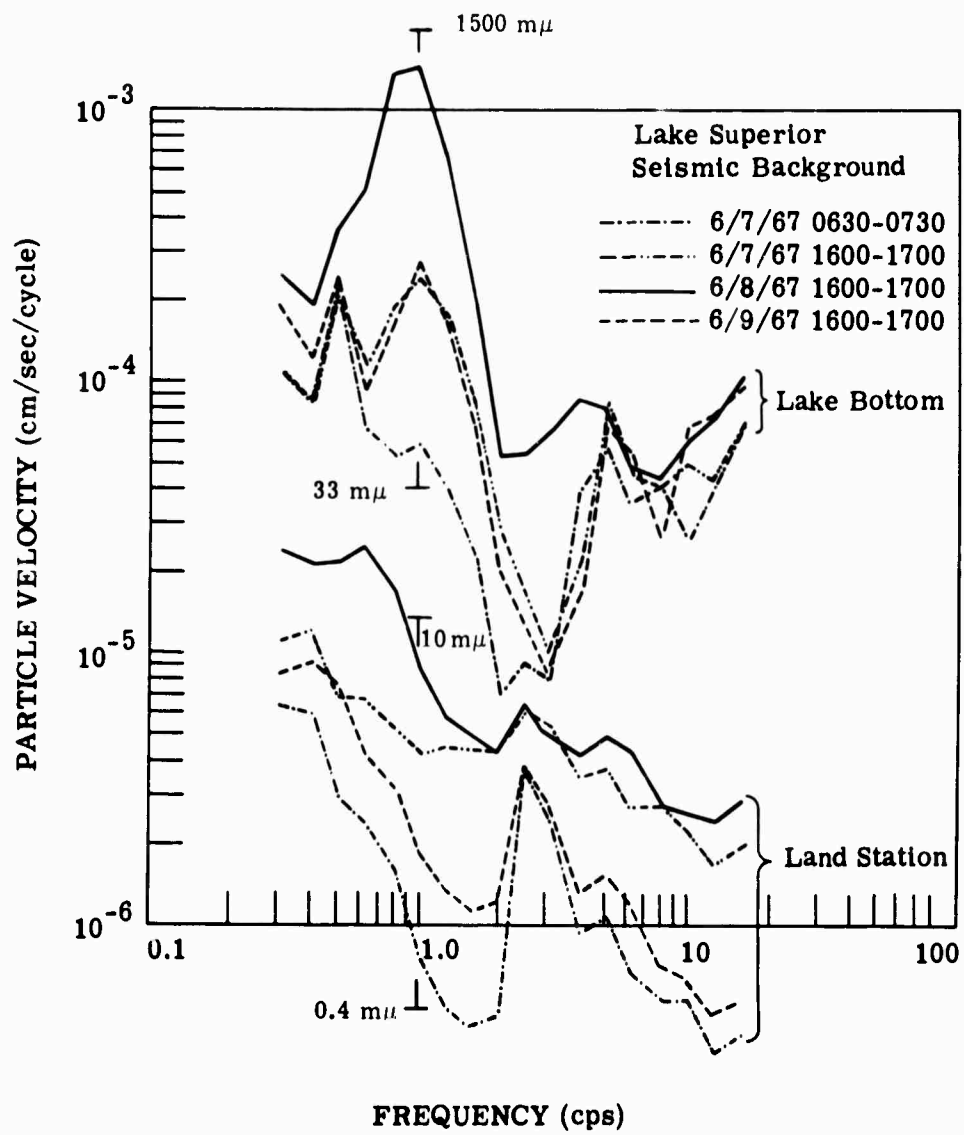
FIGURE 23. COMPARISON OF SEISMIC BACKGROUND NOISE FOR FOUR INTERVALS,
BOTH LAKE SUPERIOR STATIONS
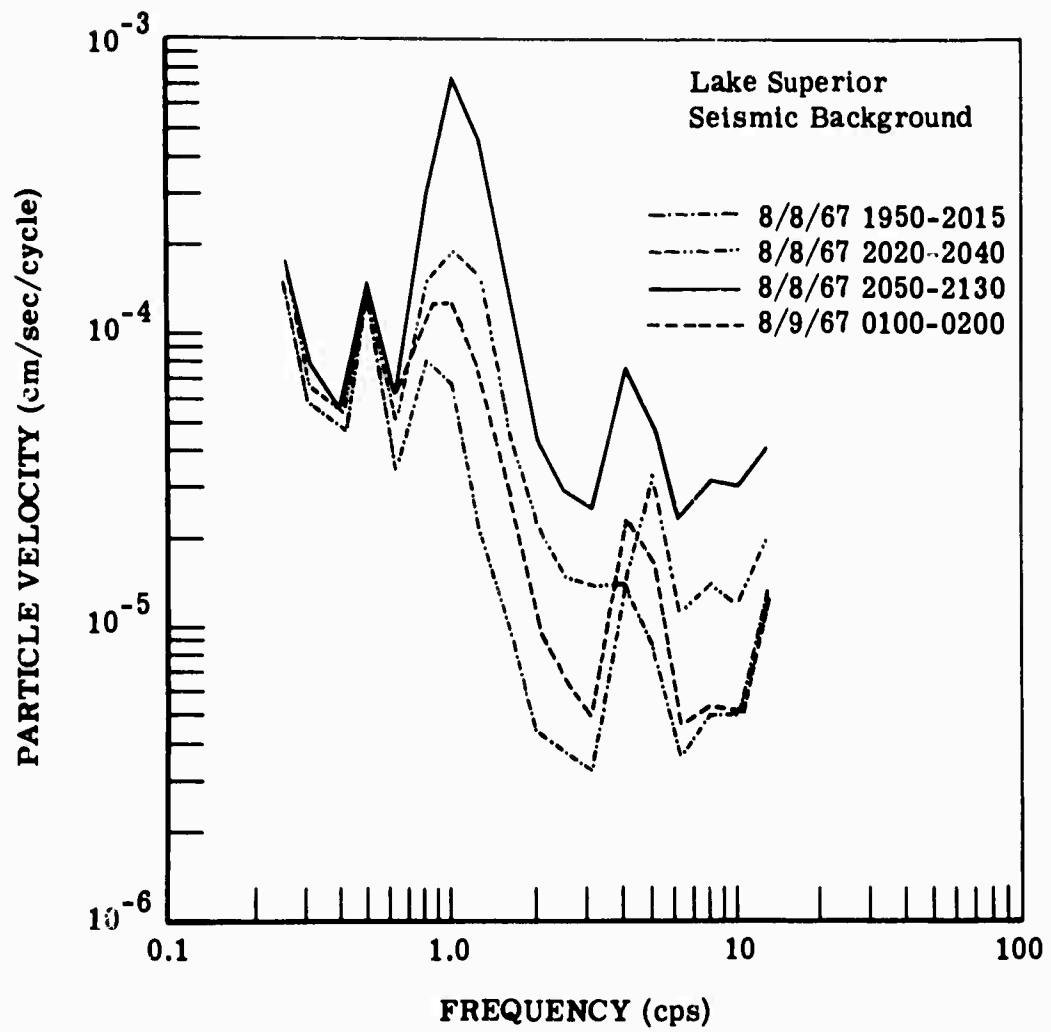
FIGURE 24. COMPARISON OF SEISMIC BACKGROUND NOISE, THIRD LAKE SUPERIOR
DROP

40

63 dB

Lake Bottom Seismograph
Buffalo, N. Y. Earthquake
6/13/67
Δ = 986 km

61 dB

63 dB

59 dB

P

1 min
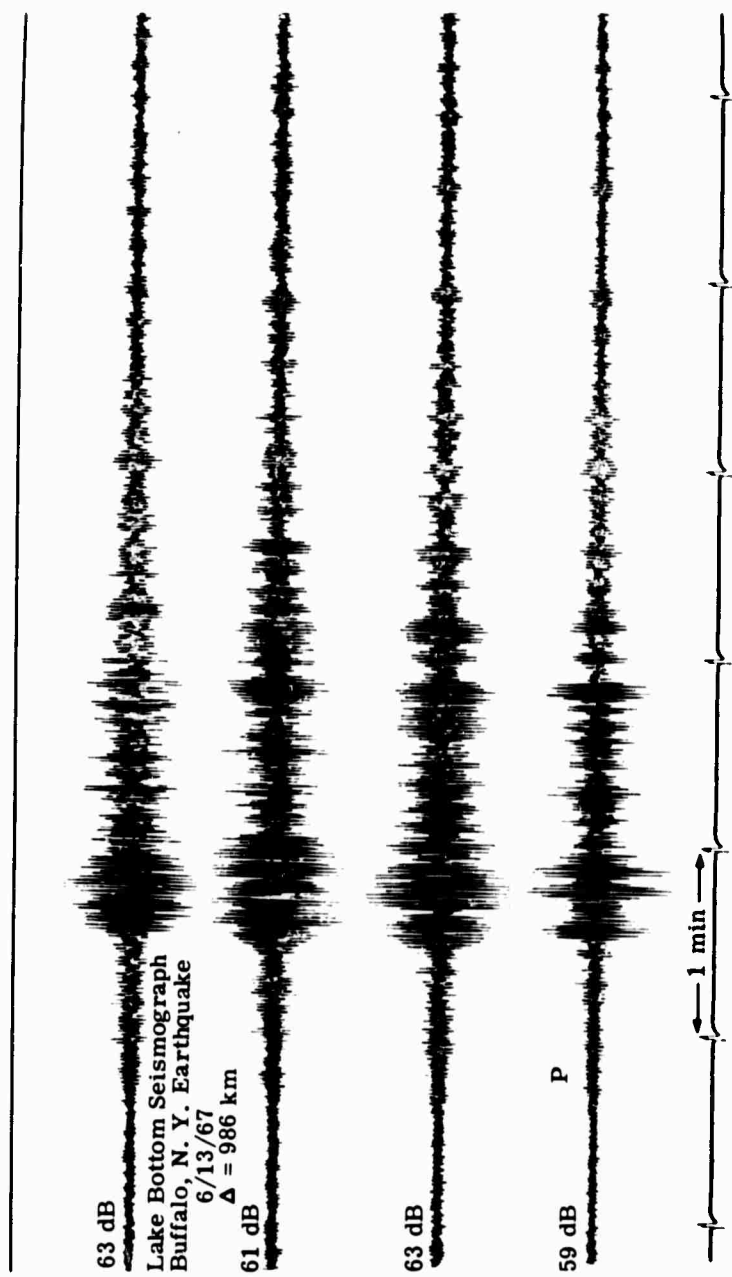
FIGURE 25.  BUFFALO, NEW YORK, EARTHQUAKE RECORDED ON LAKE-BOTTOM SEISMOGRAPH

54 dB
N-S
Land Station.
Buffalo, N. Y. Earthquake
6/13/67
$\Delta$ = 986 km

54 dB
E-W

P

60 dB
Vert.

← 1 min →
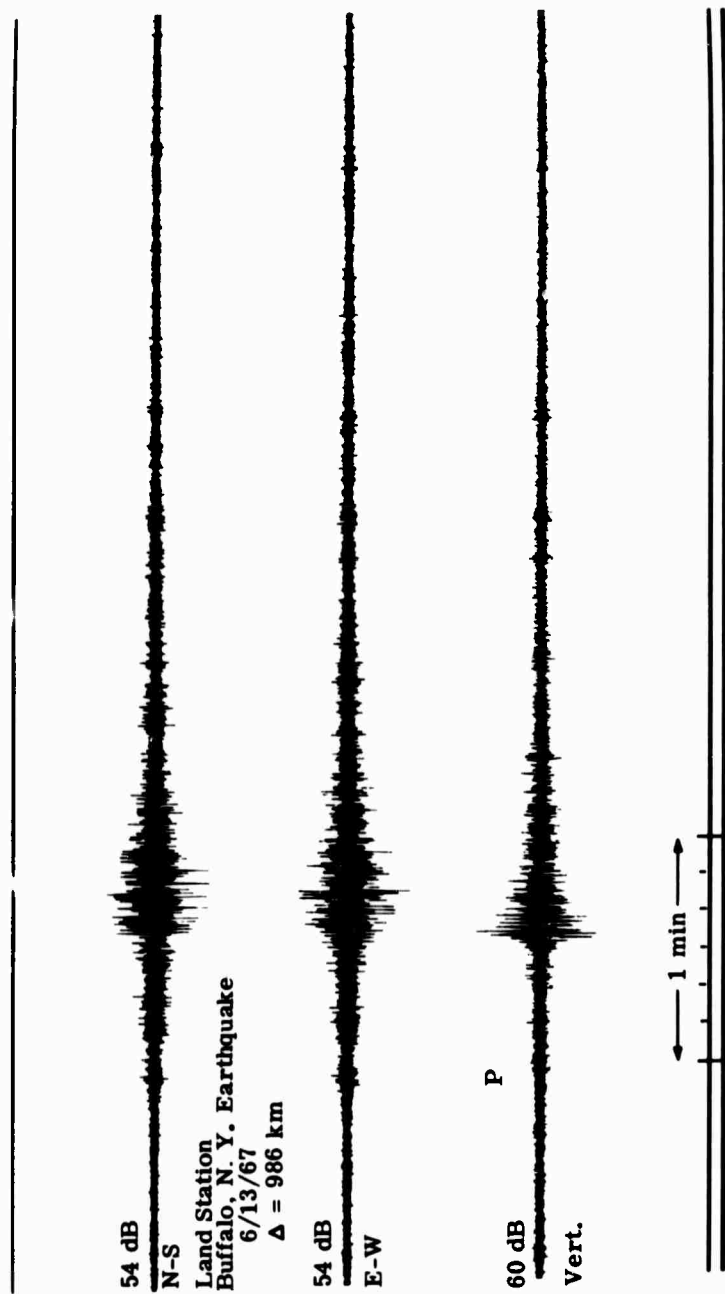
FIGURE 26. BUFFALO, NEW YORK, EARTHQUAKE RECORDED ON LAND-STATION SEISMO-
GRAPH

42
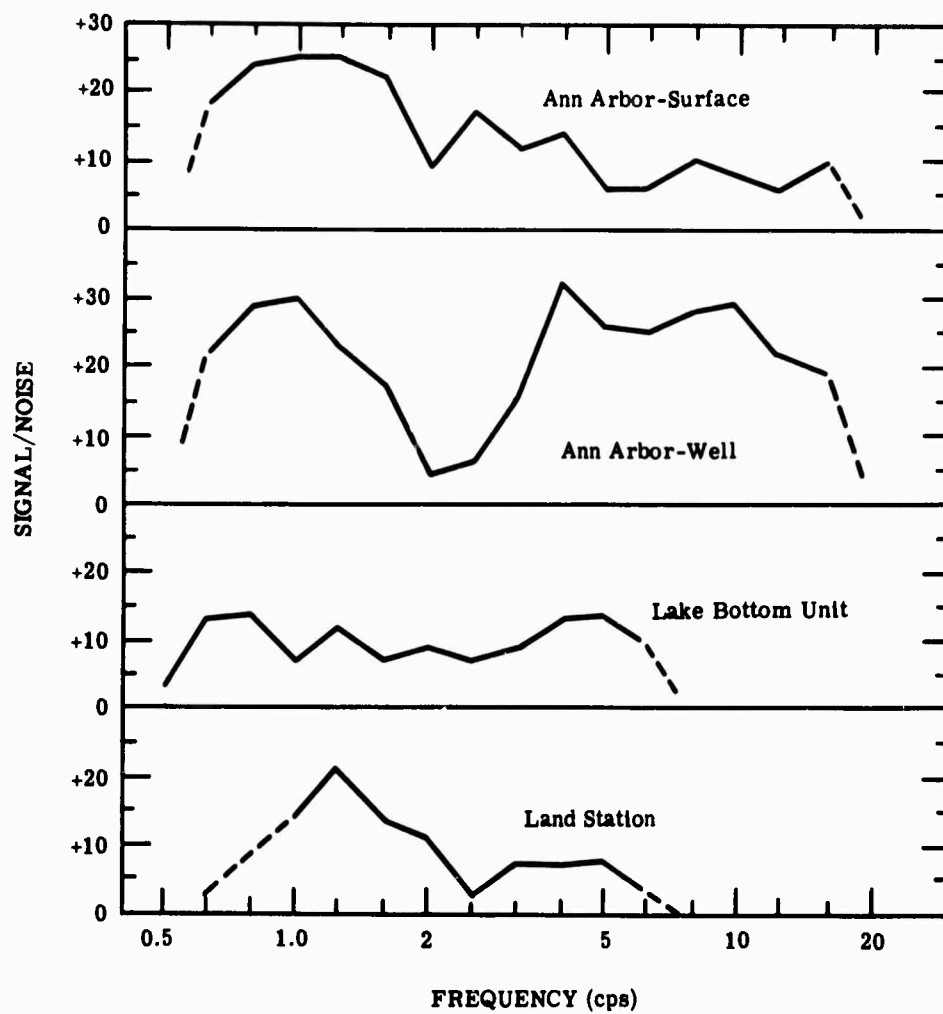
FIGURE 27. SIGNAL-TO-NOISE RATIO OF BUFFALO, NEW YORK, EARTHQUAKE OF
JUNE 13, 1967

43

# SEISMIC RADIATION FROM SHOAL

C. G. Bufe and D. E. Willis

Travel times, amplitude, and particle-velocity spectra for the SHOAL event of 26 October 1963 have been examined for distances to 1200 km and for widely distributed azimuths. A composite curve of raw travel-time data reaffirms the low $P_n$ velocities previously observed in the Basin and Range province and yields a crustal thickness of about 26 km. The travel-time data was obtained from LRSM, VELA array, USCG, Sandia Corporation, University of California, University of Michigan, and various volunteer team sources. These data, when corrected for station elevations, yield a least-square $P_n$ velocity of 7.84 km/sec. Residuals to this $P_n$ curve have been contoured for distances from 200 to 1200 km and are shown in figure 28. With the exception of the central California and southern Nevada data, these residuals bear a negative correlation to the mean station residuals obtained by Carder, Gordon, and Jordan [4] for explosive sources at teleseismic distances, and thus seem to reflect lateral variations in mantle velocity just below the crust. Paths through Herrin and Taggart's [5] high and low $P_n$ apparent velocity zones explain the observed residual pattern north and east of SHOAL.

Amplitude data from LRSM, VELA array, Sandia, and University of Michigan stations were used in a study of the attenuation of $P_n$ at distances of 200 to 1200 km. $A/T$ was found to decrease as the inverse cube of the distance (A = amplitude; T = period). Residuals from the mean inverse cube were measured in decibels and are shown in figure 29. Negative residuals are within the shaded areas. There is a zone of large positive $P_n$ amplitude residuals in northeastern Nevada, but generally the first arrivals to the east of SHOAL are lower in amplitude than those at the same distances to the south and north. Amplitude data from SHOAL and from the Fallon earthquake of July 20, 1962, contoured by Jordan, Black, and Bates [6] also indicate a pattern of anomalously high $P_n$ amplitudes in northeastern Nevada and northern Utah.

Two sets of three stations to the north, northeast, and east of SHOAL at distances of 320 and 1100 km were chosen for analysis of particle-velocity spectra. Four of these were portable stations operated by The University of Michigan and two were LRSM vans operated by the Geotechnical Corporation.

The spectra of $P_n$ at The University of Michigan's 320-km stations are shown in figure 30. Dinner Station, Nevada, which is northeast of SHOAL, displays much more energy below 2.5 Hz than the stations to the north or east. Above 3 cps, Chicken Springs, Oregon (north of SHOAL), and Dinner Station have particle velocities well above those at Berry Creek to the east. The maximum P-particle velocities (fig. 31) show a stronger similarity between stations, each peaking at 2.5 cps, although Chicken Springs sees more signal above 3.0 cps than the other 320-km stations.

The $P_n$ spectra at distances near 1100 km are shown in figure 32. At all frequencies shown, the Tres Piedres site to the southeast shows lower amplitudes than the other two stations. The spectra of maximum P as shown in figure 33 are similar at the three stations, although Shepherd displays a lower signal level between 1 and 2 cps than the other stations. Van Nostrand and Helterbran [7] have used data from other stations to compute the power spectra for the SHOAL, HARDHAT, and "Fallon earthquake" events.
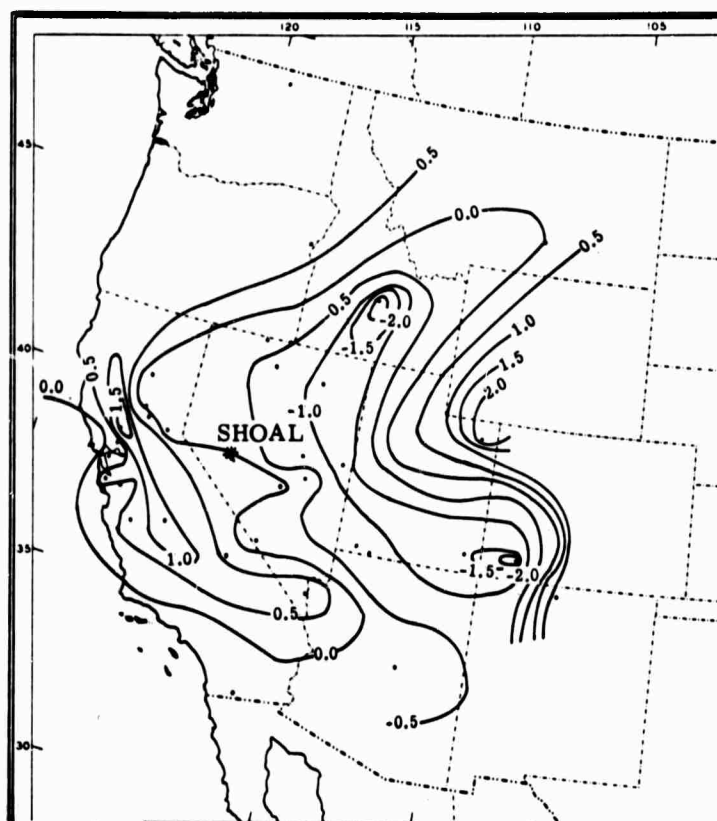
FIGURE 28. $P_n$ RESIDUALS FROM SHOAL; $P_n$ VELOCITY OF 7.84 km sec
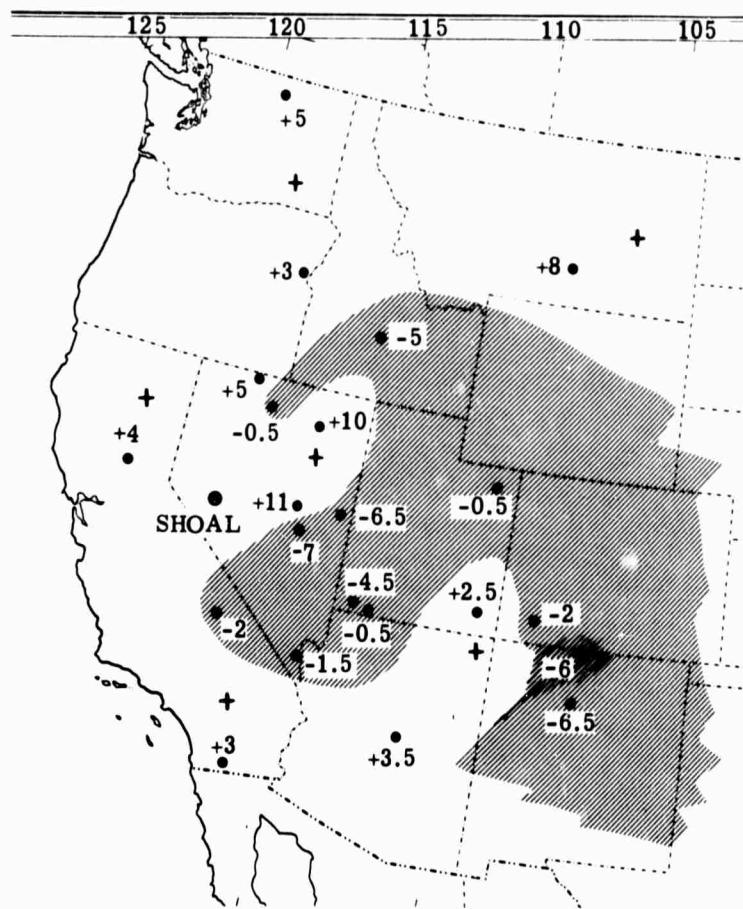
FIGURE 29. SHOAL $P_n$ AMPLITUDE RESIDUALS IN DECIBELS RELATED TO MEAN INVERSE CUBE

Channel 6 Vert.
Δ ≃ 320 Km

SHOAL
10/26/63

-dB

$10^{-2}$

PARTICLE VELOCITY (cm/sec)

$P_n$ at Berry Creek, Nev. ........................
Dinner Station, Nev. ------
Chicken Springs, Ore. ——

$10^{-3}$

$10^{-4}$

$10^{-5}$

1.0

10.0

FREQUENCY (cps)

0

20

40

60
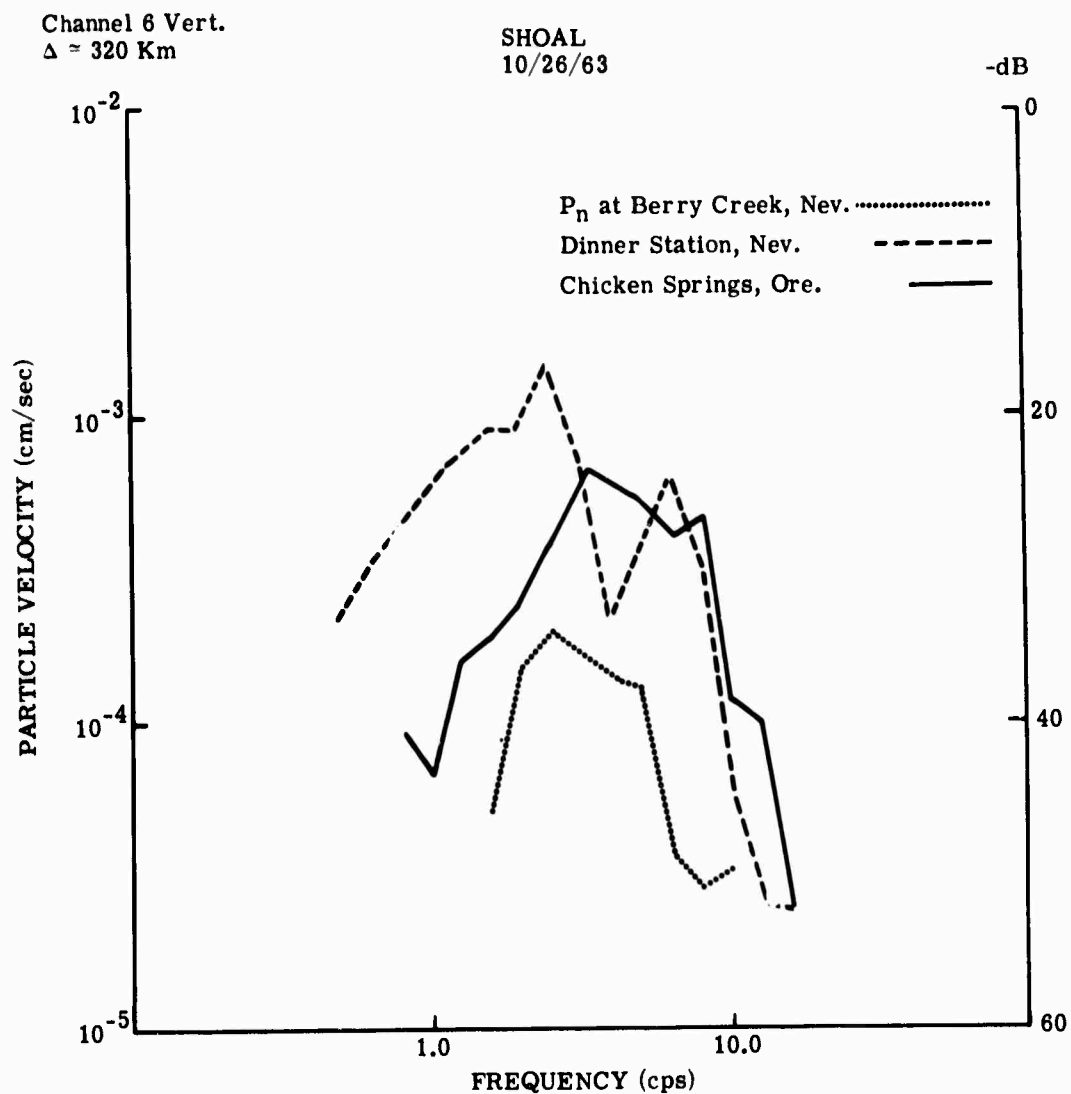
FIGURE 30.  SHOAL $P_n$ PARTICLE VELOCITIES AT 320-km SITES
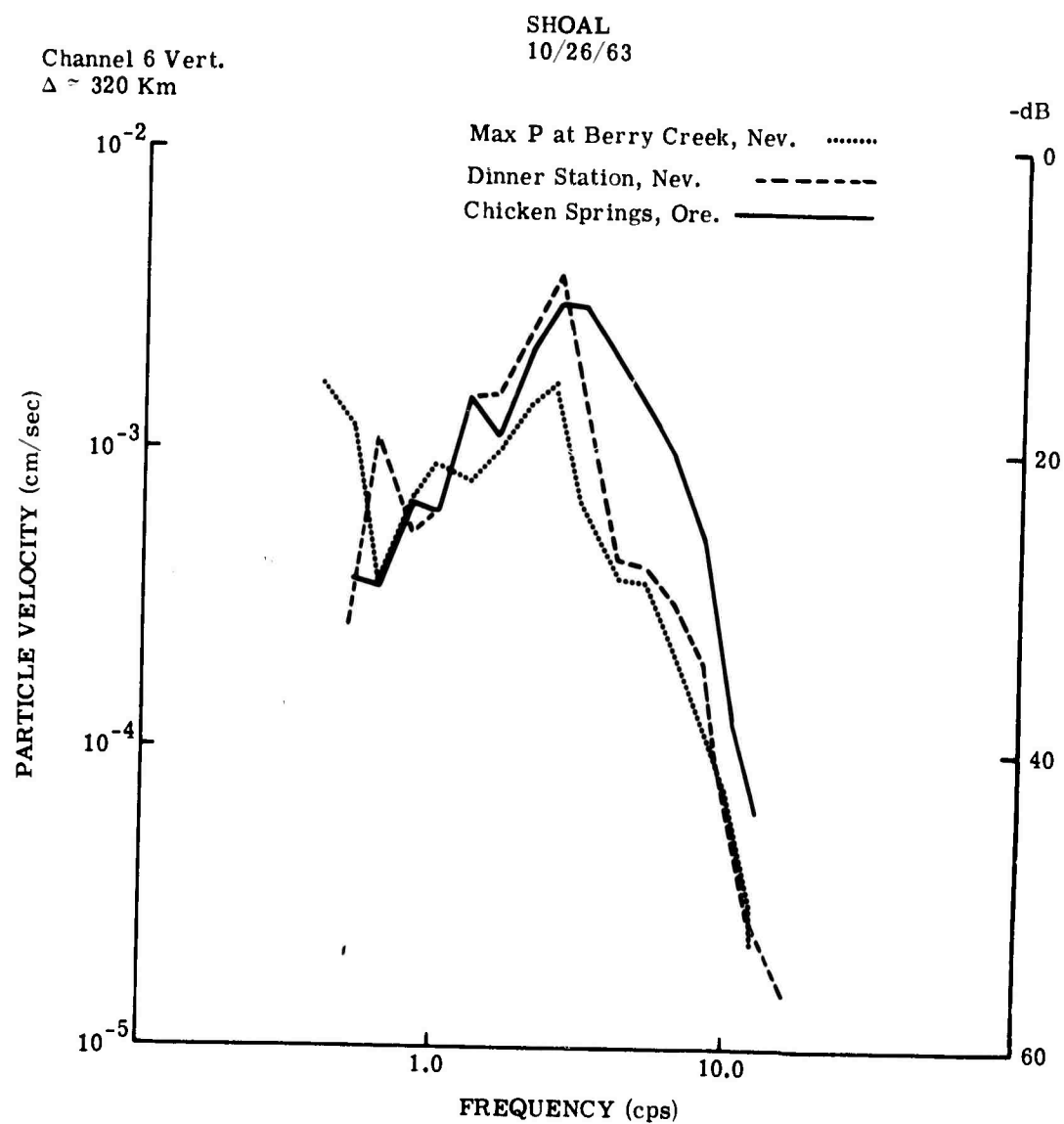
FIGURE 31. SHOAL PARTICLE VELOCITIES OF MAXIMUM P AT 320-km SITES
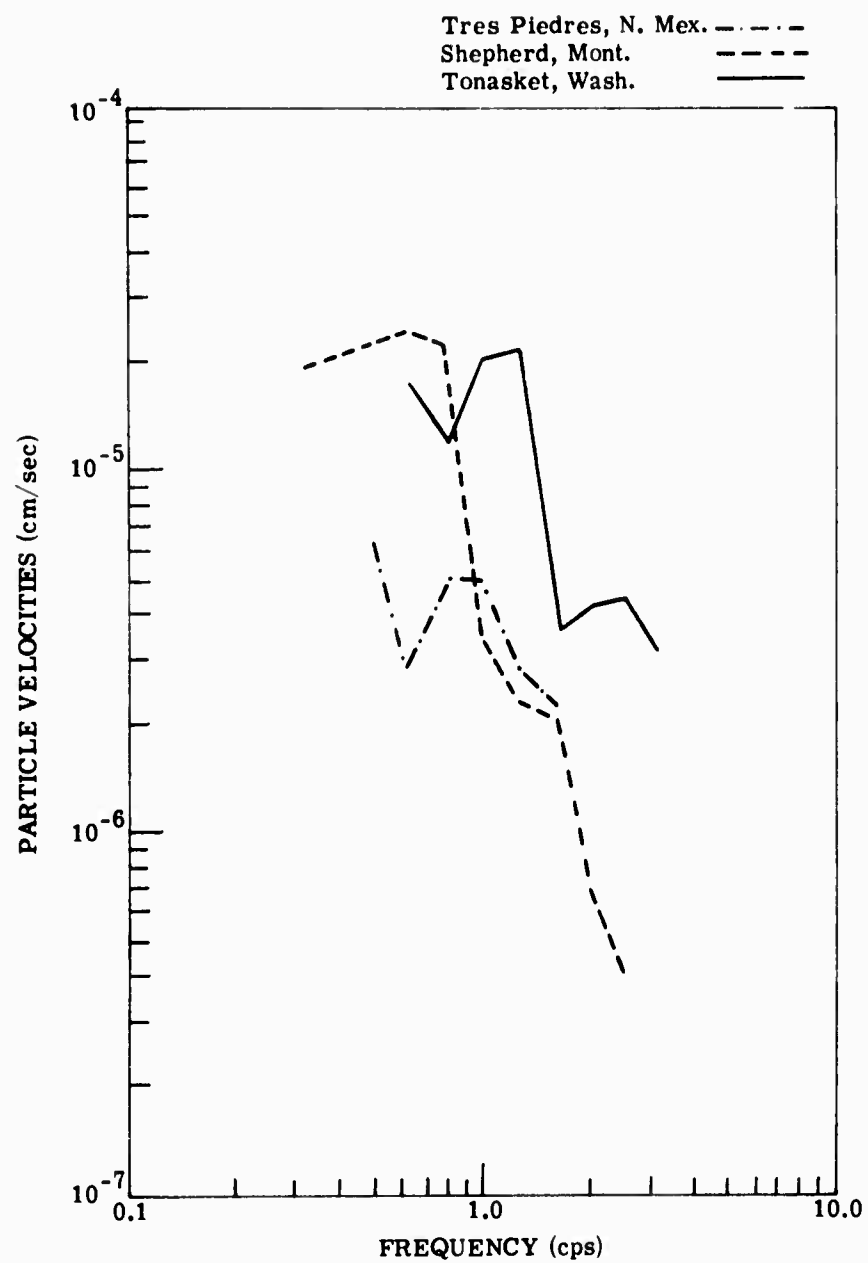
FIGURE 32. SHOAL $P_n$ PARTICLE VELOCITIES AT 1100-km SITES

50
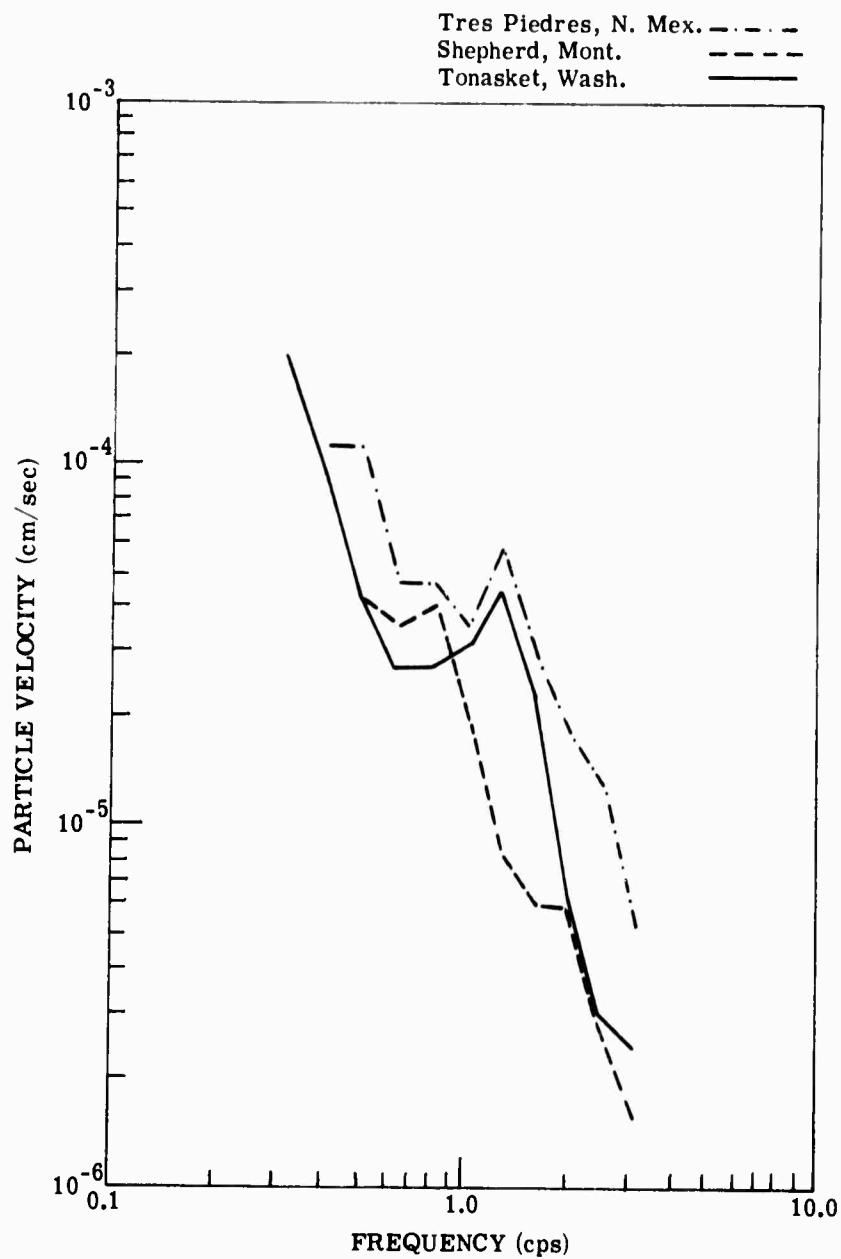
FIGURE 33. SHOAL MAXIMUM P PARTICLE VELOCITIES AT 1100-km
SITES

# MODE FILTERING
## R. M. Turpening

With the optical data processing system as a guide, work has progressed toward the understanding of present linear mode filters, development of new ones, and digital application for all of them. Much of the work was performed while the author participated in a postdoctoral program at Massachusetts Institute of Technology, and that opportunity is gratefully acknowledged.

The geometry of the system is the same as that given in reference 8. Detailed digital analysis of the square of the two-dimensional amplitude "spectrum" (diffraction patterns) of synthetic Rayleigh waves (noise) and P waves shows that fine structure exists that was not seen in optical processing. Figures 34, 35, and 36 indicate that there exist useful differences between signal and noise "spectra" at least down to a signal-to-noise ratio of 1/2 on the vertical seismometer. The contours are logarithmic, and the dashed contours are areas where the noise spectrum exceeds the signal spectrum.

The filter which seems to be indicated by the spectral differences results in the following expression for a filter output:

$$P(\alpha, t) = A(\alpha, \beta)Z(t) + B(\alpha, \beta)\tilde{Z}(t) + C(\alpha, \beta)DN(t) + D(\alpha, \beta)\widetilde{DN}(t) + E(\alpha, \beta)DTN(t) + F(\alpha, \beta)\widetilde{DTN}(t)$$

where
$Z(t)$ is vertical time trace

$DN(t)$ is time trace in direction of noise

$DTN(t)$ is time trace in direction of transverse to the noise

A, B, C, D, E, and F are weighting functions derived from the location of the filter bands in the $\omega$-$\beta$ plane and the geometry.

$\sim$ is an indication of a constant phase shift of $\pi/2$

$\alpha$ is index variable for computed projections

$\beta$ is transformed variable related to $\alpha$

$\omega$ is frequency in radians per second

Since $\tilde{f}(t)$ does not represent a phase shift of $\pi/2$ for all frequencies, phase distortion will result. Therefore, it is envisioned that the banded filter structure, shown in figures 34, 35, and 36, be applied repeatedly along some path through the $\omega$-$\beta$ plane. Figure 37 represents the two-dimensional spectrum (diffraction pattern) of a typical seismic event and thus describes a possible path for the repeated use of the banded filter structure.
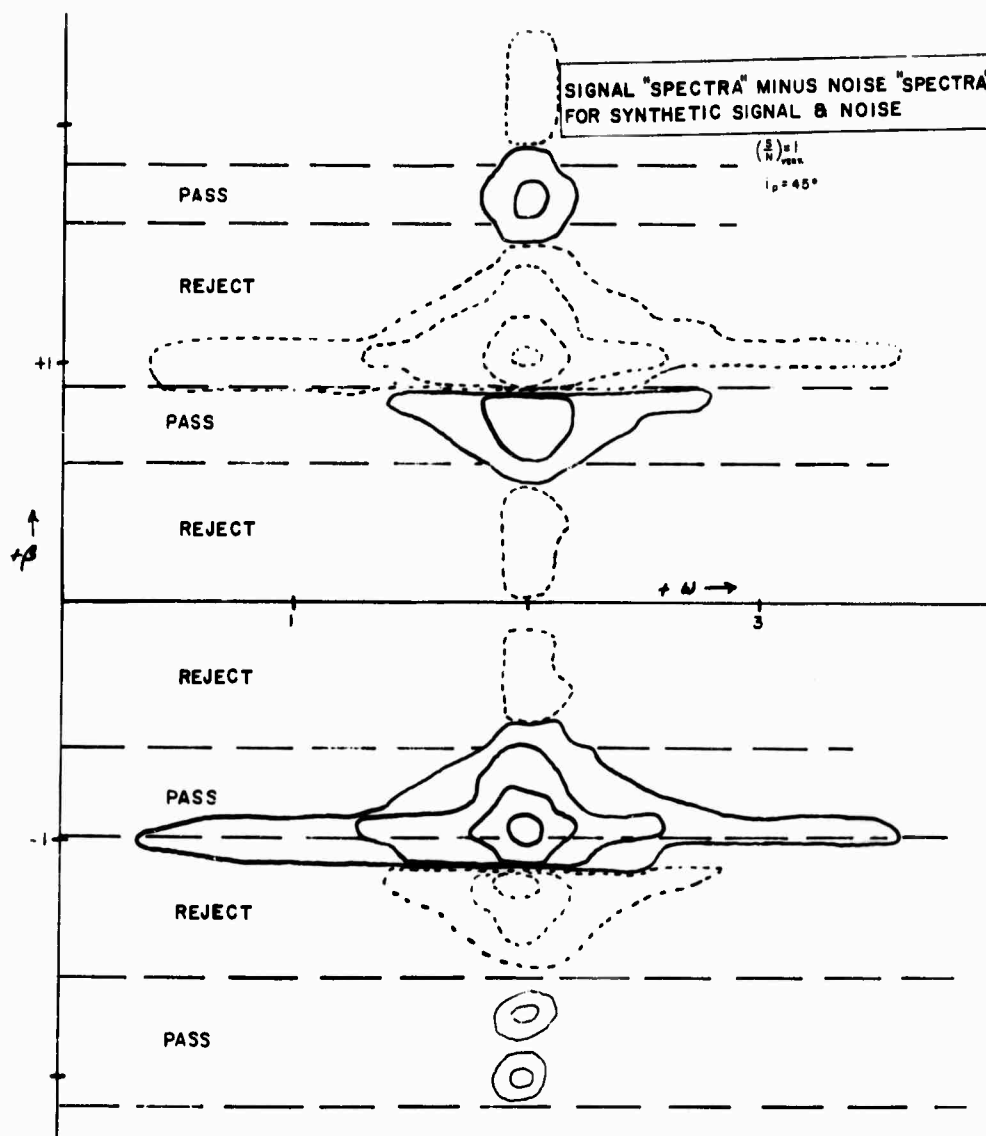
FIGURE 34. THEORETICAL DIFFERENCE OF SIGNAL AND NOISE TWO-
DIMENSIONAL AMPLITUDE "SPECTRA" (DIFFRACTION PATTERNS) FOR
NOISE-ELLIPSE HALF AXES EACH OF SIZE 1. Signal amplitude is 2 and
angle of incidence is 45°. Suggested filter is shown.

FIGURE 35. THEORETICAL DIFFERENCE OF SIGNAL AND NOISE TWO-DIMENSIONAL AMPLITUDE "SPECTRA" (DIFFRACTION PATTERNS) FOR NOISE-ELLIPSE HALF AXES OF SIZES 3/2 AND 1. Signal parameters same as figure 34. Suggested filter is shown.

54
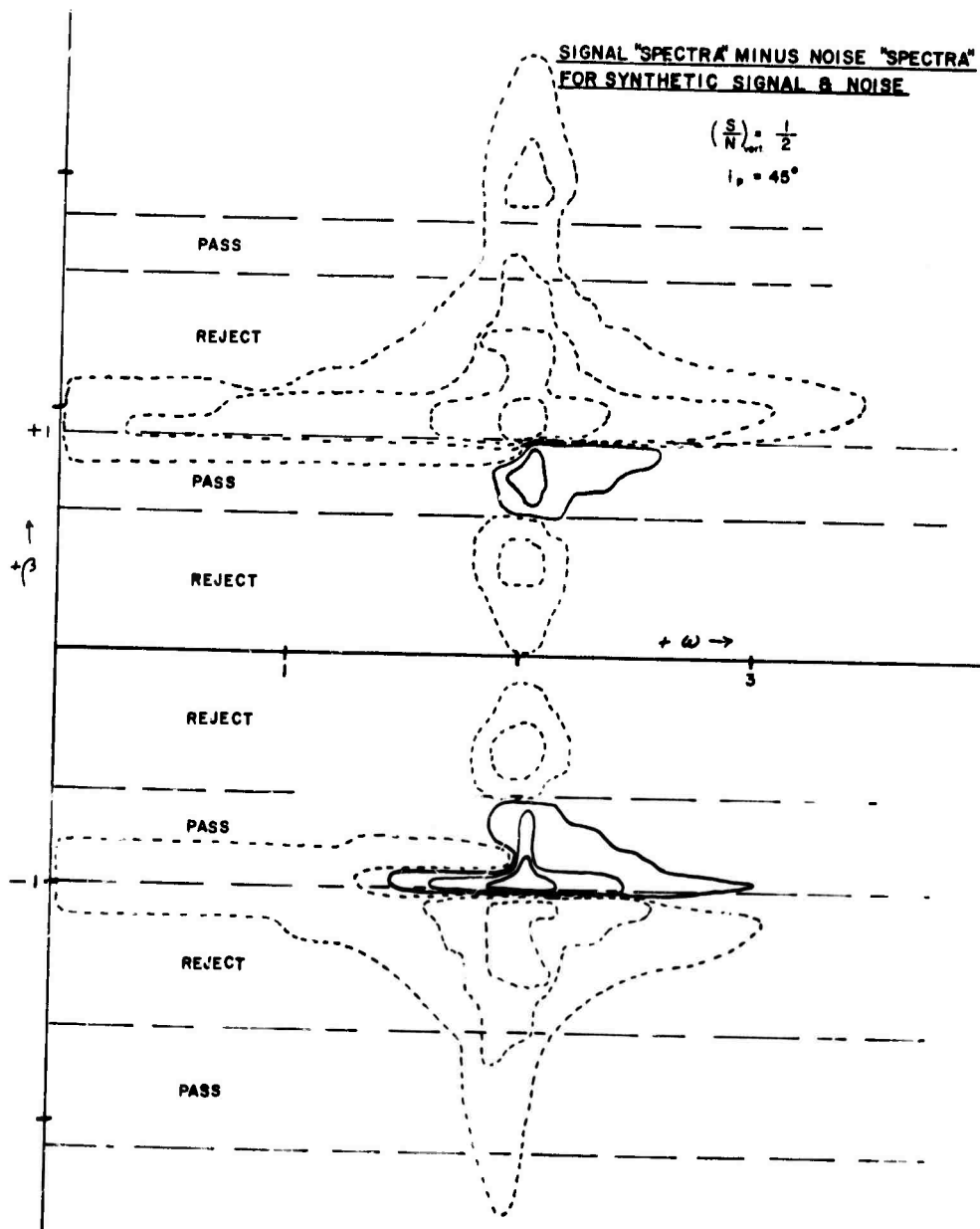
FIGURE 36. THEORETICAL DIFFERENCE OF SIGNAL AND NOISE TWO-DIMENSIONAL AMPLITUDE "SPECTRA" (DIFFRACTION PATTERNS) FOR NOISE-ELLIPSE HALF AXES OF SIZES 2 AND 1. Signal parameters same as figure 34. Suggested filter is shown.

55
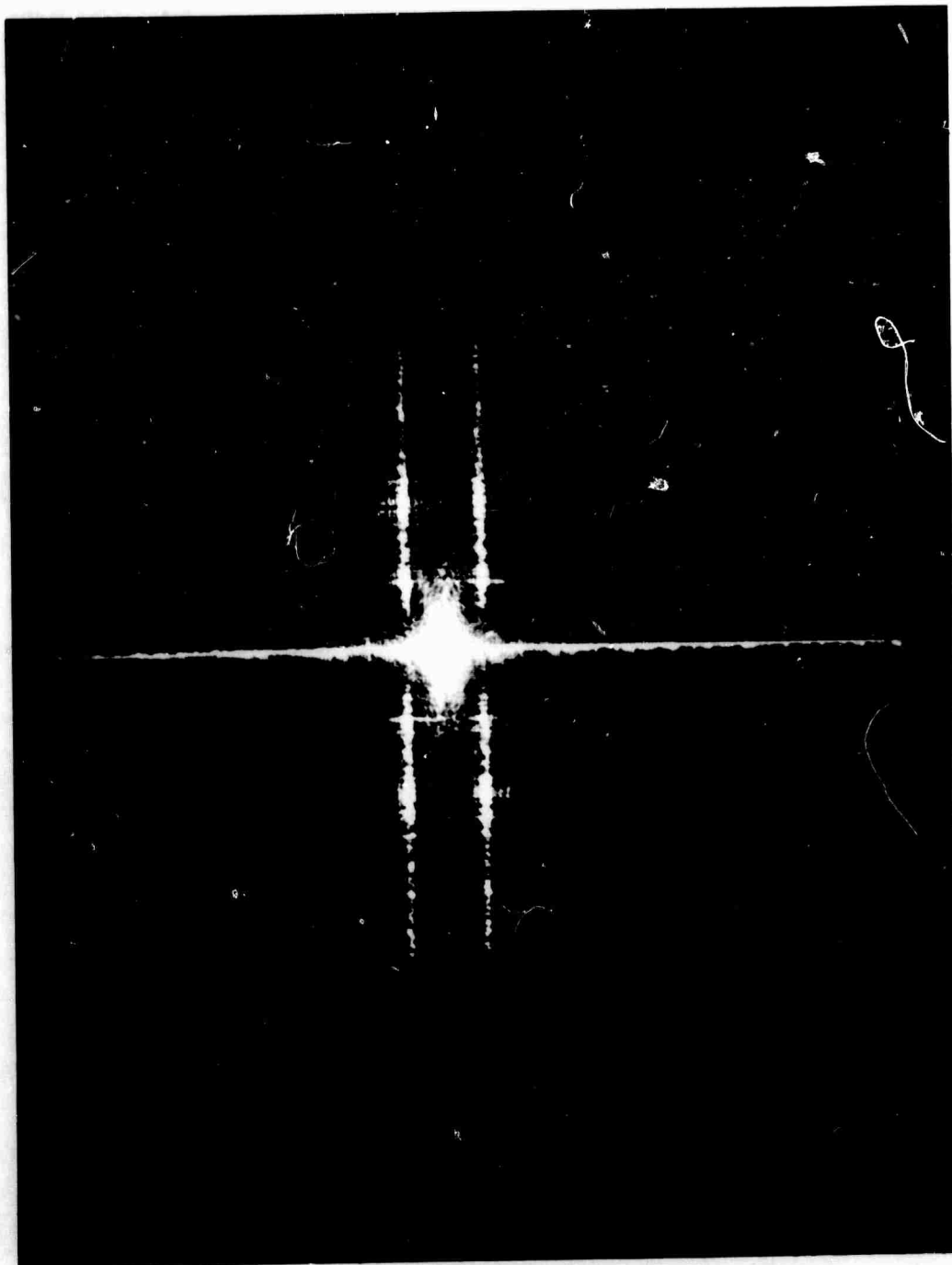
FIGURE 37. DIFFRACTION PATTERN OBTAINED FROM A TYPICAL SEISMIC EVENT

56

## 6
## LASA DATA CONVERTOR
### P. L. Jackson

A digital convertor for LASA data has been completed and is now operational. The convertor is contained in one 7-ft rack except for the digital tape playback unit. Fifty data channels can be selected from the LASA digital tape. This limited number of data channels was selected for reasons of economy, and can be augmented to as many as all the data channels, with additional expense.

The convertor is a flexible research tool in which LASA data output can be scanned or preselected, viewed either one dimensionally or two dimensionally in wiggly line or variable density, and photographed as frame-by-frame motion pictures, continuous moving strips, or still film. The output is currently designed for a CRT. Hard copy, e.g., 50 simultaneous wiggly line channels, is immediately obtainable with Polaroid photography of the CRT. As the convertor can be manually controlled to select and replay any portion of the LASA tape and visually present selected outputs for the research seismologist, it enables direct, interactive, contact with LASA data. He has immediately available both dynamic and static presentations in several different forms. Thus the convertor represents a powerful selective and interpretive tool. When further machine computation is desired, the selected data segments can be used with the University's IBM 360/67 computer.

As described in references 1 and 8, an investigation of optical techniques for initial on-line detection of significant events was planned upon completion of the convertor. However, the decision to use an entire IBM model 40 in addition to a model 2250 for detection alone will require reassessment of this plan. Although optical techniques, if proved applicable, would cost a fraction of that of model 40, the versatility and accuracy would not appear to be comparable.

Figures 38 and 39 show the convertor and a closeup of selection panel. Figure 40 shows one form of output.
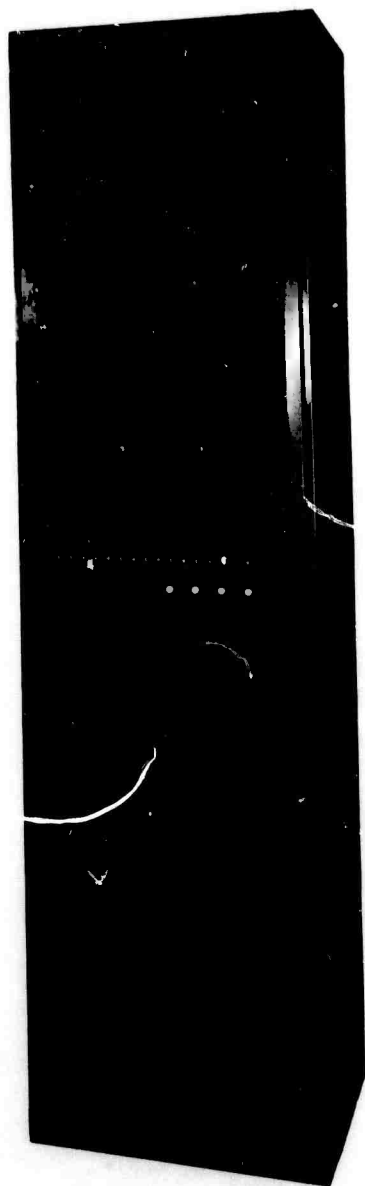
FIGURE 38. LASA DATA CONVERTOR

58
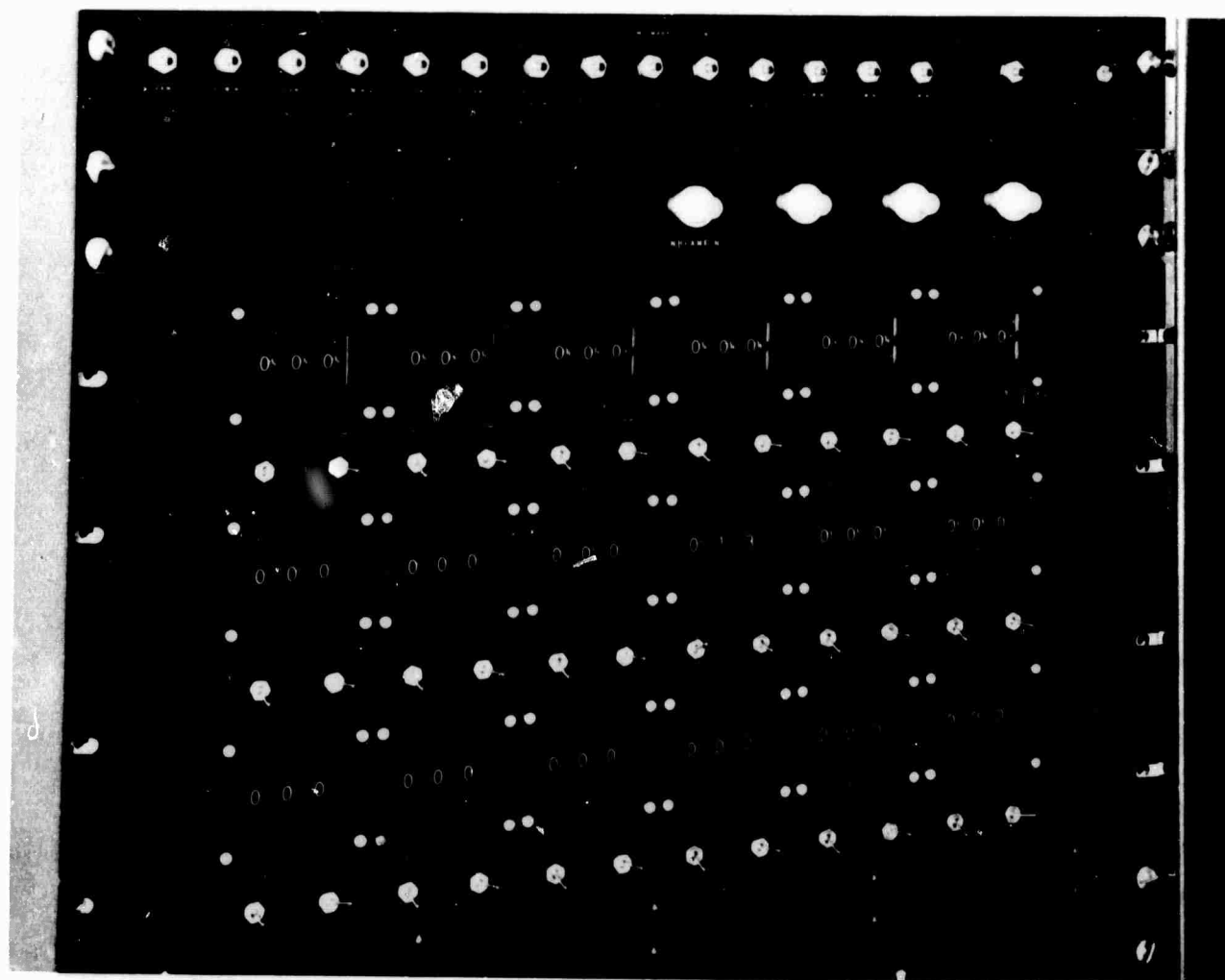
FIGURE 39. CLOSE-UP OF SELECTION PANEL OF LASA DATA CONVERTOR

CRT RECORDING OF EVENT WITH LINEAR PROJECTION
OF LASA ALONG 245° AZIMUTH. POSITION OF SEISMO-
GRAMS ON FILM SELECTED WITH LASA DATA CONVERTOR
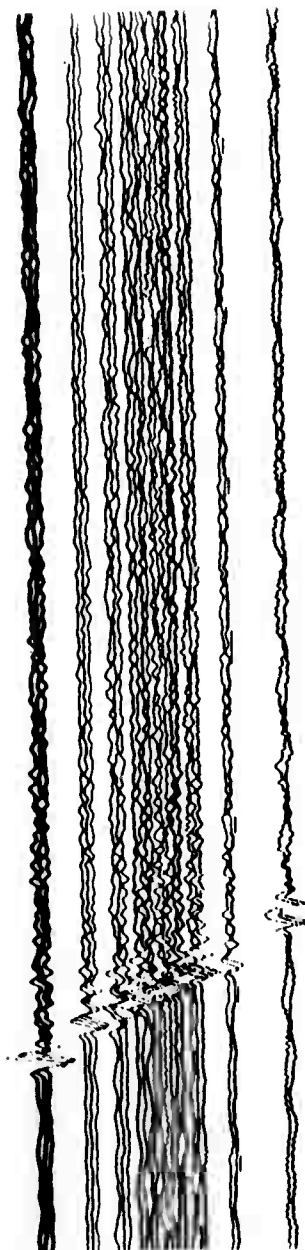
EVENT:

FIJI ISLANDS REGION

| | 12 | 09 | 65 | | | | | | | |
|---|---|---|---|---|---|---|---|---|---|---|
| DATE | TIME | | | LAT | LONG | DEPTH | MAG | DELTA | AZ | VEL | PDE |
| 12/9 | 13 | 37 | 38.2 | -17.7 | 178.3 | 650.0 | 5.1 | 90.99 | 245.11 | 24.19 | 95 1 3 |

FIGURE 40. ONE FORM OF OUTPUT OF LASA DATA CONVERTOR

60

# 7
# SEISMIC-RAY TRACING AND TRAVEL TIMES
## BY DIGITAL MODELING
### P. L. Jackson

## 7.1. INTRODUCTION

The purpose of this work is to produce seismic-ray traces through any media, no matter how inhomogeneous, with output in the form of travel times and amplitudes. The program under development is for both two- and three-dimensional representations of media. Need for such programs has recently become more severe because more precise seismology has indicated lateral inhomogeneities in almost every section and depth of the earth. The program under development will enable us to determine travel times for the entire earth or for any portion or depth of the earth. For example, a simple layered structure can be easily constructed and later perturbed in selected areas to more accurately reproduce observed travel times.

The investigation is to provide the seismologist with a tool to experimentally determine velocity and density structures. It was thought that the digital computer, with its high speed, versatility, ease of varying both the analysis and the data inputs, and particularly the capability of realistic display of its output with a CRT, offered a unique potential for this purpose. The aim was to develop a means of ray tracing through which travel times could be computed and displayed, in which the rays would be displayed along with the velocity structure. With such a display and the capacity to immediately retrace the rays after alteration of the indicated structure, an interactive tool for the interpretative seismologist would be achieved.

Until recently, ray tracing has been confined to a spherically symmetric earth, horizontal layers, or, in optics, through layers which can be represented as conic sections. Spherically symmetric ray tracing has been described by Julian and Anderson [9] and shown by Lewis and Meyer [10]. Iyer and Punton [11] have described a method to compute rays through a two-dimensional inhomogeneous velocity field first by the construction of wave fronts. Yacoub [12] has traced rays through inhomogeneous media and has computed amplitude by means of Zoeppritz's equations. However, information on Yacoub's process has not yet been made available to the author.

This approach has been successful though by no means perfected or completed. Instead of taking a mathematical representation of the velocity structure, a method was devised of sampling the structure and allowing the rays to traverse the samples in a step-by-step fashion. As computer storage is often limited, a method was devised to use an arbitrary portion of the data, save the information of the emerging rays and their travel times and amplitudes, read in (or construct) the velocity data for the succeeding portion, and continue the computations through the succeeding portion. The number of portions is not limited.

Multiple reflections were included by continuing with a reflected ray while saving the information of the ray that was incident on the interface. After tracing the reflected rays, the program returns to the preceding incident rays and continues tracing through the interface. As many as ten multiple reflections have been allowed for in the exploratory programs, but, again, this number can be as high as wished, and can be terminated either by limiting the number or monitoring the amplitude upon reflection.

An extension to three-dimensional ray tracing was developed. For the purpose of investigation, a simple $10 \times 10 \times 10$ grid was employed with good results.

Thus far a simple approximation has been employed. Only velocity data has been used. Snell's law is employed with Fresnel reflection coefficients. The amplitude has been computed by fixed exponential decrement and spherical spreading where the initial amplitude is divided by the distance propagated.

However, the use of these simple computations are considered preliminary. Extension to more accurate seismological approximations will naturally follow. With inclusion of density and S-wave data, Zoeppritz's equations can be implemented. As the travel times are computed, diffractive effects can be investigated for given frequencies. Ground roll can be added. Synthetic seismograms may be possible. Although it does not appear that propagation computed with the wave equations will naturally follow as an extension of this method, Keller's geometric diffraction theory may. Also, by dynamic programming, changing of the velocity structure with iterations appears to be a natural extension of the method.

Previously, an IBM 7090 computer and Calcomp plots were used for batch processing. The University's time-sharing IBM 360/67 computer has recently become operational, and a change-over is being made to this facility. This computer has about $2 \times 10^7$ bytes of storage. Testing programs have been run on the 360, for example, for development of the equations for ray tracing in any direction ($360°$ freedom) with any slope. CRT output is available with the new computer. The batch processing on the 7090 was slow, as a minimum 24-hr turnaround time was required. Difficulties have been encountered in the changeover, and during some periods the program has seemed to retrogress, which is all too common with computer program development. When new, more demanding data were added, deficiencies have successively been discovered. For example, channelizing through successive critical reflections due to the sampling interval and computing the first segment after reflection have been recent problems.

The author presented a paper on this method in April 1968 [13].

Preliminary results are shown in figures 41-44. These are not presented as finished products but as illustrations of the potential of the method. Program glitches have been deliberately left in to give an idea of some of the problems which have been encountered. The average execution time during computation of the figures has been 30 sec, with plotting times of about 2 min. Of particular significance are figure 45, where the Jeffrey-Bullen p-wave travel-time curve is closely duplicated with only 40 samples of the radial velocity profile, and figure 43, where an isometric

projection of the results of three-dimensional ray tracing is shown. For the case of the spherical earth, the power in this method lies in the capability of introducing lateral inhomogeneities.

When used for structural determination with regional disturbances, this ray-tracing technique can be used as shown in figure 46. For local structural determination from teleseisms, it can be used as shown in figure 47.

## 7.2. CURRENT PROGRESS

Currently, FORTRAN IVG is being used on the 360 computer for two-dimensional ray tracing with complete ray-direction and slope freedom. (In MAD language, for the 7090 computer, three-dimensional ray traces were made with a representation of a simplified structure.) A "patchwork" program, in which data can be successively read in after tracing through and retaining values from the preceding data, has been perfected and the resulting travel-time curves produced by the emerging rays have been drawn by the computer. This program will obviate the need for large memory for detailed ray tracing. A program for including head waves has been written. A method of using Zoeppritz' equations has been checked out and is the next planned addition to the basic program.

## 7.3. DISCUSSION

The program in the appendix will reproduce most of the waves produced in the half-earth (with the exception of the diffracted P), such as P, PP, PcP, PKP in all branches, PKIKP, PKiKP. With minor modification PKKP can be obtained. When this program is tested with 102 P-wave velocity values sampled from the Jeffrey-Bullen velocity vs. depth graph, the travel times for the various waves are usually within 1% of those found in the Jeffrey-Bullen travel-time tables. The errors are due to the inaccuracies of taking velocity values from a small graph, the margin of error in the original formulation of the velocity values, and the result of sampling a relatively few values. In ray tracing, any error due to sampling in the initial portion of the rays tends to become exaggerated by a "lever-arm" effect. The length of the two legs of PP often differ by several percent, but the travel times are more accurate due to the fact that they are propagating through the proper velocity structure. The available memory of the computer, of course, dictates the amount of data which can be handled at one time. For the program in the appendix, all the data are accepted at one pass.

In the computer runs with 102 samples to the earth's center, the average time to trace each ray and obtain the travel time was 1 sec of central processing unit time.

At the present time graphical output has not yet been incorporated into the computer using the program listed in the appendix.

63

SEISMIC RAY TRACES, TRAVEL TIMES, AND AMPLITUDES

FIGURE 41. ILLUSTRATION OF SEISMIC DATA DISPLAY. $20 \times 80$ sample points read in $20 \times 40$ "patches."

64

| TRAVEL TIMES | DISTANCES | AMPLITUDES |
|---|---|---|
| 2.83 | 4.49 | 9.24 |
| 5.10 | 4.26 | .15 |
| 4.67 | 9.05 | 2.32 |
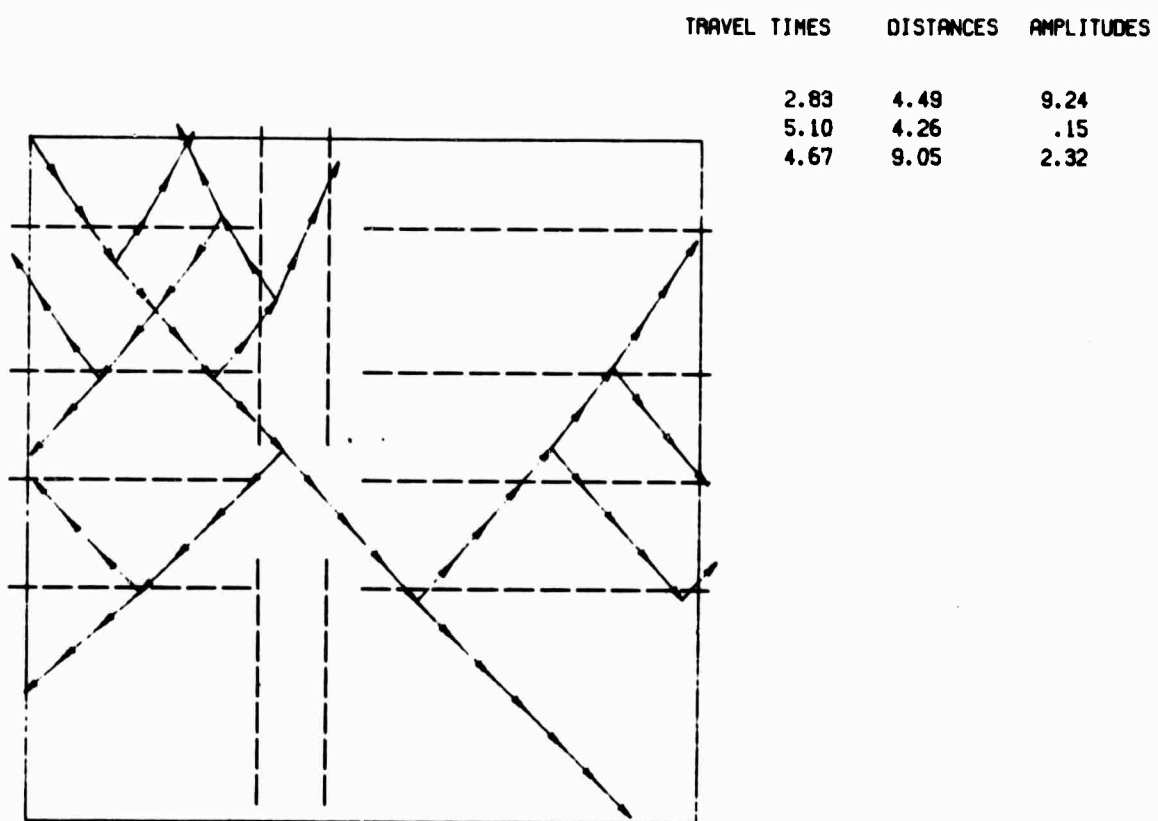
FIGURE 42. ILLUSTRATION OF MULTIPLE REFLECTIONS WITH A VERTICAL DIKE

65
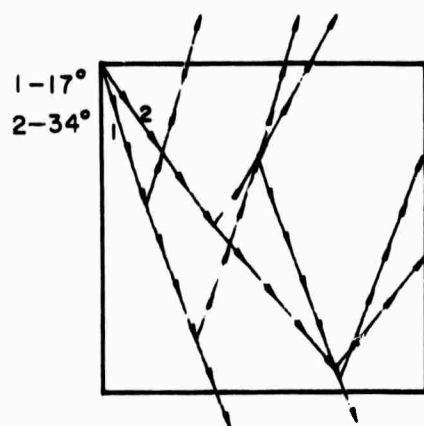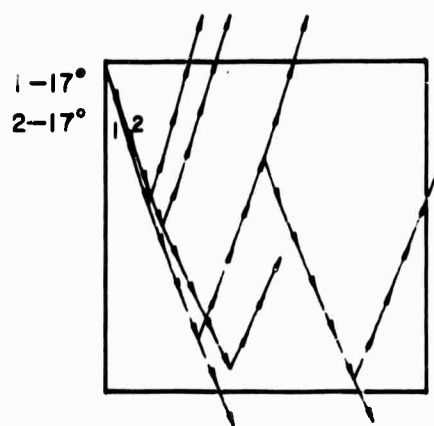
FRONT VIEW (I,J)          SIDE VIEW (I,K)

THREE-DIMENSIONAL 10X10X10 SAMPLES

BOTTOM VIEW (J,K)
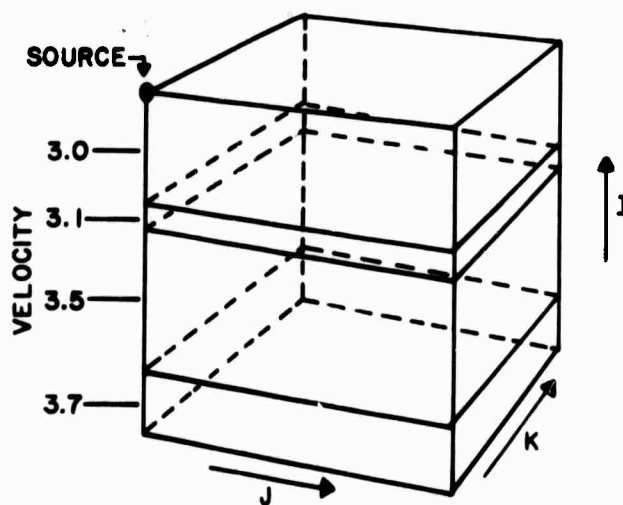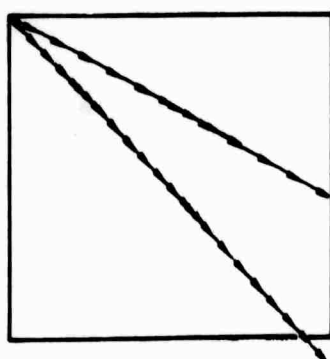
FIGURE 43.  THREE-DIMENSIONAL RAY TRACING THROUGH A VERY SIMPLE CUBE WITH
HORIZONTAL LAYERS

66
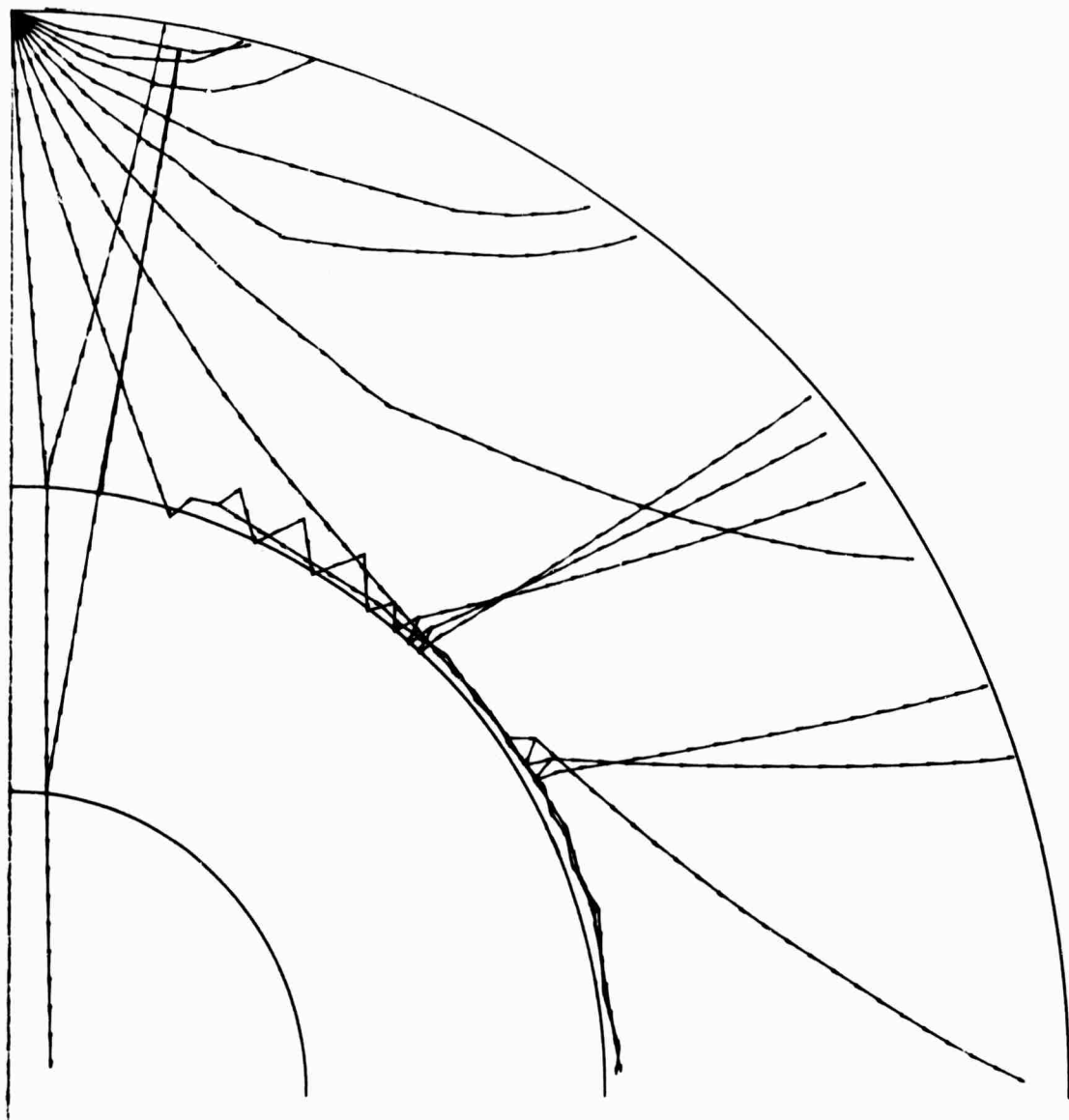
FIGURE 44.  SOME DIFFICULTIES ENCOUNTERED IN DIGITAL MODELING
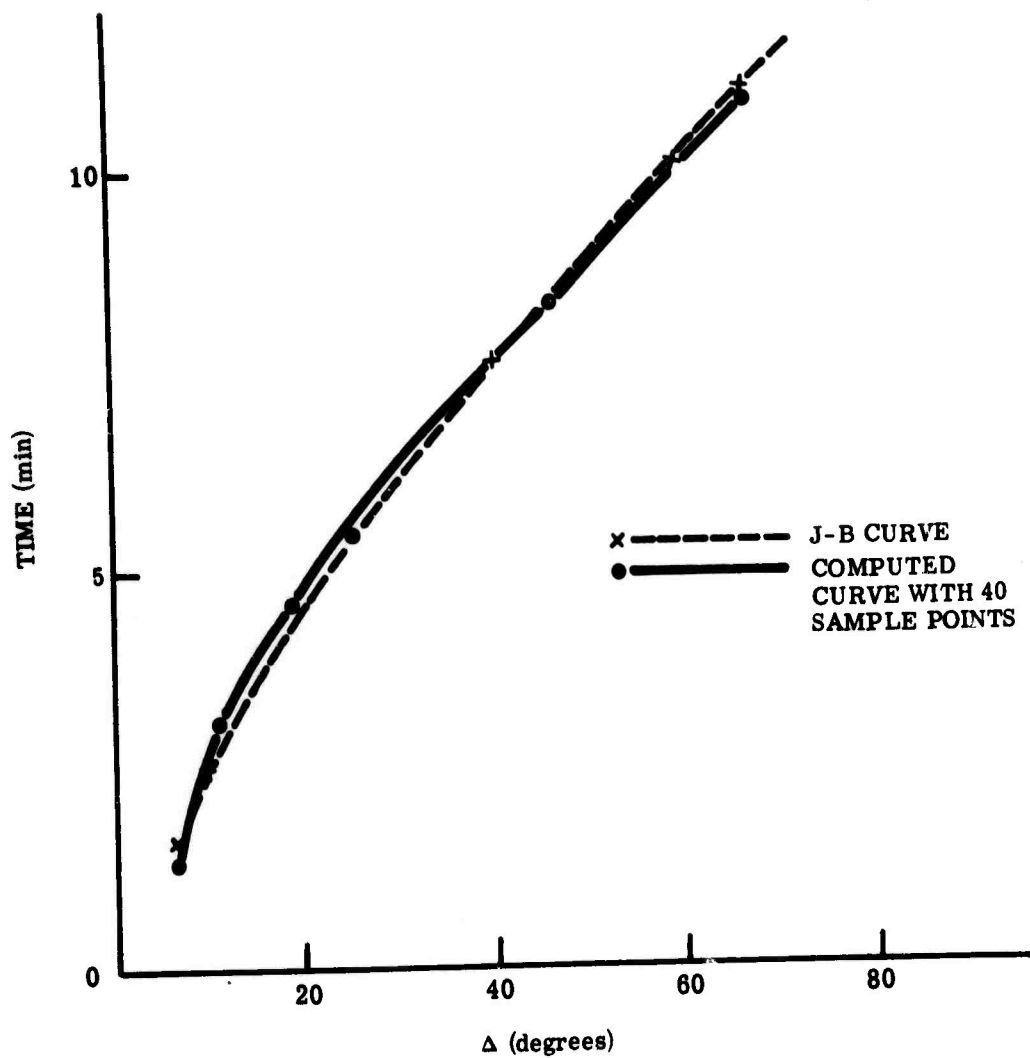
FIGURE 45.  TRAVEL-TIME CURVE PLOTTED WITH SAMPLED JEFFREY-BOLLEN
RADIAL P-WAVE VELOCITY PROFILE

68
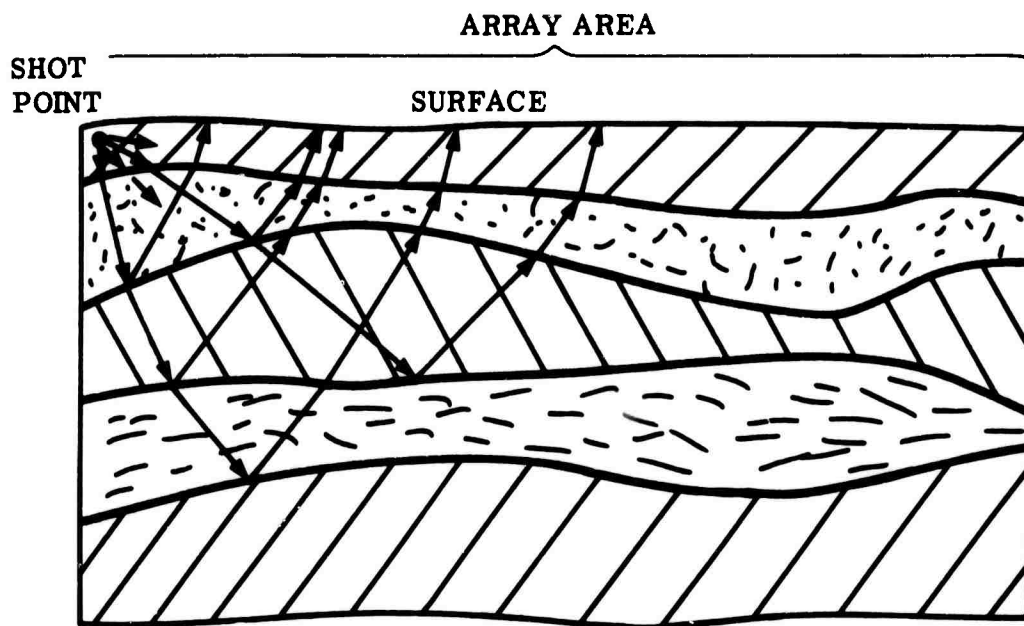
FIGURE 46. RAY TRACING FOR REGIONAL SHOTS. Travel times, amplitudes, and angle of emergence also computed.

**ARRAY AREA**

DISTRIBUTION OF EMERGENCE INDICATES STRUCTURE

INITIALIZATION OF RAYS FROM EACH SAMPLING POINT
INITIAL RAY DIRECTIONS FROM SPHERICALLY SPREADING WAVES

FIGURE 47. RAY TRACING FOR TELESEISMS. Travel times, amplitudes, and angles
of emergence also computed.

70

# Appendix
## SEISMIC-RAY TRACING BY DIGITAL MODELING
### P. L. Jackson

Seismic rays can be traced through velocity and density structures of any degree of in-homogeneity. A digital computer is used to trace and graphically present the rays, and to compute the travel times and amplitudes of those emerging at the surface. The number of multiple reflections can be selected or can be limited by a minimum amplitude upon reflection. A sampling of the structure on two- or three-dimensional grids comprises the data for the ray tracing. As the data can be "patched" together and the continuation of rays traced through each data "patch," only a small amount of computer memory is required; thus detail is not limited by computer memory. Calcomp plots of ray traces through several representative velocity structures have been made. Included is an earth quadrant in which the Jeffrey-Bullen P-wave velocity profile was used for data. The program can be extended to include more techniques of seismic interest, such as Zoeppretz's equations, head waves, Rayleigh waves. One goal of this work is to present the output on a CRT so that the results of velocity and density data changes can be immediately perceived.

Because ray tracing for a spherical earth is the only present program written in FORTRAN IVG, only this program will be described in this report. This program displays the basic approach of the ray-tracing procedure, and can be expanded or altered by the reader. The program and the flow diagram (fig. 48) follow the appendix.

Snell's law is used to iteratively penetrate through an array (in this description a two-dimensional array). Each element of the array is a velocity value representing the velocity at a depth corresponding to the row of the array and a distance corresponding to the column of the array. A corresponding array represents the slope found at each velocity value. As the ray penetrates a fixed distance at an angle determined by Snell's law, the velocity for the incident value and slope value nearest to the extent of penetration are taken to compute the angle of the next penetration of the fixed distance through the array. A "probing" extension of the fixed distance at the preceding angle is made to determine the velocity of the emerging region. The velocity of the incident region, the angle of incidence, and the velocity of the emergent region are thus determined 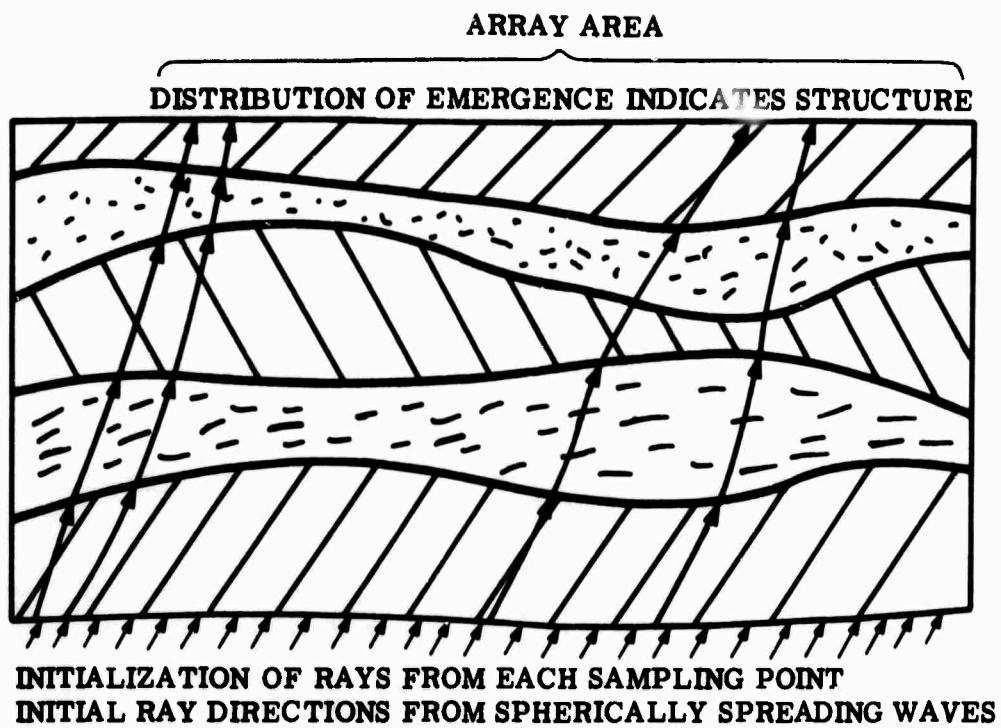for a succeeding application of Snell's law. If desired, a change of one set of indices can be made to use the slope of the emergent region instead of the incident region.

As each fixed distance of the penetrating ray is incremented, this distance is divided by the velocity value through which the ray is penetrating to compute the travel time for this increment. These segmental travel times are successively summed so that upon emergence at the surface the total travel time is retained.

71

When the ray "probes" into an emerging region whose velocity differs by a specified amount and in a region which can be limited, reflection occurs. The value of the reflecting angle is determined by the angle of incidence, and the penetration continues with the initialized angle of reflection. In case of critical reflection no values are retained from the reflecting interface. With noncritical reflection, the value of the incident angle is retained, along with the summed travel times to the interface. After the reflected ray emerges or exceeds the bounds of the array, control is returned to the incident ray so that it can penetrate beyond the interface. The number of multiple reflections can be specified or, if desired, terminated if the amplitude is sufficiently small, although this latter condition is not in the accompanying program.

When any ray is sufficiently close to the representation of the surface of the earth, its azimuthal distance and its length (in kilometers), the travel time, and the amplitude are printed out before a new direction from the source or returning to a reflection point is initiated for continuation of the incident ray.

The program contains two subroutines. The first, entitled "WORLD," accepts radial velocity samples to any depth and constructs the two-dimensional velocity and slope arrays to correspond to a curved earth. When the half-earth is used, it constructs the array for half of the earth. The second, entitled "SINDET," accepts the angle from the vertical, the velocity value of the incident region and its slope, and the velocity value from the emerging region. It then computes the emerging angle by means of Snell's law. Any angle from the vertical from $0^\circ$ to $360^\circ$ and any slope from $-90^\circ$ to $+90^\circ$ is accepted by SINDET. In case of angles which are critical or beyond, this information is returned to the main program so that a reflection will take place.

Because a rectangular array is used, the conversion to flat earth is straightforward. The subroutine "WORLD" is not used for flat earth, and the rays emerge at the first row of the array. Actually the flat earth is more economical to compute because an arctangent computation is not required for each element of the array.

```
 >     1              DIMENSION A(203,102),B(203,102),PI(10),PJ(10),
 >     2             1CIJ(10),ON(10),ANT(10),D(102),AT(10)
 >     3              ICRIT=0
 >     4              NAMELIST/NAM1/NOIN,DELN,BEGIN,NMULT,ORIGV,ORIGH,H·
 >     5             1,ISAMP,IPORSH,JPORSH,DIFRAC
 >     6              READ(4,NAM1)
 >     7              READ(5,500)(D(I),I=1,IPORSH)
 >     8              CALL WORLD(D,A,B,ISAMP,IPORSH,JPORSH)
 >     9              WRITE(1,600)((A(I,J),I=1,203),J=1,102)
 >    10              WRITE(1,600)((B(I,J),I=1,203),J=1,102)
 >    11              DATA PIT/3.1415927/
 >    12              DATA DEC/-.00003/
 >    13    C
 >    14    C                         17 CALCOMP CARDS
 >    15    C
 >    16              DO 20 L=1,NOIN
 >    17              IF(BEGIN.GT.1.57) CALL SYSTEM
 >    18              III=0
 >    19              WRITE(7,501) BEGIN
 >    20              ANGLE2=BEGIN
 >    21              PNM=1000.
 >    22              DO 30 I=1,10
 >    23              AT(I)=0.
 >    24    30        ON(I)=0.
 >    25              IVW=0
 >    26              IZ=1
 >    27              ANT(IZ)=1.
 >    28              PI(IZ)=ORIGV
 >    29              PJ(IZ)=ORIGH
 >    30              I=PI(IZ)+.5001
 >    31              J=PJ(IZ)+.5001
 >    32    40        IF(IZ) 20,20,60
 >    33    60        IU=I
 >    34              IV=J
 >    35              ANGLE1=ANGLE2
 >    36    C
 >    37    C                          2 CALCOMP CARDS
 >    38    C
 >    39              IF(ANGLE1.GT.7.) GOTO 52
 >    40              G=H*A(I,J)/13.62
 >    41              HHH=G*COS(ANGLE1)
 >    42              GGG=G*SIN(ANGLE1)
 >    43              PI(IZ)=PI(IZ)+HHH
 >    44              PJ(IZ)=PJ(IZ)+GGG
 >    45              AT(IZ)=AT(IZ)+DIFRAC*G/(A(I,J)*60.)
 >    46              ON(IZ)=ON(IZ)+DIFRAC*G
 >    47              PII=ISAMP-PI(IZ)
 >    48              PJJ=PJ(IZ)-1.
 >    49              RAD=SQRT(PII*PII+PJJ*PJJ)
 >    50              IF(RAD-ISAMP+1.) 70,70,80
 >    51    80        IF(B(I,J).LE.0.) DISTA=-57.2957795*B(I,J)
 >    52              IF(B(I,J).GT.0.) DISTA=57.2958*(PIT-B(I,J))
 >    53              AMPL=(PNM*ANT(IZ)/ON(IZ))*EXP(DEC*ON(IZ))
 >    54              DKM=111.4726*DISTA
 >    55              WRITE(7,501) DISTA,DKM,AT(IZ),AMPL
 >    56              III=III+1
 >    57              IF(IZ.EQ.1.AND.ICRIT.EQ.0) GOTO 210
 >    58              GOTO 52
 >    59    70        IF(PI(IZ).GT..5.AND.PJ(IZ).GT..5.AND.PI(IZ).LT.202.5
 >    60             1.AND.PJ(IZ).LT.101.5) GOTO 90
 >    61    52        IVW=0
 >    62              ANT(IZ-1)=(1-ANT(IZ))*ANT(IZ-1)
 >    63              IZ=IZ-1
 >    64              IF(IZ) 20,20,100
```

73

```
>    65     100   I=PI(IZ)+.5
>    66           J=PJ(IZ)+.5
>    67           ANGLE2=CIJ(IZ)
>    68           GOTO 40
>    69      90   I=PI(IZ)+.5
>    70           J=PJ(IZ)+.5
>    71   C                          3 CALCOMP CARDS
>    72   C
>    73           PII=PI(IZ)+HHH
>    74           PJJ=PJ(IZ)+GGG
>    75           IM=PII+.5
>    76           IS=PJJ+.5
>    77           PII=ISAMP-PII
>    78           PJJ=PJJ-1.
>    79   C********COMPUTE RADIUS********
>    80           RAD=SQRT(PII*PII+PJJ*PJJ)
>    81           WRITE(1,501) PI(IZ),PJ(IZ),A(I,J),B(I,J)
>    82   C********CHECK FOR BEING IN BOUNDARIES********
>    83           IF(RAD.GT.ISAMP-1) GOTO 80
>    84           IF(IM.GT.2*IPORSH-1.OR.IM.LT.1.OR.IS.GT.JPORSH
>    85          1.OR.IS.LT.1) GOTO 52
>    86           IF(A(IM,IS)-A(I,J)) 120,40,120
>    87   C********CALL SUBROUTINE TO COMPUTE DIRECTIONS********
>    88     120   CALL SINDET(ANGLE1,ANGLE2,A(I,J),A(IM,IS),B(I,
>    89          1J),ICRIT)
>    90           IF(ICRIT+IVW.GE.2) GOTO 40
>    91           IF(ICRIT.GE.1) GOTO 230
>    92     130   IF(ABS(A(I,J)-A(IM,IS)).GE.1.2.AND.IZ.LE.NMULT
>    93          1.AND.IVW.LT.1.AND.A(IM,IS).GT.3..AND.RAD.LT.64.
>    94          2) GOTO 135
>    95           IVW=0
>    96           GOTO 40
>    97     135   IZ=IZ+1
>    98           ON(IZ)=ON(IZ-1)
>    99           AT(IZ)=AT(IZ-1)
>   100           PI(IZ)=PI(IZ-1)
>   101           PJ(IZ)=PJ(IZ-1)
>   102           ANT(IZ)=ANT(IZ-1)*(A(I,J)-A(IU,IV))/(A(I,J)+A(IU,IV))
>   103           CIJ(IZ-1)=ANGLE2
>   104     230   IF(IZ-NMULT) 210,220,220
>   105     220   IZ=IZ-1
>   106           GOTO 40
>   107     210   ANGLE2=PIT-ANGLE1+2.*B(I,J)
>   108           IF(ANGLE2.GE.2.*PIT) ANGLE2=ANGLE2-2.*PIT
>   109           IF(ANGLE2.LT.0.) ANGLE2=ANGLE2+2.*PIT
>   110           IF(III.GT.1) GOTO 52
>   111           IVW=1
>   112           GOTO 40
>   113      20   BEGIN=BEGIN+DELN
>   114   C
>   115   C                          1 CALCOMP CARD
>   116   C
>   117     500   FORMAT(10F4.2)
>   118     501   FORMAT(6F10.2)
>   119     700   FORMAT(F3.2)
>   120     600   FORMAT(' '10F5.2)
>   121           CALL SYSTEM
>   122           END
>   123   C
>   124   C
>   125           SUBROUTINE WORLD(D,VEL,SLP,ISAMP,IPORSH,JPORSH)
>   126           DIMENSION D(102),VEL(203,102),SLP(203,102)
>   127           PPI=3.1415926/2.
>   128           DO 10 I=1,IPORSH
>   129           SLP(IPORSH,I)=PPI
>   130           SLP(I,1)=0.
```

74

```
  >    131              VEL(IPORSH,I)=D(IPORSH+1-I)
  >    132         10   VEL(I,1)=D(I)
  >    133              IPOR=IPORSH-1
  >    134              DO 20 I=1,IPOR
  >    135              DO 20 J=2, JPORSH
  >    136              P=IPORSH-I
  >    137              Q=J-1
  >    138              PQ=P*P+Q*Q
  >    139              H=SQRT(PQ)
  >    140              IF(H.GT.IPOR+.5001) GOTO 20
  >    141              R=P/Q
  >    142              THETA=ATAN(R)
  >    143              SLP(I,J)=THETA-PPI
  >    144              K=IPORSH-H+.5001
  >    145              VEL(I,J)=D(K)
  >    146         20   CONTINUE
  >    147              IF(IPORSH.NE.ISAMP) GOTO 40
  >    148              DO 30 I=1,IPOR
  >    149              DO 30 J=1,JPORSH
  >    150              VEL(I+IPORSH,J)=VEL(IPORSH-I,J)
  >    151         30   SLP(I+IPORSH,J)=-SLP(IPORSH-I,J)
  >    152         40   RETURN
  >    153              END
  >    154     C
  >    155     C
  >    156              SUBROUTINE SINDET(CIU,CIJ,AIJ,AMS,BIJ,ICRIT)
  >    157              ICRIT=0
  >    158              DATA PI/3.1415927/
  >    159              DATA PPI/1.57579631/
  >    160              AA=AMS/AIJ
  >    161              GH=0.
  >    162              HG=1.
  >    163              CC=CIU-BIJ
  >    164              IF(CC.EQ.0..OR.CC.EQ.PI.OR.CC.EQ.2.*PI) GOTO 11
  >    165              IF(CIU.GT.0..AND.CIU.LE.PI) GOTO 101
  >    166              IF(CC.LT.3.*PPI) GOTO 112
  >    167              GH=2.*PI
  >    168              GOTO 1000
  >    169        101   IF(CC.GT.PPI) GOTO 112
  >    170              GOTO 1000
  >    171        112    H=PI
  >    172              HG=-1.
  >    173       1000   FFF=AA*SIN(CC)
  >    174              IF(ABS(FFF).GE.1.) GOTO 13
  >    175              ARC=HG*ARSIN(FFF)
  >    176              CIJ=ARC+BIJ+GH
  >    177              IF(CIJ.GT.2.*PI) CIJ=CIJ-2.*PI
  >    178              IF(CIJ.LT.0.) CIJ=CIJ+2.*PI
  >    179              GOTO 14
  >    180        13    ICRIT=1
  >    181              GOTO 14
  >    182        11    CIJ=CIU
  >    183        14    RETURN
  >    184              END
  #  END OF FILE
  #
```

FIGURE 48.  FLOW CHART FOR MAIN PROGRAM SUBROUTINE WORLD AND SUB-
ROUTINE SINDET

FIGURE 48. FLOW CHART FOR MAIN PROGRAM SUBROUTINE WORLD AND SUB-
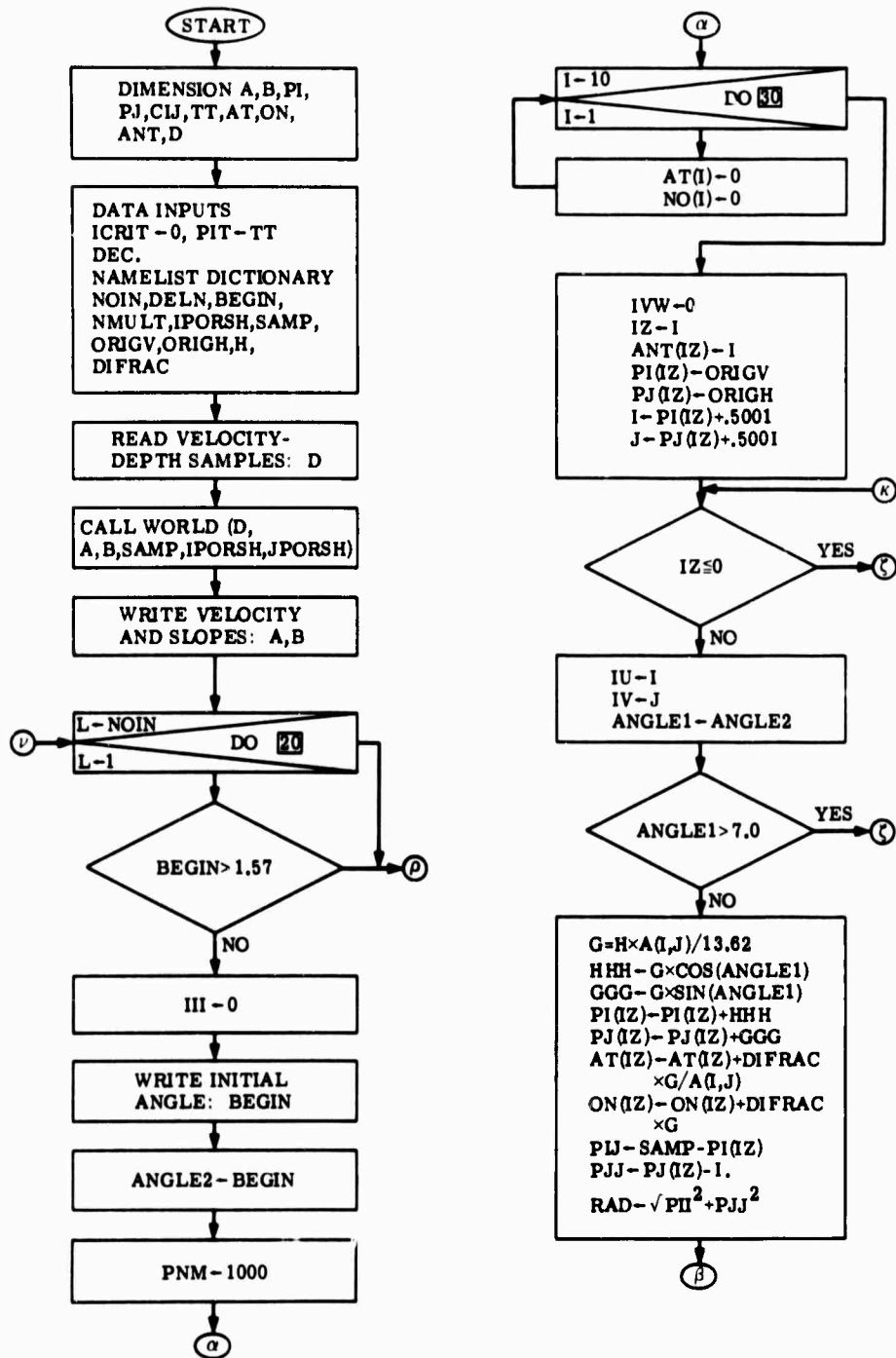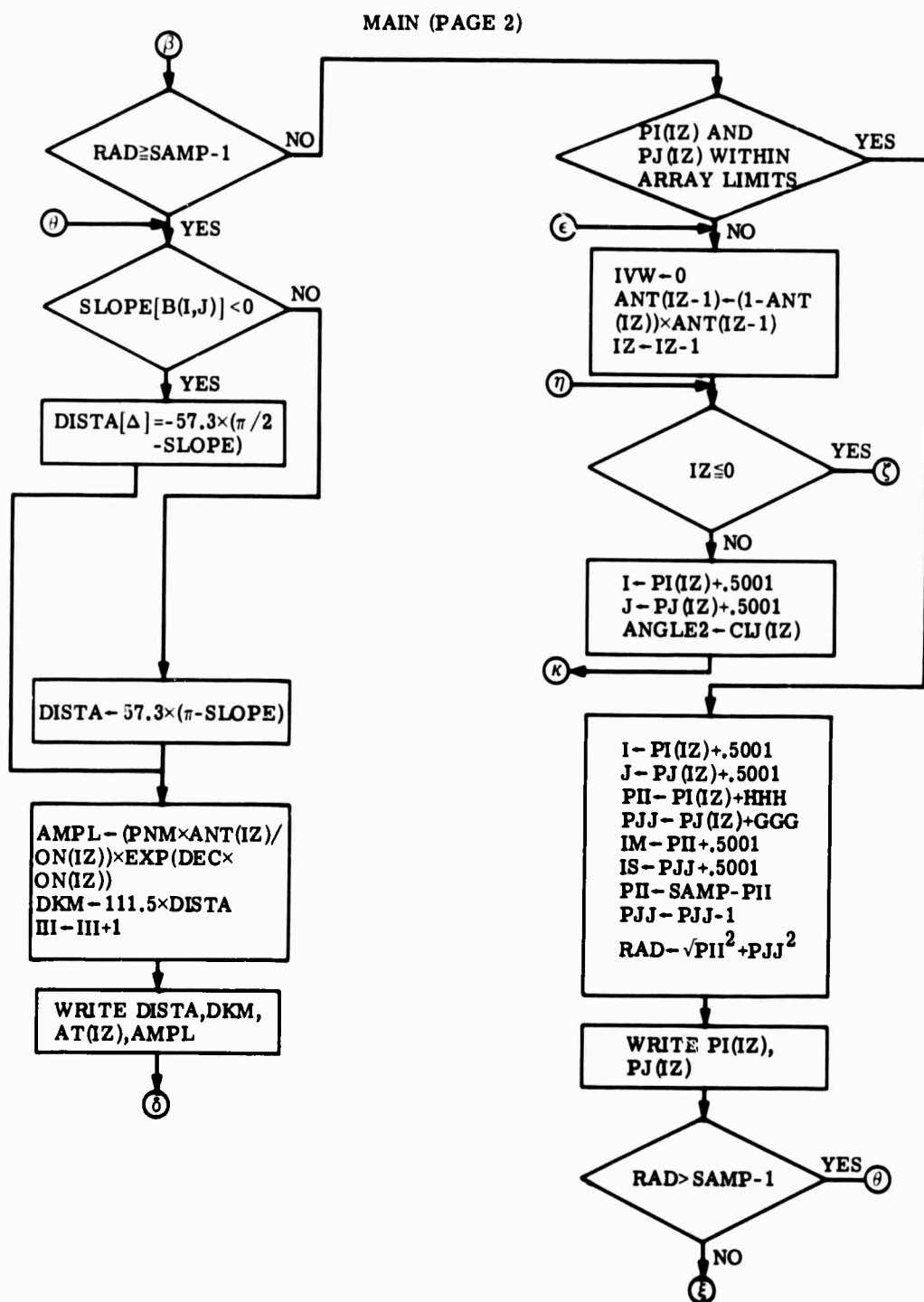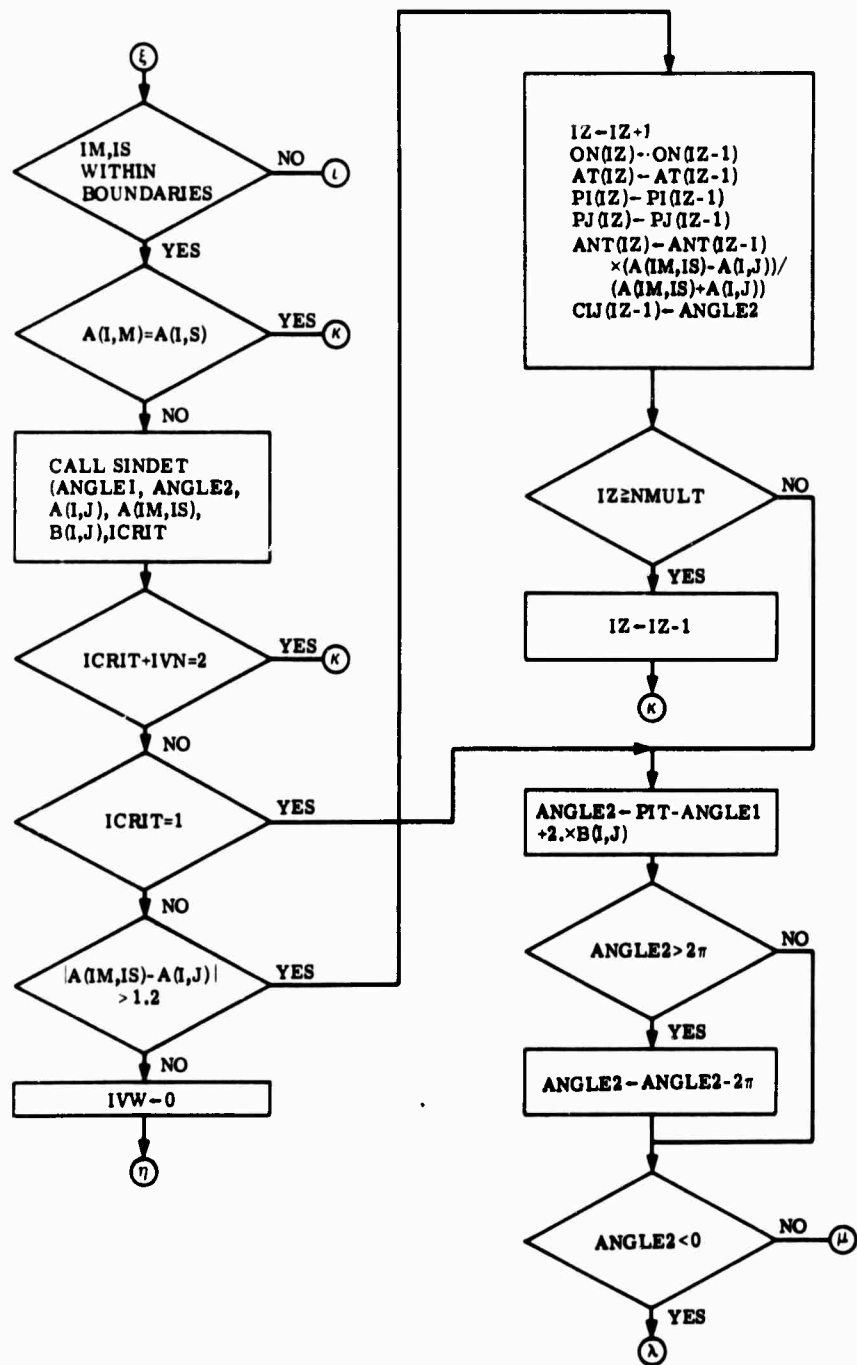ROUTINE SINDET (Continued)

FIGURE 48. FLOW CHART FOR MAIN PROGRAM SUBROUTINE WORLD AND SUB-
ROUTINE SINDET (Continued)
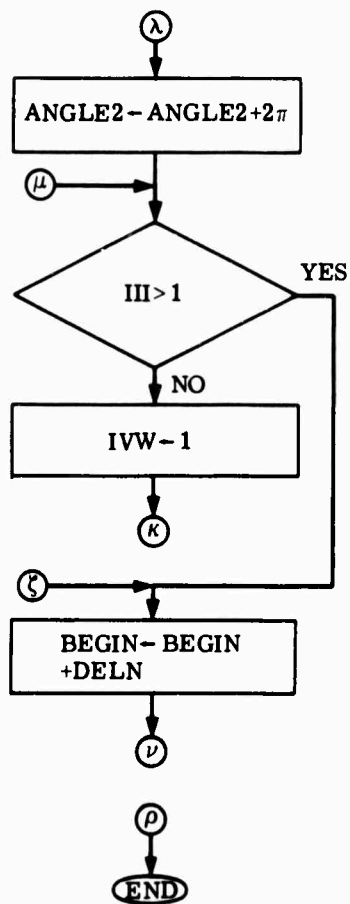
FIGURE 48. FLOW CHART FOR MAIN PROGRAM SUBROUTINE WORLD AND SUB-
ROUTINE SINDET (Continued)

SUBROUTINE SINDET(CIV,CIJ,AIJ,AMS,BIJ,ICRIT)
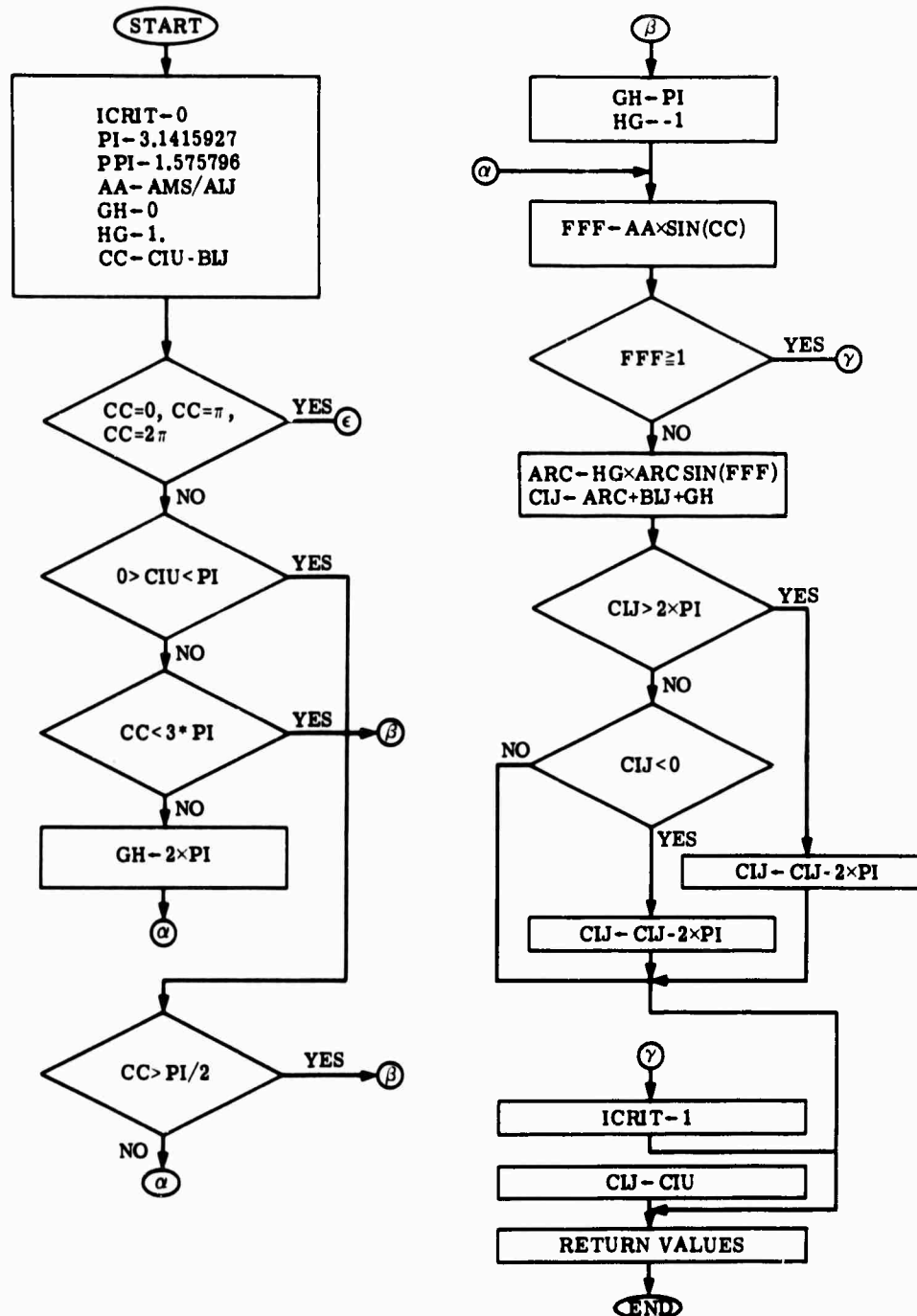


FIGURE 48.  FLOW CHART FOR MAIN PROGRAM SUBROUTINE WORLD AND SUB-
ROUTINE SINDET (Continued)

SUBROUTINE WORLD (D,VEL,SLP,SAMP,IPORSH,JPORSH)

START

DIMENSION D,VEL,SLP

PPI← 3.1415926/2.

I=IPORSH
DO 10
I=1

SLP(IPORSH,I← PPI
SLP(I,1)← 0.
VEL(IPORSH,I)← D
(IPORSH+1-I)

VEL(I,1)← D(I)

I=IPORSH
DO 20
I=1

J=JPORSH
DO 20
J=2

P← IPORSH-I
Q← J-1
PQ← P* P+Q*Q
H← SQRT(PQ)

CONTINUE

α

α

H>ISAMP
YES
NO

R← P/Q
THETA← ARCTAN(R)
SLP(I,J)← THETA-PPI
Y← ISAMP-H+.5
VEL(I,J)← D(K)

I=IPOR
DO 30
I=1,1

J=SAMP
DO 30
J=1,1

VEL(I+IPORSH,J)← VEL
(IPORSH-I,J)

SLP(I+IPORSH,J← SLP
(IPORSH-I,J)

RETURN

END

FIGURE 48. FLOW CHART FOR MAIN PROGRAM SUBROUTINE WORLD AND SUB-
ROUTINE SINDET (Concluded)

81

# REFERENCES

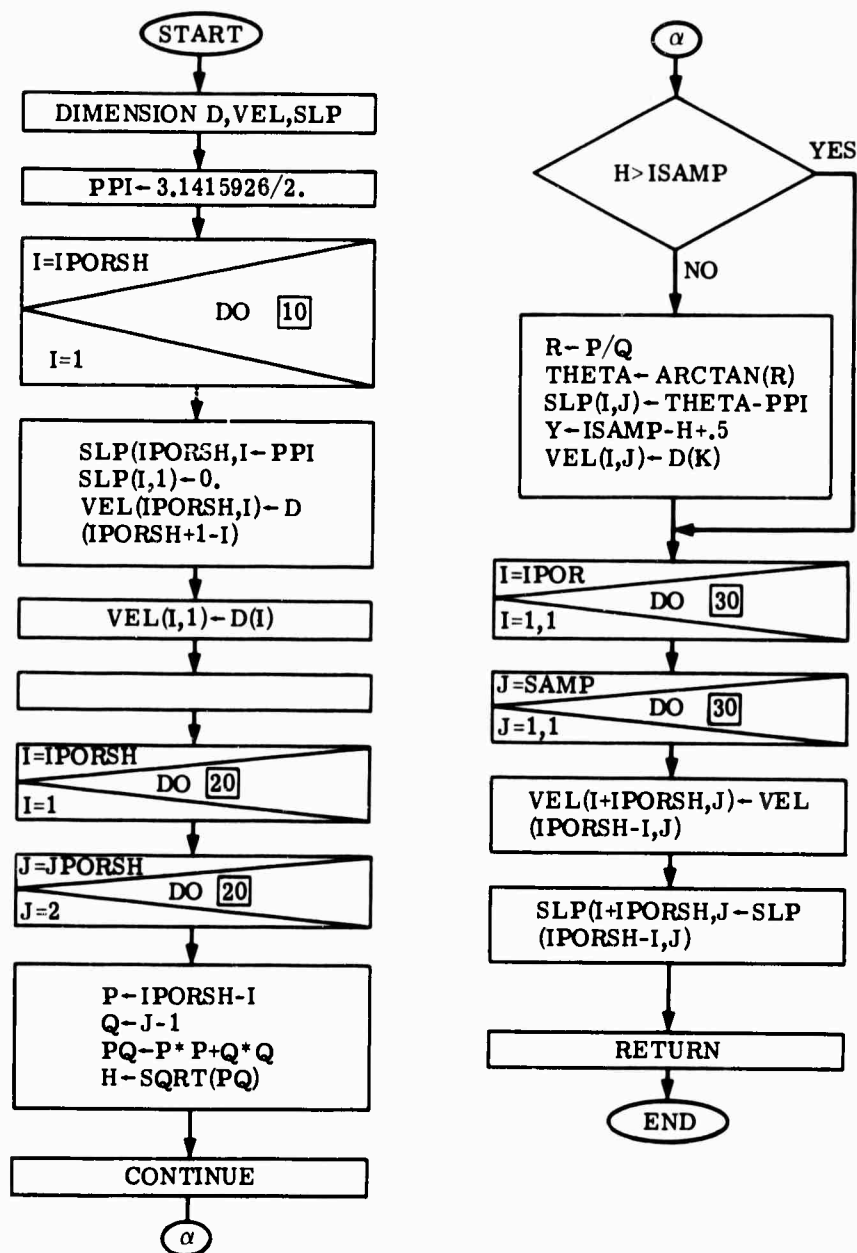1. David E. Willis and Philip L. Jackson, Collection and Analysis of Seismic Wave Propagation Data (Annual Report), Rept. No. 8071-6-P, Willow Run Laboratories of the Institute of Science and Technology, The University of Michigan, Ann Arbor, August 1967.

2. J. L. Hough, Geology of the Great Lakes, University of Illinois Press, Urbana, 1958.

3. Hugh Bradner and J. G. Dodds, "Comparative Seismic Noise on the Ocean Bottom and on Land," J. Geophys. Res., Vol. 69, No. 20, pp. 4339-4354, 1964.

4. D. S. Carder, D. W. Gordon, and J. N. Jordan, "Analysis of Surface Focus Travel Times," Bulletin of the Seismological Society of America, Vol. 56, No. 4, pp. 815-840, 1966.

5. E. Herrin and J. Taggart, "Regional Variations in $P_n$ Velocity and Their Effect on the Location of Epicenters," Bulletin of the Seismological Society of America, Vol. 52, No. 5, pp. 1037-1046, 1962.

6. J. Jordan, R. Black, and C. C. Bates, "Patterns of Maximum Amplitudes of $P_n$ and P Waves Over Regional and Continental Areas," Bulletin of the Seismological Society of America, Vol. 55, No. 4, pp. 693-720, 1965.

7. R. Van Nostrand and W. Helterbran, A Comparative Study of the SHOAL Event, Seismic Data Laboratory Rept. No. 109, prepared for AFTAC, Contract AF 33(657)-12447, VT/2037, 1964.

8. David E. Willis and Philip L. Jackson, Collection and Analysis of Seismic Wave Propagation Data (Final Report), Rept. No. 5178-64-F, Willow Run Laboratories of the Institute of Science and Technology, The University of Michigan, Ann Arbor, August 1966.

9. B. R. Julian and D. L. Anderson, "Travel Times, Apparent Velocities and Amplitudes of Body Waves," Bulletin of the Seismological Society of America, Vol. 58, No. 1, pp. 339-366, 1968.

10. B. T. R. Lewis and Robert P. Meyer, "A Seismic Investigation of the Upper Mantle to the West of Lake Superior," Bulletin of the Seismological Society of America, Vol. 58, No. 2, pp. 565-569, April 1968.

11. H. M. Iyer and V. W. Punton, "A computer Program for Plotting Wavefronts and Rays from a Point Source in Dispersive Mediums," J. Geophys. Res., Vol. 68, No. 11, June 1, 1968.

12. Personal Communication from Nazieh Yacoub, U. S. G. S., Special Projects Branch, Denver, Colo. 80226

13. Philip L. Jackson, "Two- and Three-Dimensional Ray Tracing, Travel Time, and Amplitude Computation," Paper presented to the Seismological Society of America, Tucson, Ariz., April 13, 1968.

## DOCUMENT CONTROL DATA - R & D

*(Security classification of title, body of abstract and indexing annotation must he entered when the overall report is classified)*

| 1. ORIGINATING ACTIVITY *(Corporate author)* | 2a. REPORT SECURITY CLASSIFICATION |
|---|---|
| Willow Run Laboratories of the Institute of Science and Technology, The University of Michigan, Ann Arbor | Unclassified |
| | 2b. GROUP |

3. REPORT TITLE

COLLECTION AND ANALYSIS OF SEISMIC-WAVE PROPAGATION DATA

4. DESCRIPTIVE NOTES *(Type of report and inclusive dates)*

Annual Report, 1 June 1967 Through 31 May 1968

5. AUTHOR(S) *(First name, middle initial, last name)*

David E. Willis and Philip L. Jackson

| 6. REPORT DATE | 7a. TOTAL NO. OF PAGES | 7b. NO. OF REFS |
|---|---|---|
| September 1968 | viii + 83 | 13 |

| 8a. CONTRACT OR GRANT NO. | 9a. ORIGINATOR'S REPORT NUMBER(S) |
|---|---|
| AF 49(638)-1759 | 8071-15-P |
| b. PROJECT NO. ARPA Order No. 292, Amendments 32 & 37 | |
| c. | 9b. OTHER REPORT NO(S) *(Any other numbers that may be assigned this report)* |
| d. | |

10. DISTRIBUTION STATEMENT

Distribution of this document is unlimited.

| 11. SUPPLEMENTARY NOTES | 12. SPONSORING MILITARY ACTIVITY |
|---|---|
| | Advanced Research Projects Agency, Washington, D.C.; Air Force Office of Scientific Research, Arlington, Va. |

13. ABSTRACT

This report discusses the results of an extensive long-range reversed refraction profile which traverses the Michigan Basin and the Appalachian Mountains. Particular emphasis is placed on the attenuation of first compressional wave arrivals and on crustal-upper mantle structure. Also included are results of a survey on lake bottom seismic background noise in Lake Superior. Although large signal levels were obtained in the lake bottom, long periods of high background noise indicated that land based seismographs are superior. Theoretical studies in elastic wave scattering were made to evaluate the effect of nonhomogeneities on the propagation of elastic waves. Theoretical development of mode filtering (previously demonstrated empirically), is nearly completed. A LASA digital data convertor was designed, constructed, and put into operation. Two- and three-dimensional seismic ray-tracing techniques using digital modeling were developed. These techniques enable the seismologist to determine the effects of lateral inhomogeneities and irregularities in velocity interfaces on travel time and attenuation of seismic waves.

**DD FORM 1 NOV 65 1473**

| 14. KEY WORDS | LINK A | | LINK B | | LINK C | |
|---|---|---|---|---|---|---|
| | ROLE | WT | ROLE | WT | ROLE | WT |
| Seismic waves | | | | | | |
| Seismic-wave propagation | | | | | | |
| Seismic-wave attenuation | | | | | | |
| Seismic-wave travel time | | | | | | |
| Elastic-wave scattering | | | | | | |
| Seismic-noise studies | | | | | | |
| Mode filtering | | | | | | |
| Seismic-ray tracing | | | | | | |
| Digital modeling | | | | | | |